Title: The non-superconducting states of the cuprates

Date: Jul 07, 2015 10:00 AM

URL: http://pirsa.org/15070060

Abstract: The most interesting states of the cuprate compounds are not the superconductors with high critical temperatures. Instead, the novelty lies primarily in the higher temperature metallic "normal" states from which the superconductors descend, and in competing low temperature states with density wave order. I will review recent experimental and theoretical progress in understanding these states. The experimental evidence is compatible with the presence of a metal with topological order in the 'pseudogap' regime of low carrier density.


The non-superconducting states of the cuprates
Perimeter Institute, Waterloo
July 7, 2015
Subir Sachdev
PI
NSF
JOHN TEMPLETON FOUNDATION
PHYSICS
VE RI TAS
HARVARD
Talk online: sachdev.physics.harvard.edu


Debanjan Chowdhury
Andrea Allais
Aavishkar Patel
Andrew Lucas
Alexandra Thomson
Philipp Strack Cologne
Matthias Punk (Innsbruck)

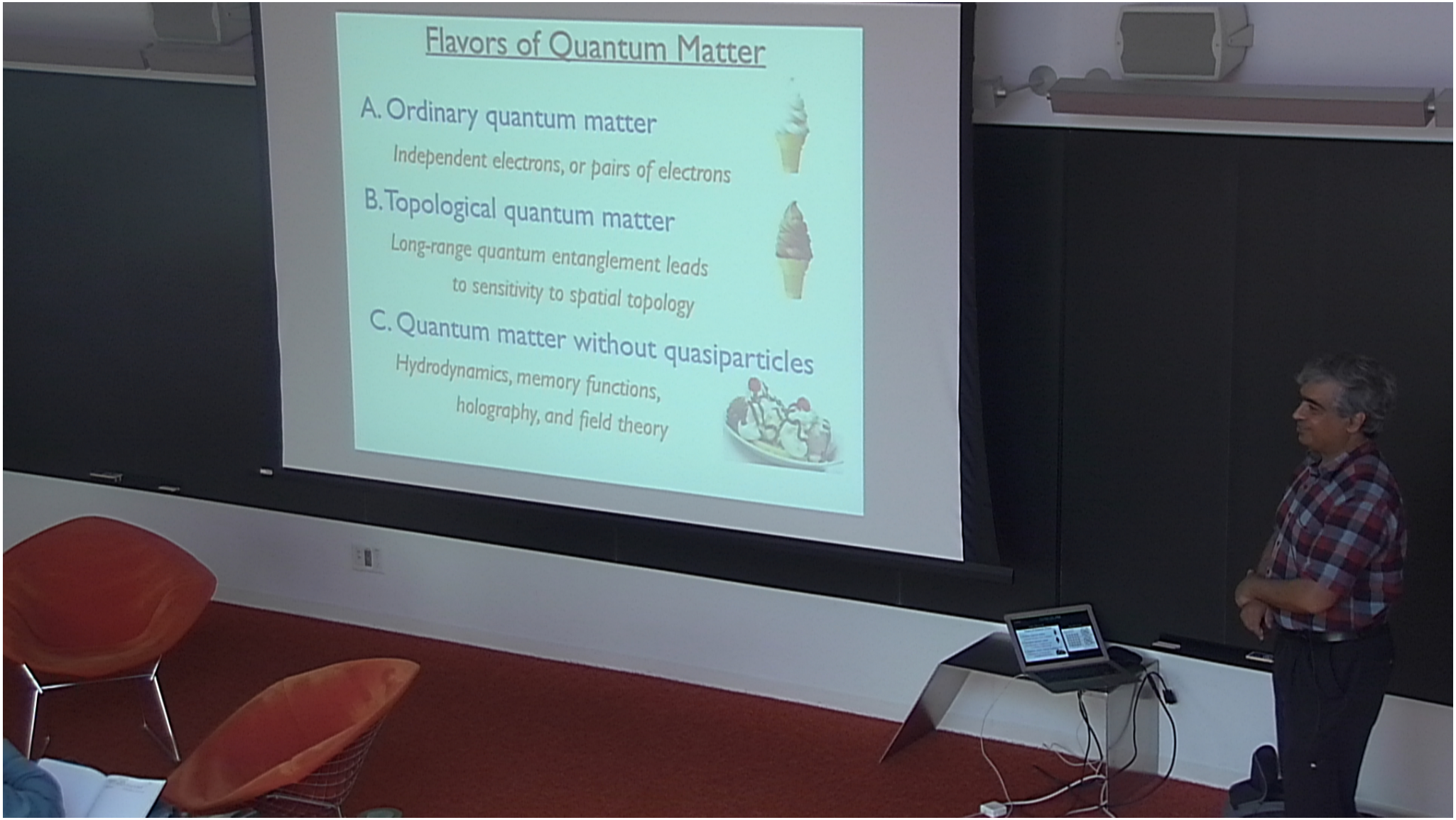
Flavors of Quantum Matter
A. Ordinary quantum matter
Independent electrons, or pairs of electrons
B. Topological quantum matter
Long-range quantum entanglement leads
to sensitivity to spatial topology
C. Quantum matter without quasiparticles
Hydrodynamics, memory functions,
holography, and field theory

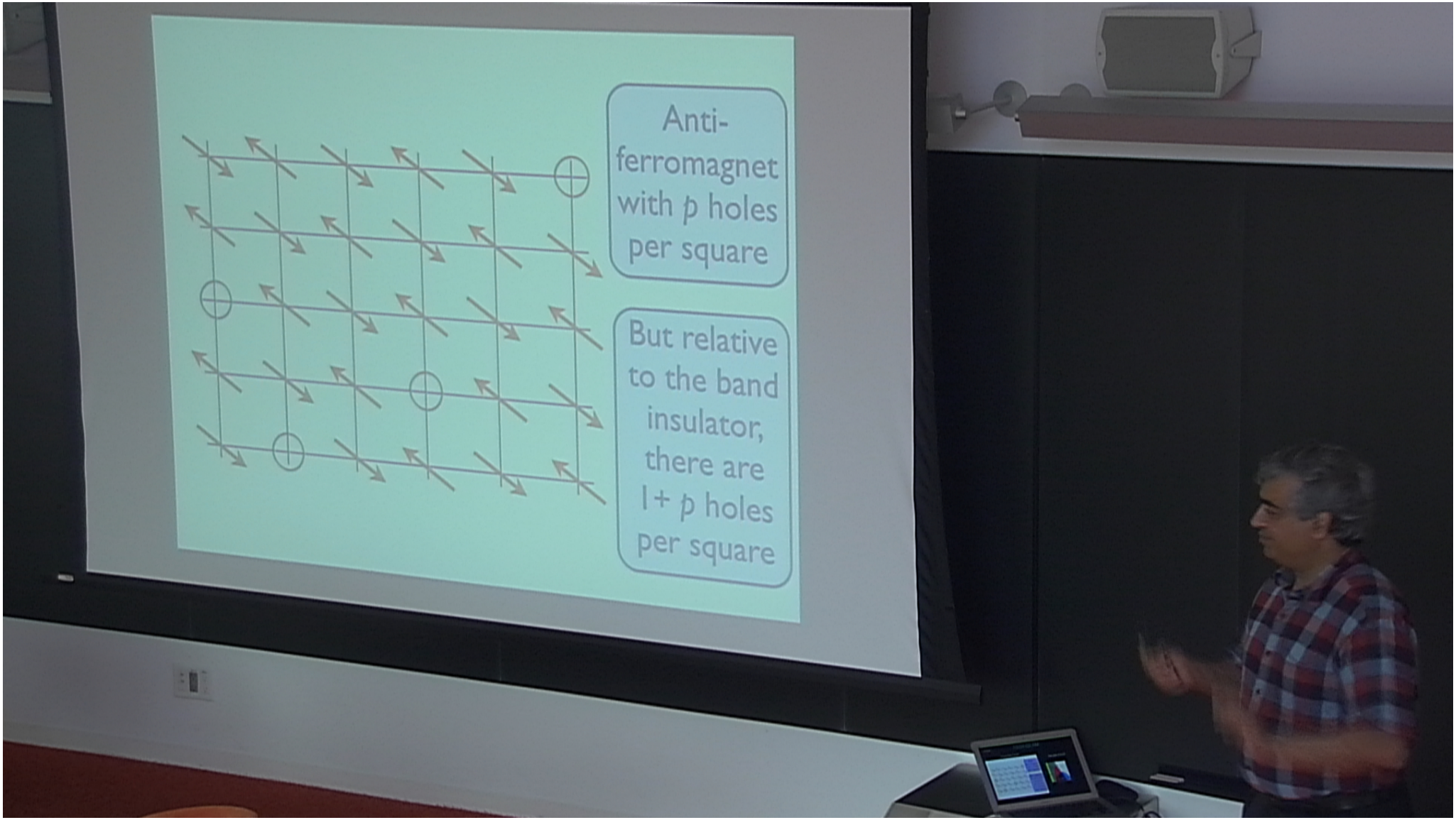
Anti-ferromagnet with p holes per square
But relative to the band insulator, there are 1+ p holes per square

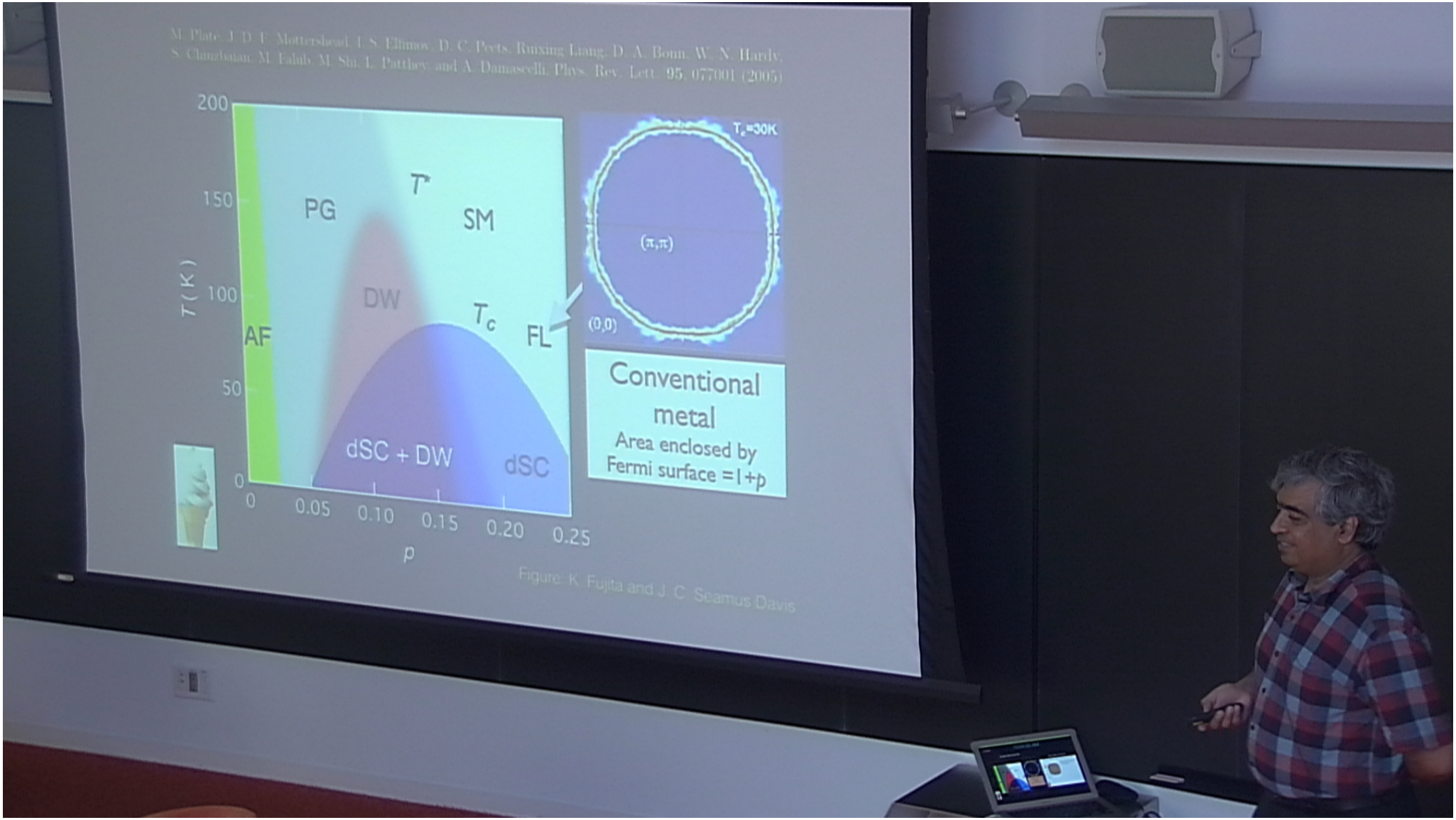
M. Plate, J. D. F. Mottershead, I. S. Elfimov, D. C. Peets, Ruixing Liang, D. A. Bonn, W. N. Hardy, S. Chiuzbaian, M. Falub, M. Shi, L. Patthey, and A. Damascelli, Phys. Rev. Lett. 95, 077001 (2005)
200
150
100
50
0
T (K)
PG
T*
SM
DW
Tc
AF
FL
dSC + DW
dSC
0
0.05
0.10
0.15
0.20
0.25
p
Tc=30K
(π,π)
(0,0)
Conventional metal
Area enclosed by Fermi surface = 1+p
Figure: K. Fujita and J. C. Seamus Davis

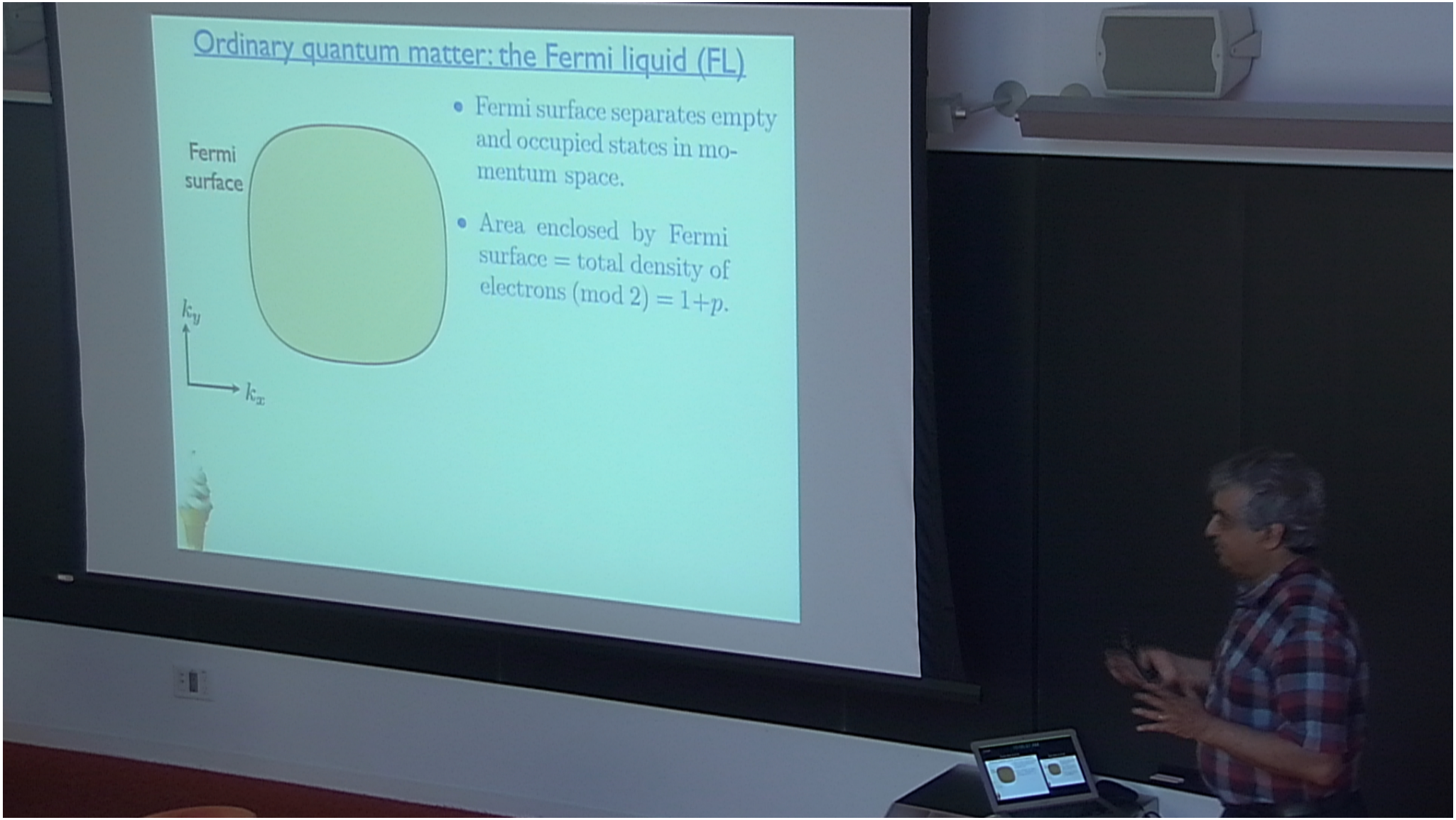
Ordinary quantum matter: the Fermi liquid (FL)
Fermi surface
k_y
k_x
• Fermi surface separates empty and occupied states in momentum space.
• Area enclosed by Fermi surface = total density of electrons (mod 2) = 1+p.

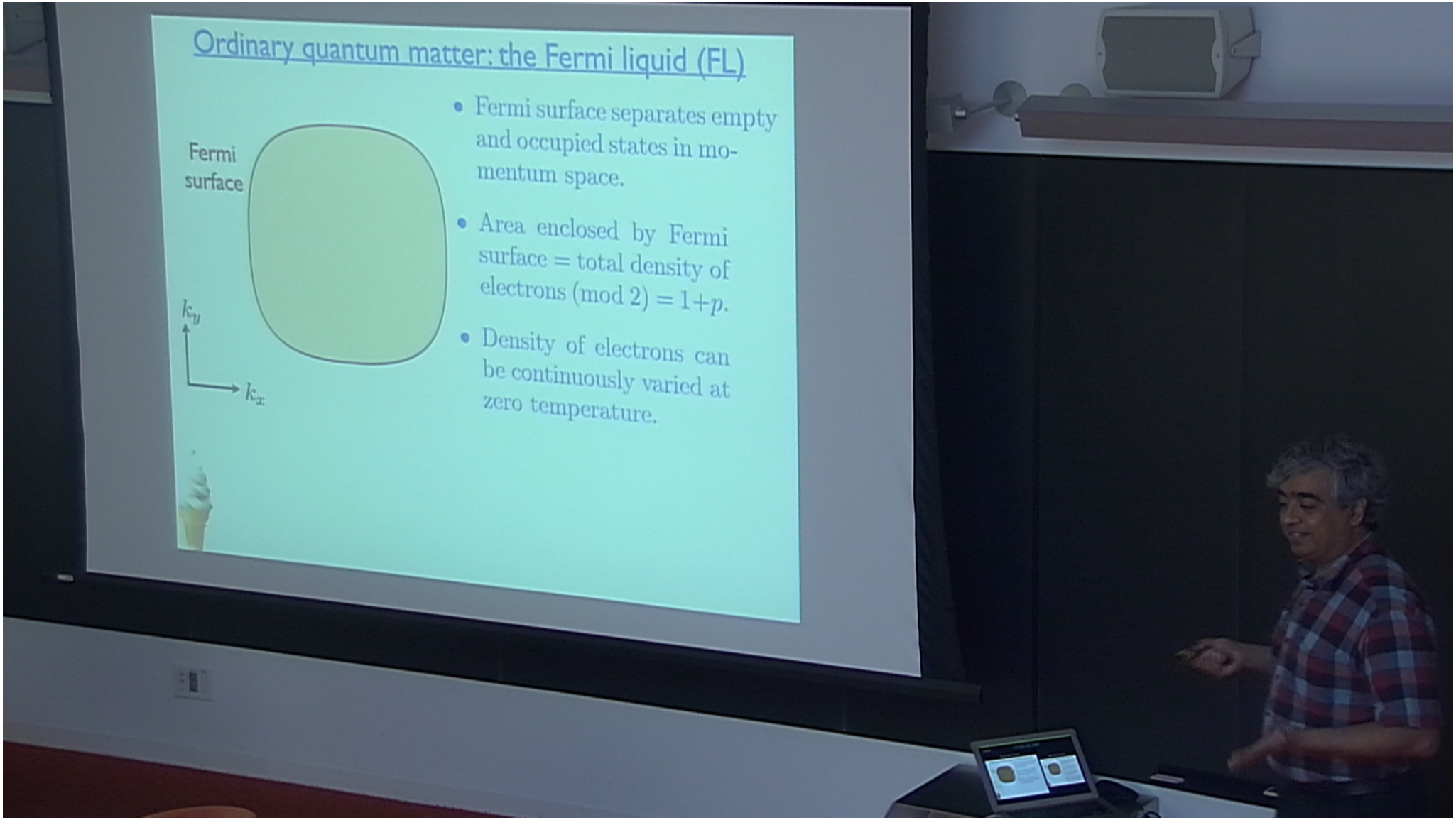
Ordinary quantum matter: the Fermi liquid (FL)
Fermi surface
k_y
k_x
• Fermi surface separates empty and occupied states in momentum space.
• Area enclosed by Fermi surface = total density of electrons (mod 2) = 1+p.
• Density of electrons can be continuously varied at zero temperature.

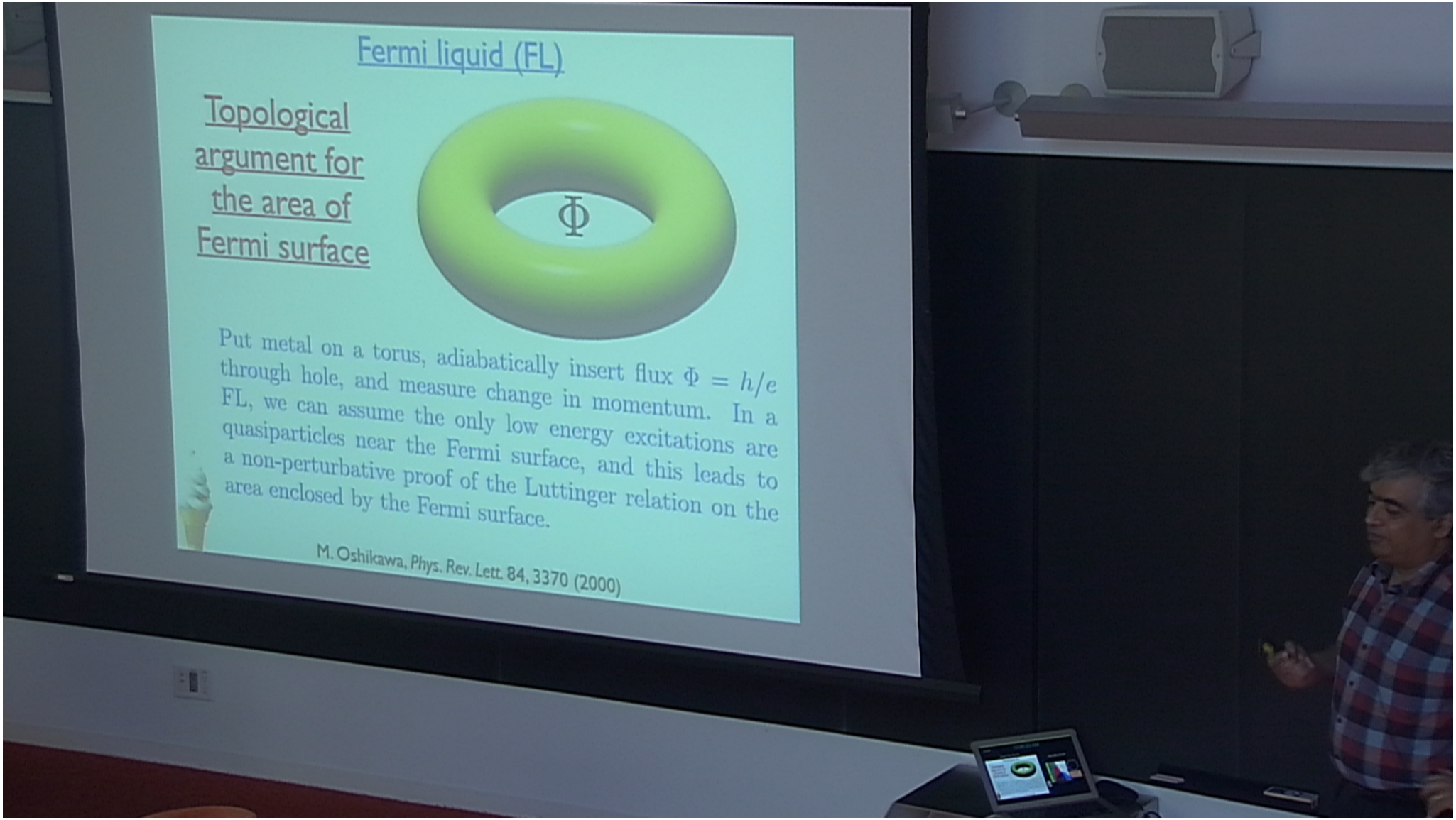
Fermi liquid (FL)
Topological argument for the area of Fermi surface
Φ
Put metal on a torus, adiabatically insert flux $\Phi = h/e$ through hole, and measure change in momentum. In a FL, we can assume the only low energy excitations are quasiparticles near the Fermi surface, and this leads to a non-perturbative proof of the Luttinger relation on the area enclosed by the Fermi surface.
M. Oshikawa, Phys. Rev. Lett. 84, 3370 (2000)

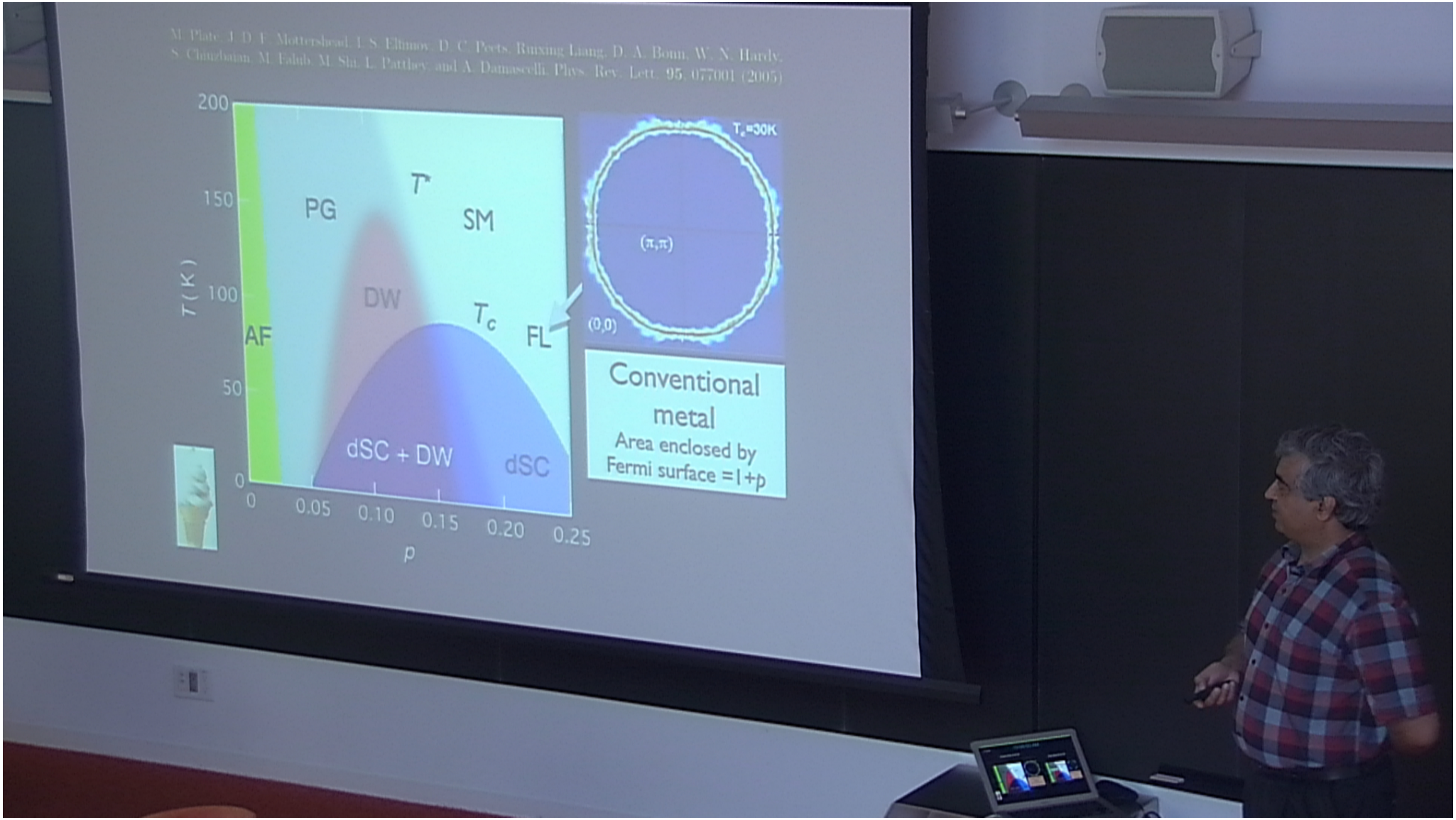
M. Plate, J. D. F. Mottershead, I. S. Elfimov, D. C. Peets, Ruixing Liang, D. A. Bonn, W. N. Hardy, S. Chiuzbaian, M. Falub, M. Shi, L. Patthey, and A. Damascelli, Phys. Rev. Lett. 95, 077001 (2005)
200
150
100
50
0
T (K)
PG
T*
SM
DW
Tc
AF
FL
dSC + DW
dSC
0
0.05
0.10
0.15
0.20
0.25
p
(π,π)
(0,0)
Conventional metal
Area enclosed by Fermi surface = 1+p

Electrical and optical evidence for Fermi surface of long-lived quasiparticles of density p

Evolution of the Hall Coefficient and the Peculiar Electronic Structure of the Cuprate Superconductors

Yoichi Ando,* Y. Kurita,† Seiki Komiya, S. Ono, and Kouji Segawa

PRL 92, 197001 (2004)

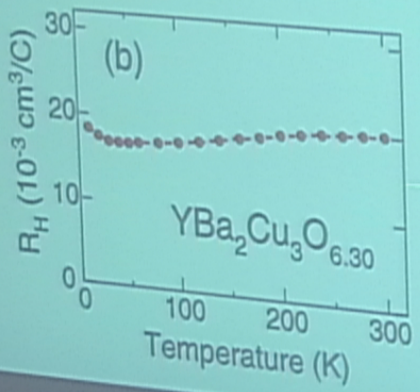

T-independent Hall effect in a magnetic field of fermions of charge +e and density p

Electrical and optical evidence for Fermi surface of long-lived quasiparticles of density p

Spectroscopic evidence for Fermi liquid-like energy and temperature dependence of the relaxation rate in the pseudogap phase of the cuprates

Seyed Iman Mirzaei[a], Damien Stricker[a], Jason N. Hancock[a,b], Christophe Berthod[a], Antoine Georges[a,c,d], Erik van Heumen[a,e], Mun K. Chan[f], Xudong Zhao[f,g], Yuan Li[h], Martin Greven[f], Neven Barisic[f,i], and Dirk van der Marel[a,1]

PNAS 110, 5774 (2013)

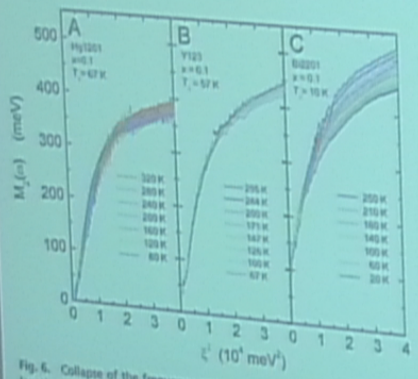

Fig. 6. Collapse of the frequency and temperature dependence of the relaxation rate of underdoped cuprate materials. Normal state $M_2(\omega, T)$ as a function of $\xi^2 \equiv (\hbar\omega)^2 + (\pi k_B T)^2$

$$\sigma_{xx} \sim \frac{1}{(-i\omega + 1/\tau)}$$

$$\text{with } \frac{1}{\tau} \sim \omega^2 + T^2$$

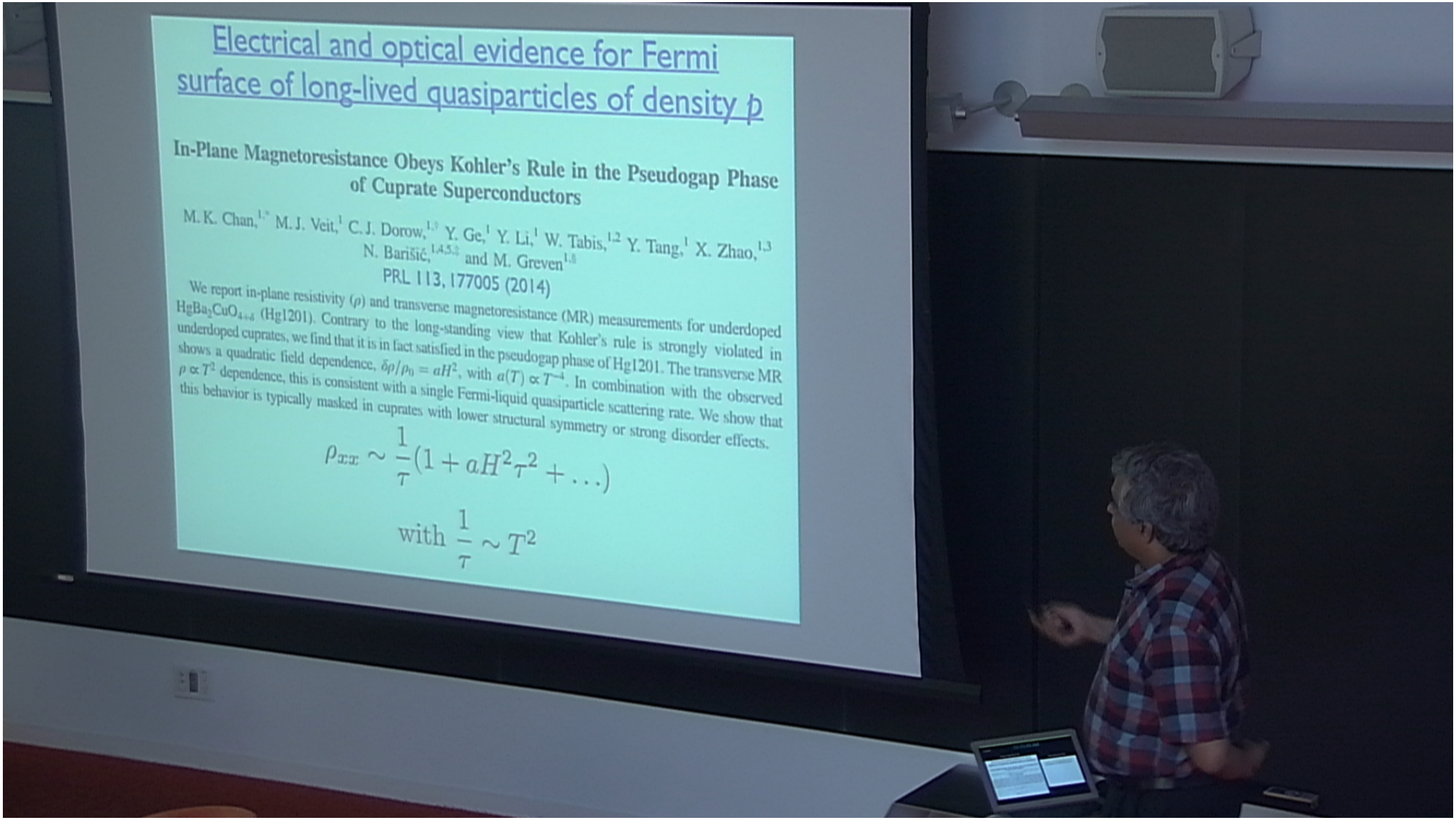
Electrical and optical evidence for Fermi surface of long-lived quasiparticles of density p
In-Plane Magnetoresistance Obeys Kohler's Rule in the Pseudogap Phase of Cuprate Superconductors
M. K. Chan, M. J. Veit, C. J. Dorow, Y. Ge, Y. Li, W. Tabis, Y. Tang, X. Zhao, N. Barišić and M. Greven
PRL 113, 177005 (2014)
We report in-plane resistivity (ρ) and transverse magnetoresistance (MR) measurements for underdoped $HgBa_2CuO_{4+\delta}$ (Hg1201). Contrary to the long-standing view that Kohler's rule is strongly violated in underdoped cuprates, we find that it is in fact satisfied in the pseudogap phase of Hg1201. The transverse MR shows a quadratic field dependence, $\delta\rho/\rho_0 = aH^2$, with $a(T) \propto T^{-4}$. In combination with the observed $\rho \propto T^2$ dependence, this is consistent with a single Fermi-liquid quasiparticle scattering rate. We show that this behavior is typically masked in cuprates with lower structural symmetry or strong disorder effects.
$$\rho_{xx} \sim \frac{1}{\tau}(1 + aH^2\tau^2 + \ldots)$$
$$\text{with } \frac{1}{\tau} \sim T^2$$

Electrical and optical evidence for Fermi surface of long-lived quasiparticles of density p

In-Plane Magnetoresistance Obeys Kohler's Rule in the Pseudogap Phase of Cuprate Superconductors

M. K. Chan,[1,*] M. J. Veit,[1] C. J. Dorow,[1,†] Y. Ge,[1] Y. Li,[1] W. Tabis,[1,2] Y. Tang,[1] X. Zhao,[1,3] N. Barišić,[1,4,5,‡] and M. Greven[1,§]

PRL 113, 177005 (2014)

We report in-plane resistivity (ρ) and transverse magnetoresistance (MR) measurements for underdoped $HgBa_2CuO_{4+\delta}$ (Hg1201). Contrary to the long-standing view that Kohler's rule is strongly violated in underdoped cuprates, we find that it is in fact satisfied in the pseudogap phase of Hg1201. The transverse MR shows a quadratic field dependence, $\delta\rho/\rho_0 = aH^2$, with $a(T) \propto T^{-4}$. In combination with the observed $\rho \propto T^2$ dependence, this is consistent with a single Fermi-liquid quasiparticle scattering rate. We show that this behavior is typically masked in cuprates with lower structural symmetry or strong disorder effects.

$$\rho_{xx} \sim \frac{1}{\tau}(1 + aH^2\tau^2 + \ldots)$$

$$\text{with } \frac{1}{\tau} \sim T^2$$

M. Plate, J. D. F. Mottershead, I. S. Elfimov, D. C. Peets, Ruixing Liang, D. A. Bonn, W. N. Hardy, S. Chiuzbaian, M. Falub, M. Shi, L. Patthey, and A. Damascelli, Phys. Rev. Lett. **95**, 077001 (2005)

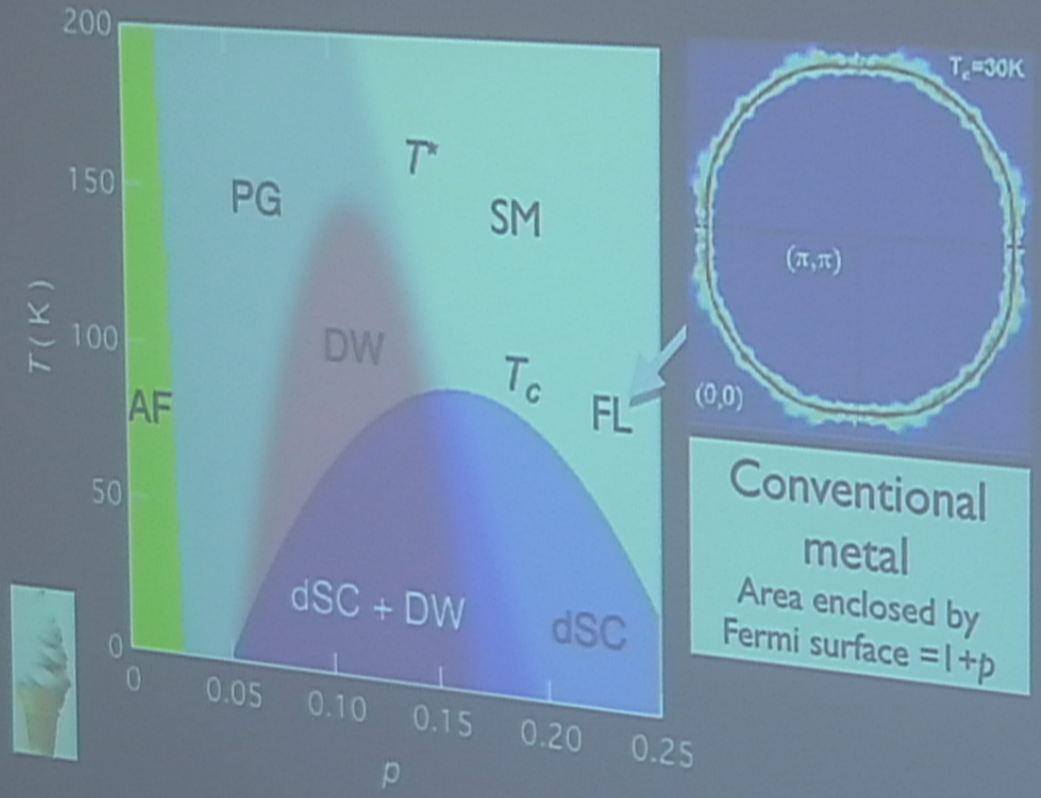

Conventional metal

Area enclosed by Fermi surface = 1 + *p*

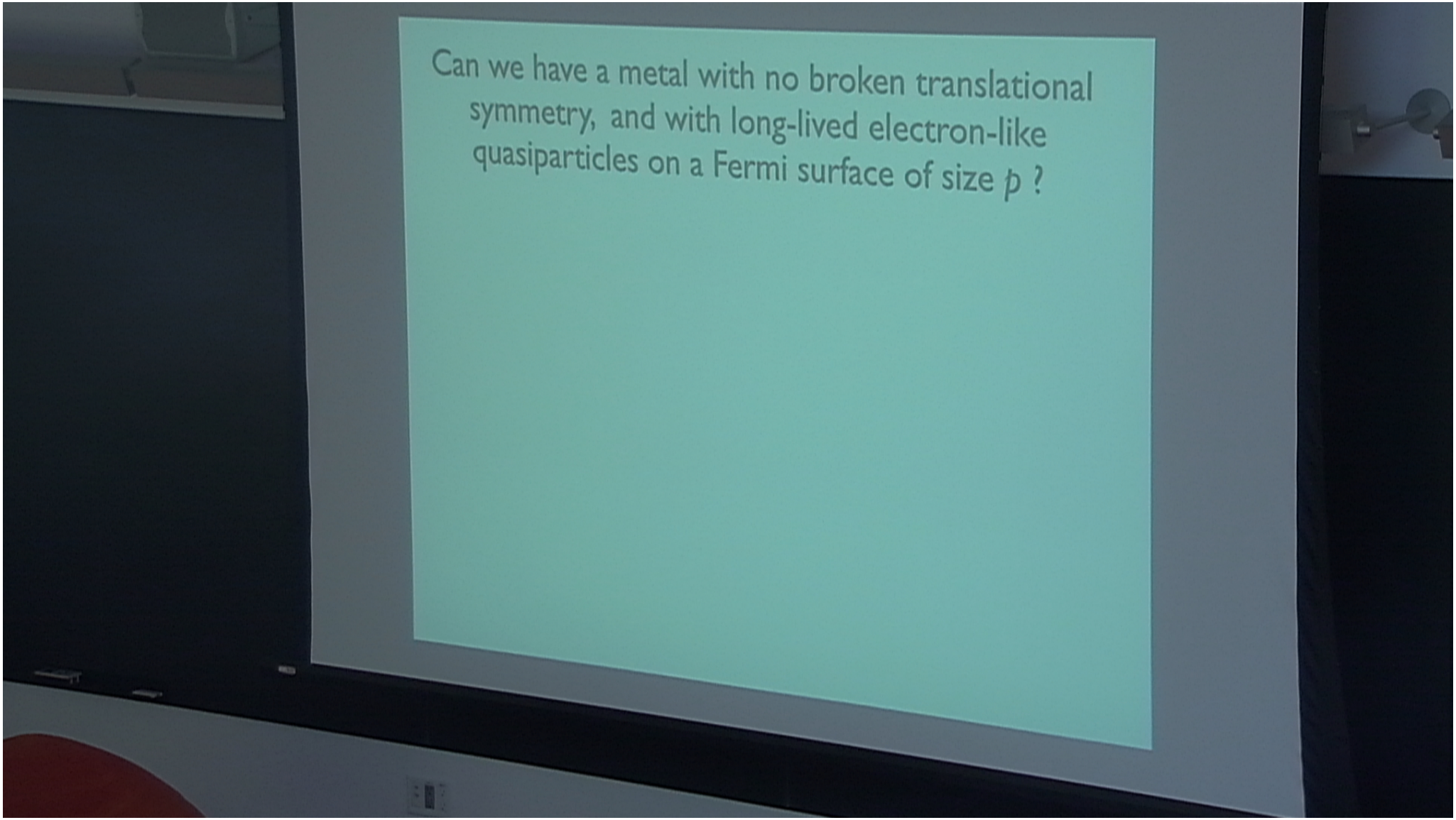
Can we have a metal with no broken translational symmetry, and with long-lived electron-like quasiparticles on a Fermi surface of size p ?

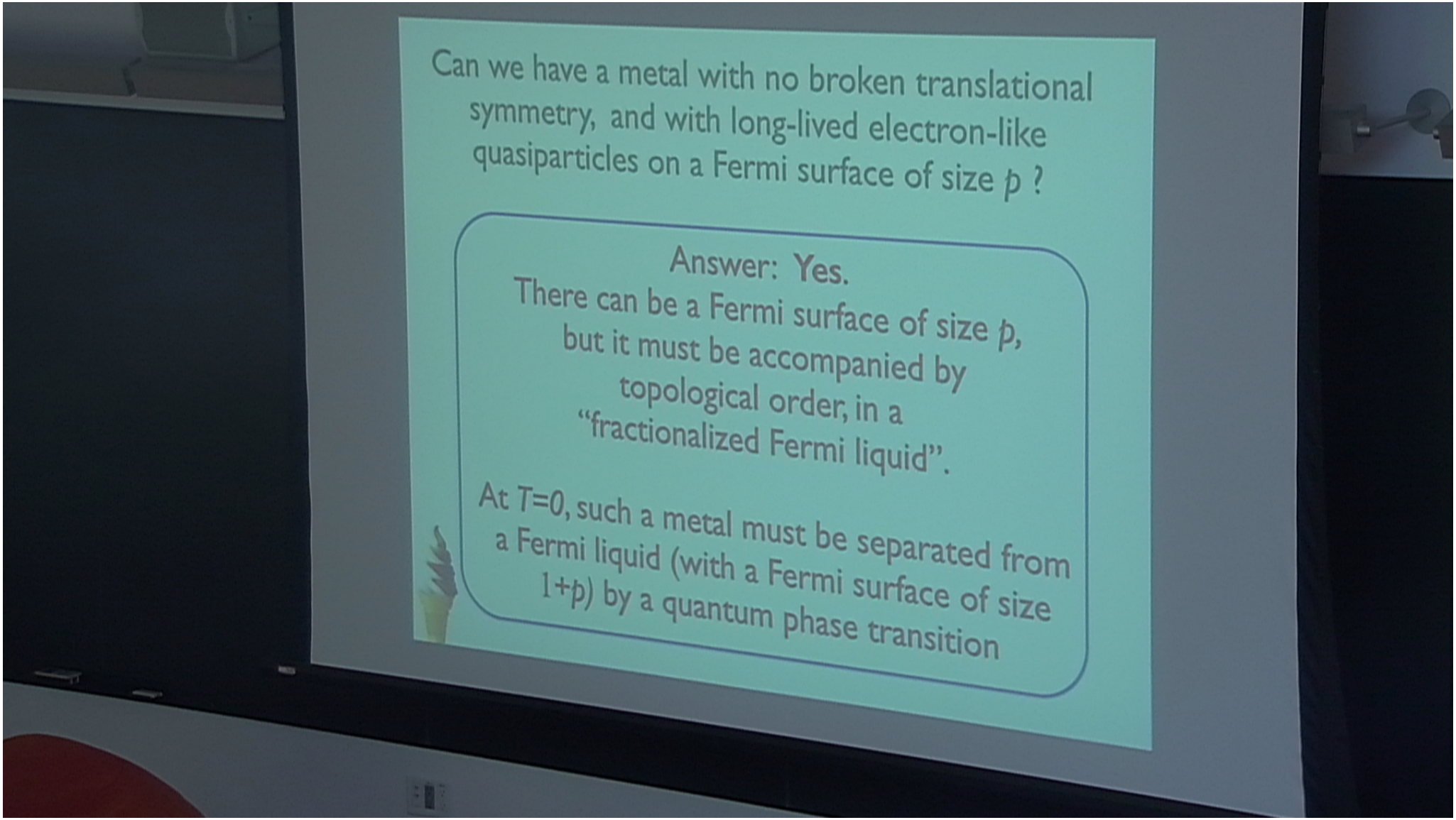
Can we have a metal with no broken translational symmetry, and with long-lived electron-like quasiparticles on a Fermi surface of size p ?
Answer: Yes.
There can be a Fermi surface of size p, but it must be accompanied by topological order, in a "fractionalized Fermi liquid".
At T=0, such a metal must be separated from a Fermi liquid (with a Fermi surface of size 1+p) by a quantum phase transition

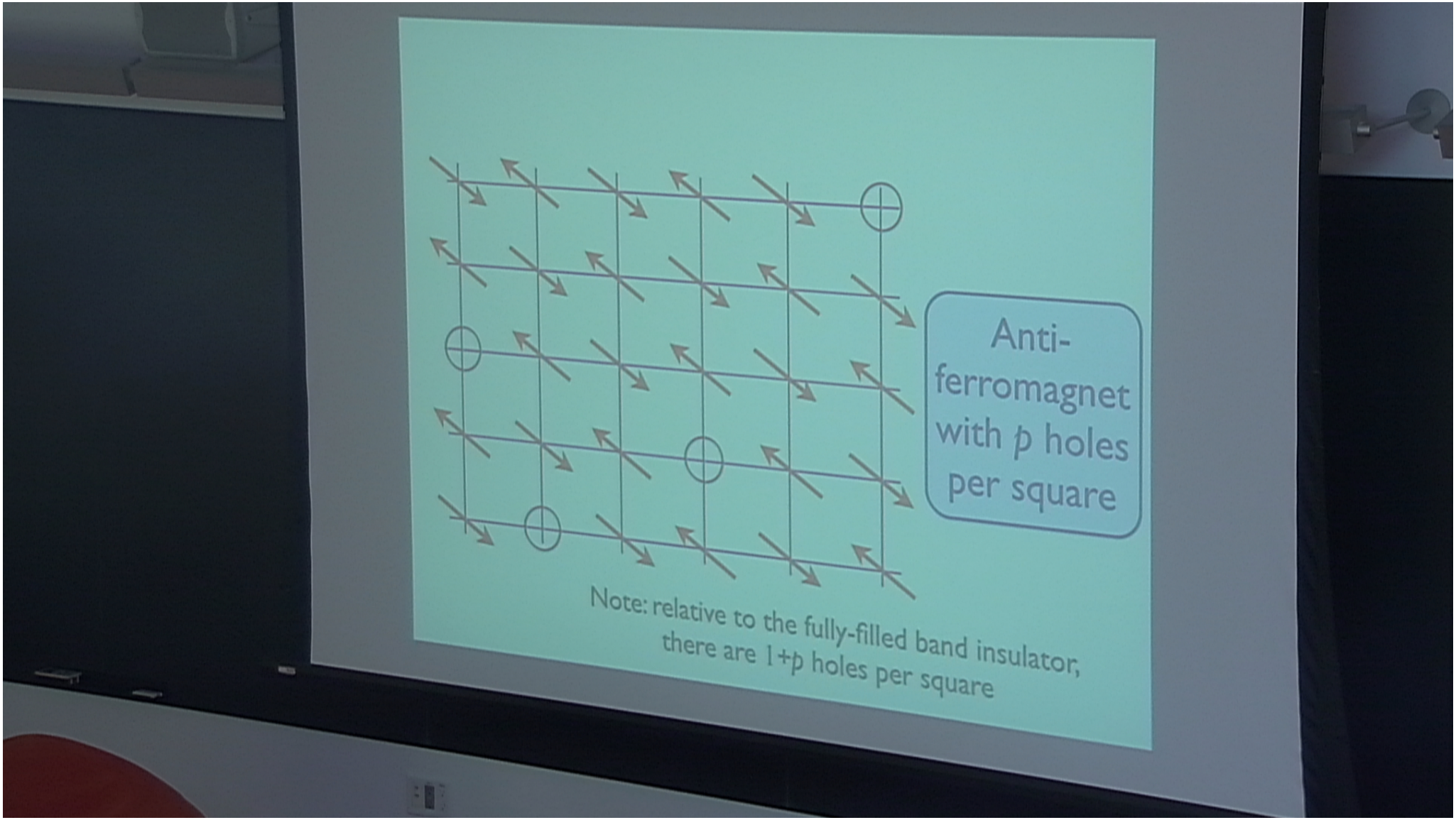
Anti-ferromagnet with p holes per square
Note: relative to the fully-filled band insulator, there are $1+p$ holes per square

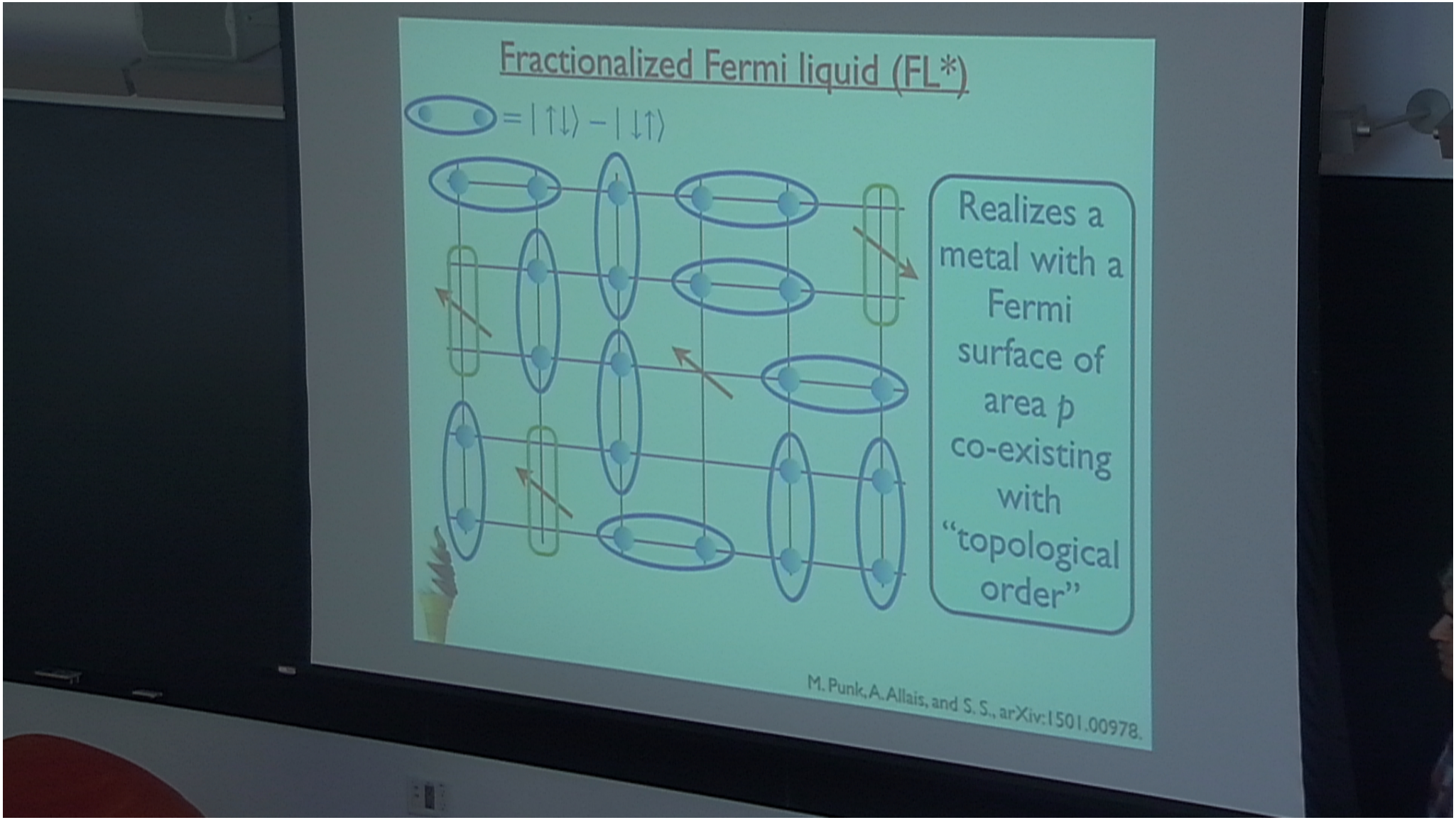
Fractionalized Fermi liquid (FL*)
$= |\uparrow\downarrow\rangle - |\downarrow\uparrow\rangle$
Realizes a metal with a Fermi surface of area p co-existing with "topological order"
M. Punk, A. Allais, and S. S., arXiv:1501.00978.

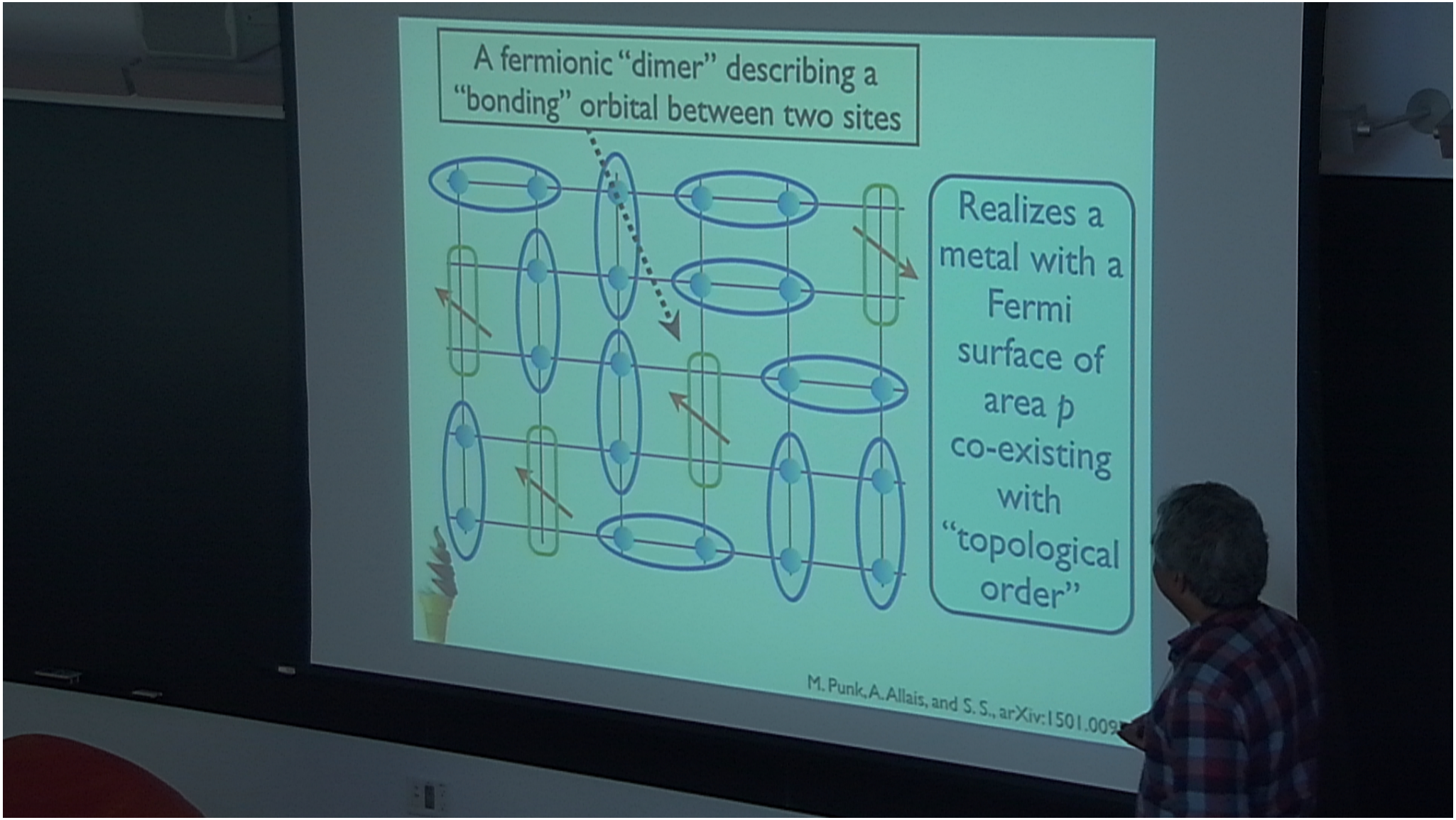
A fermionic "dimer" describing a "bonding" orbital between two sites
Realizes a metal with a Fermi surface of area p co-existing with "topological order"
M. Punk, A. Allais, and S. S., arXiv:1501.009

Topological order

Place pseudogap metal on a torus; obtain "topological" states nearly degenerate with the ground state: change sign of every dimer across red line

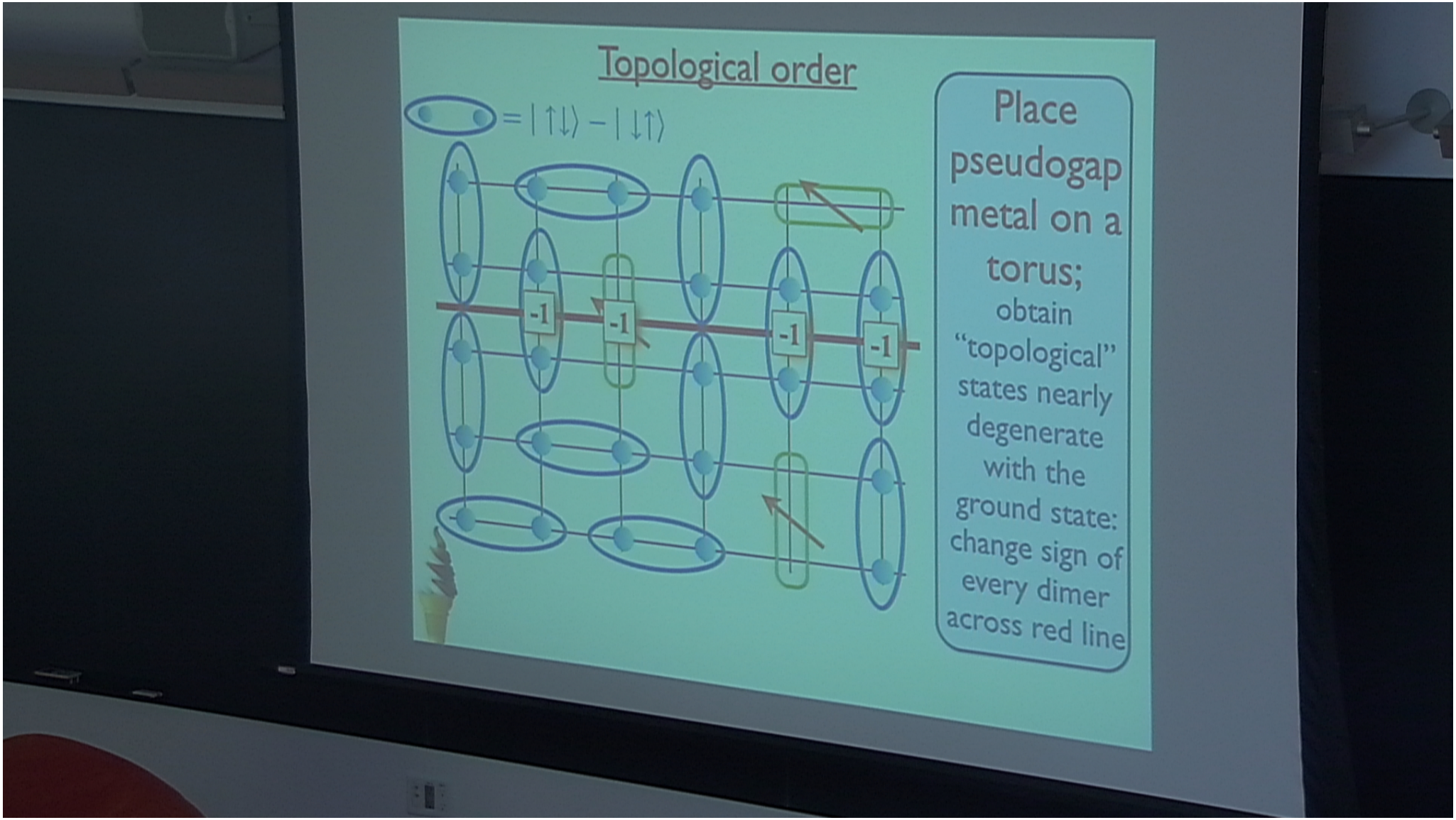
Topological order
$= |\uparrow\downarrow\rangle - |\downarrow\uparrow\rangle$
-1
-1
-1
-1
Place pseudogap metal on a torus;
obtain "topological" states nearly degenerate with the ground state:
change sign of every dimer across red line

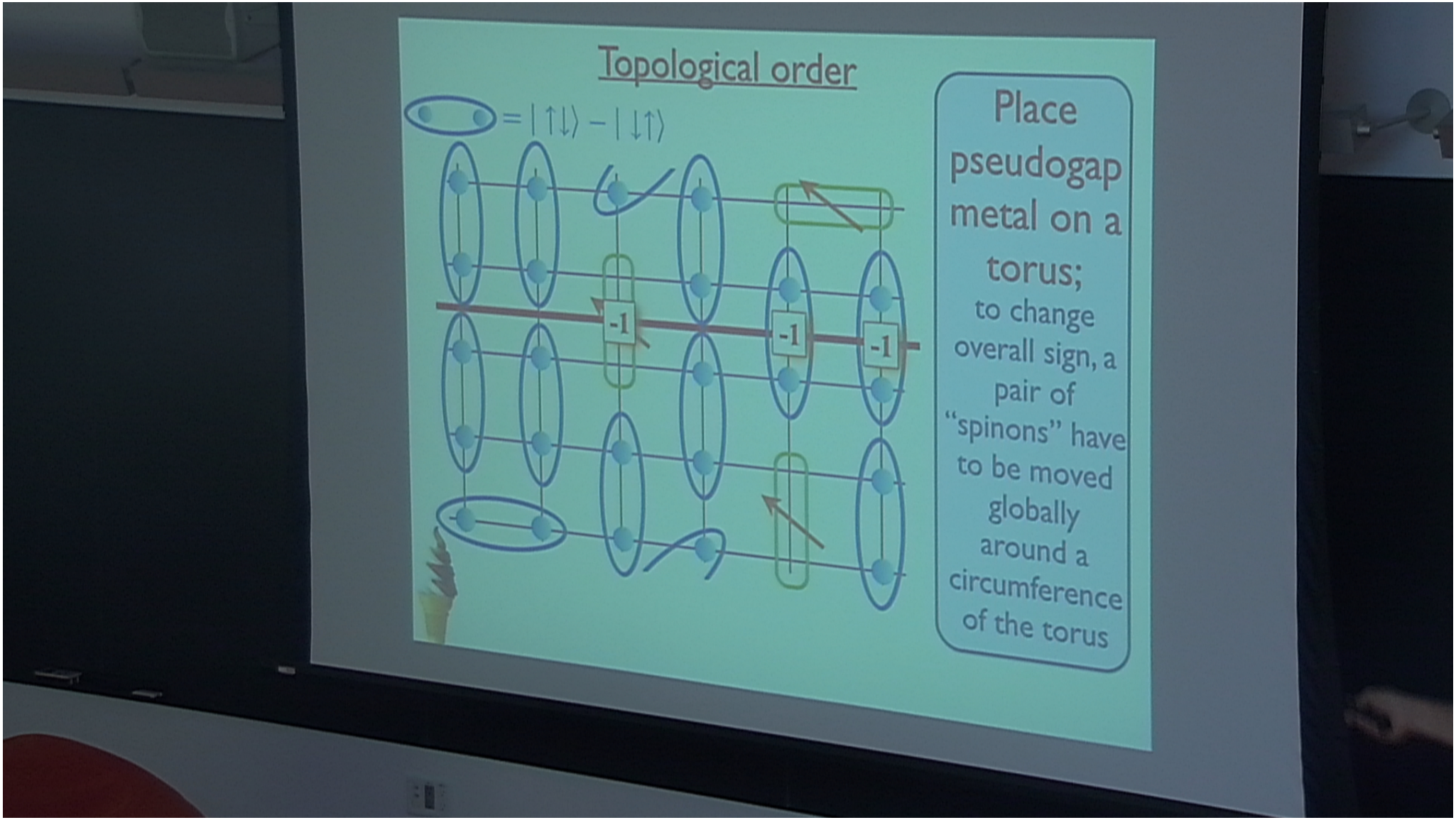
Topological order
$= |\uparrow\downarrow\rangle - |\downarrow\uparrow\rangle$
-1
-1
-1
Place pseudogap metal on a torus;
to change overall sign, a pair of "spinons" have to be moved globally around a circumference of the torus

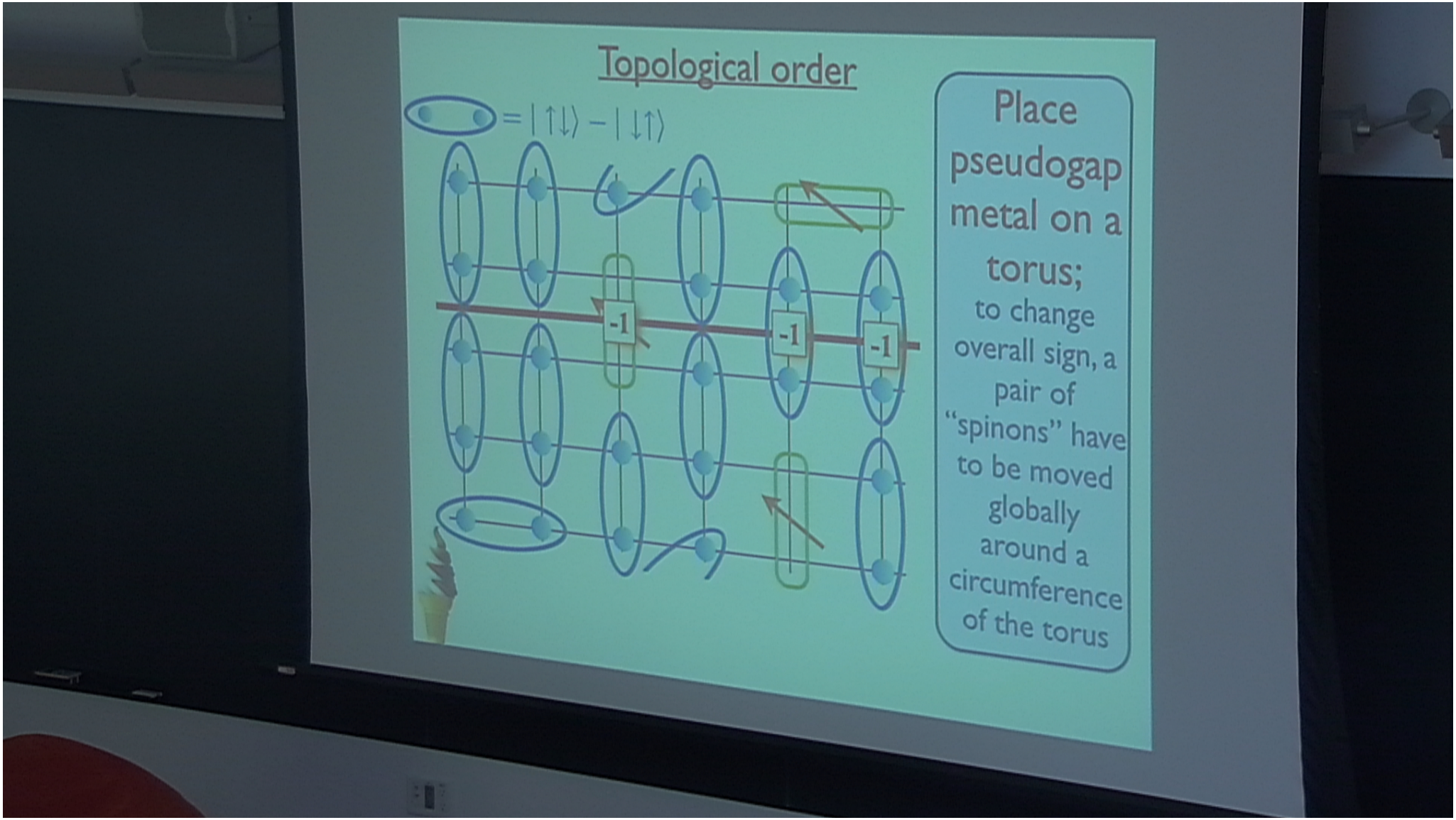
Topological order
$= |\uparrow\downarrow\rangle - |\downarrow\uparrow\rangle$
-1
-1
-1
Place pseudogap metal on a torus;
to change overall sign, a pair of "spinons" have to be moved globally around a circumference of the torus

Fermi liquid (FL)

Topological argument for the area of Fermi surface

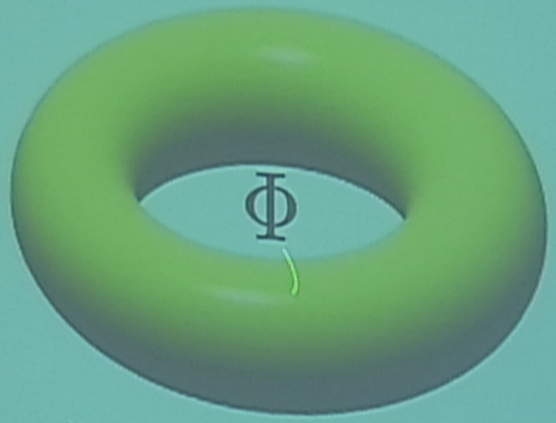

Put metal on a torus, adiabatically insert flux $\Phi = h/e$ through hole, and measure change in momentum. In a FL, we can assume the only low energy excitations are quasiparticles near the Fermi surface, and this leads to a non-perturbative proof of the Luttinger relation on the area enclosed by the Fermi surface.

M. Oshikawa, *Phys. Rev. Lett.* 84, 3370 (2000)

Quantum dimer model with bosonic and fermionic dimers

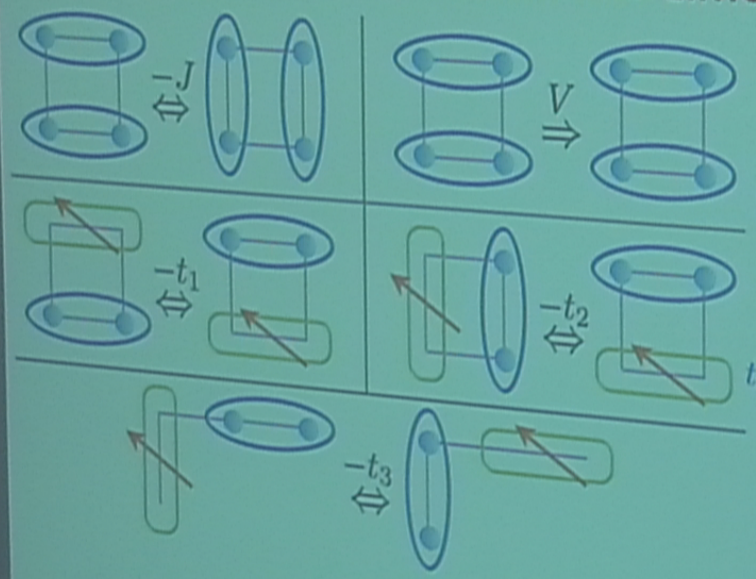

Connection to the t-t'-t''-J model:

$t_1 = -(t+t')/2$

$t_2 = (t-t')/2$

$t_3 = -(t+t'+t'')/4$

M. Punk, A. Allais, and S. Sachdev, arXiv:1501.00978

Quantum dimer model with bosonic and fermionic dimers

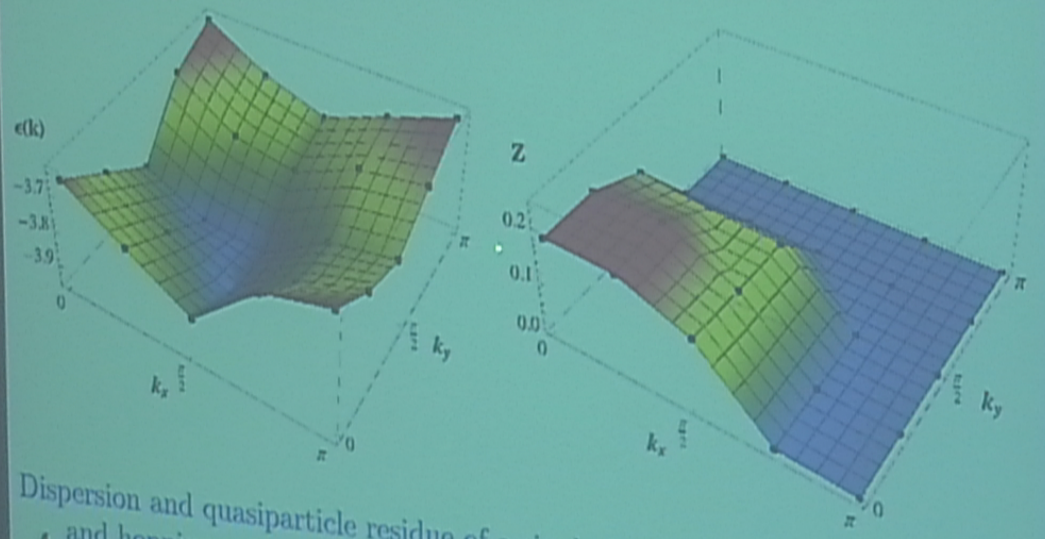

Dispersion and quasiparticle residue of a single fermionic dimer for $J = V = 1$, and hopping parameters obtained from the t-J model for the cuprates, $t_1 = -1.05$, $t_2 = 1.95$ and $t_3 = -0.6$, on a 8×8 lattice.

M. Punk, A. Allais, and S. Sachdev, arXiv:1501.00978

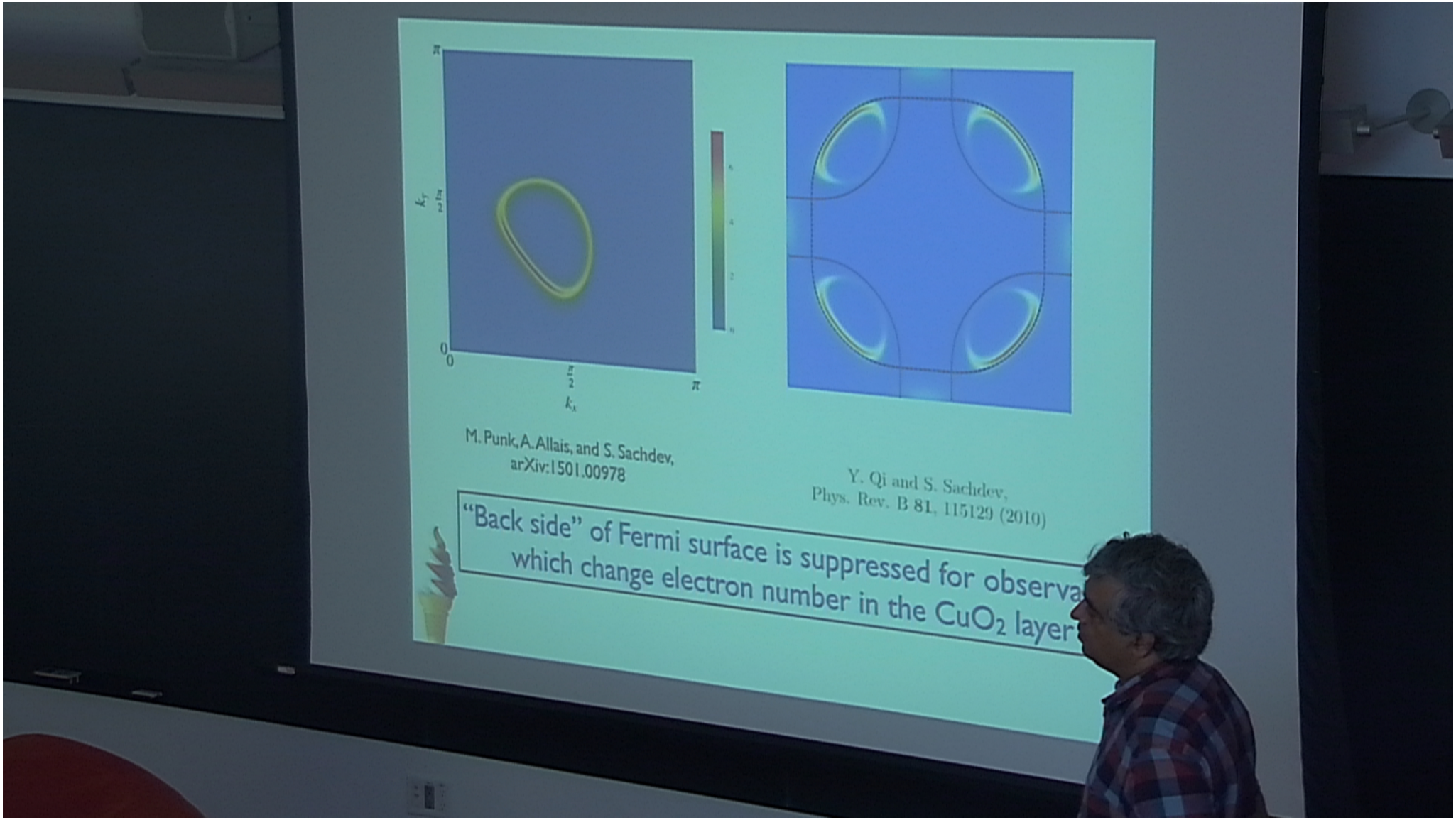
M. Punk, A. Allais, and S. Sachdev,
arXiv:1501.00978
Y. Qi and S. Sachdev,
Phys. Rev. B 81, 115129 (2010)
"Back side" of Fermi surface is suppressed for observa
which change electron number in the CuO_2 layer

Y. Qi and S. Sachdev, Phys. Rev. B **81**, 115129 (2010)
M. Punk, A. Allais, and S. Sachdev, arXiv:1501.00978

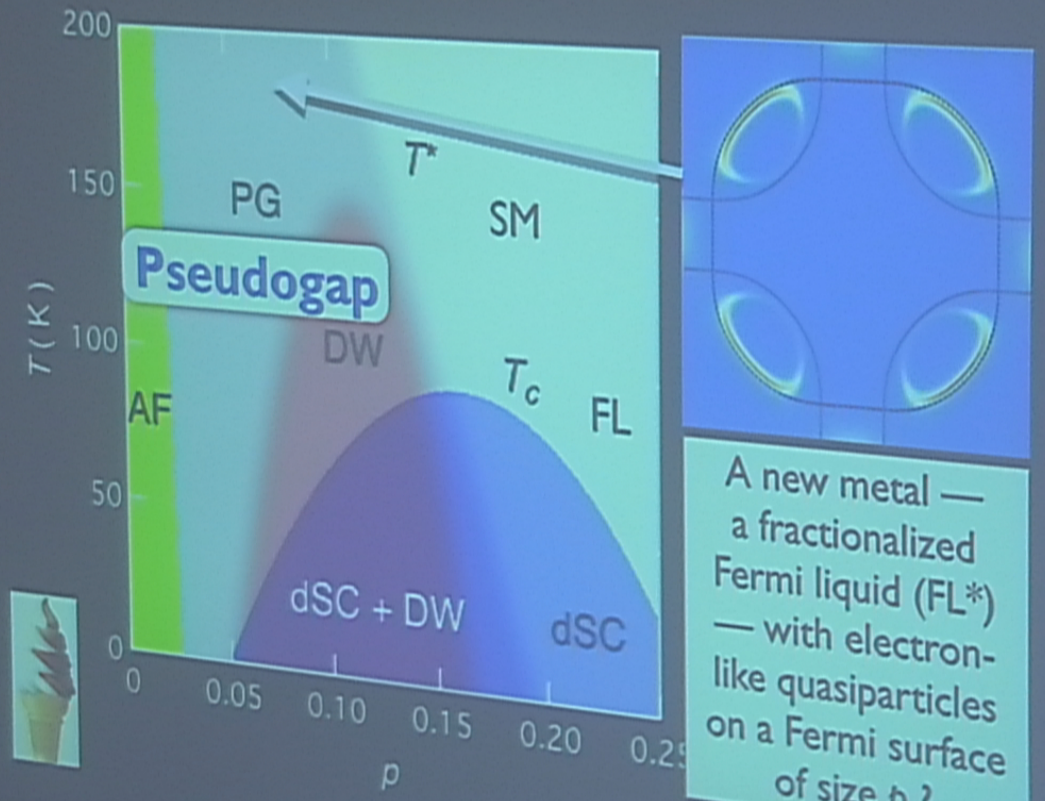

A new metal — a fractionalized Fermi liquid (FL*) — with electron-like quasiparticles on a Fermi surface of size p ?

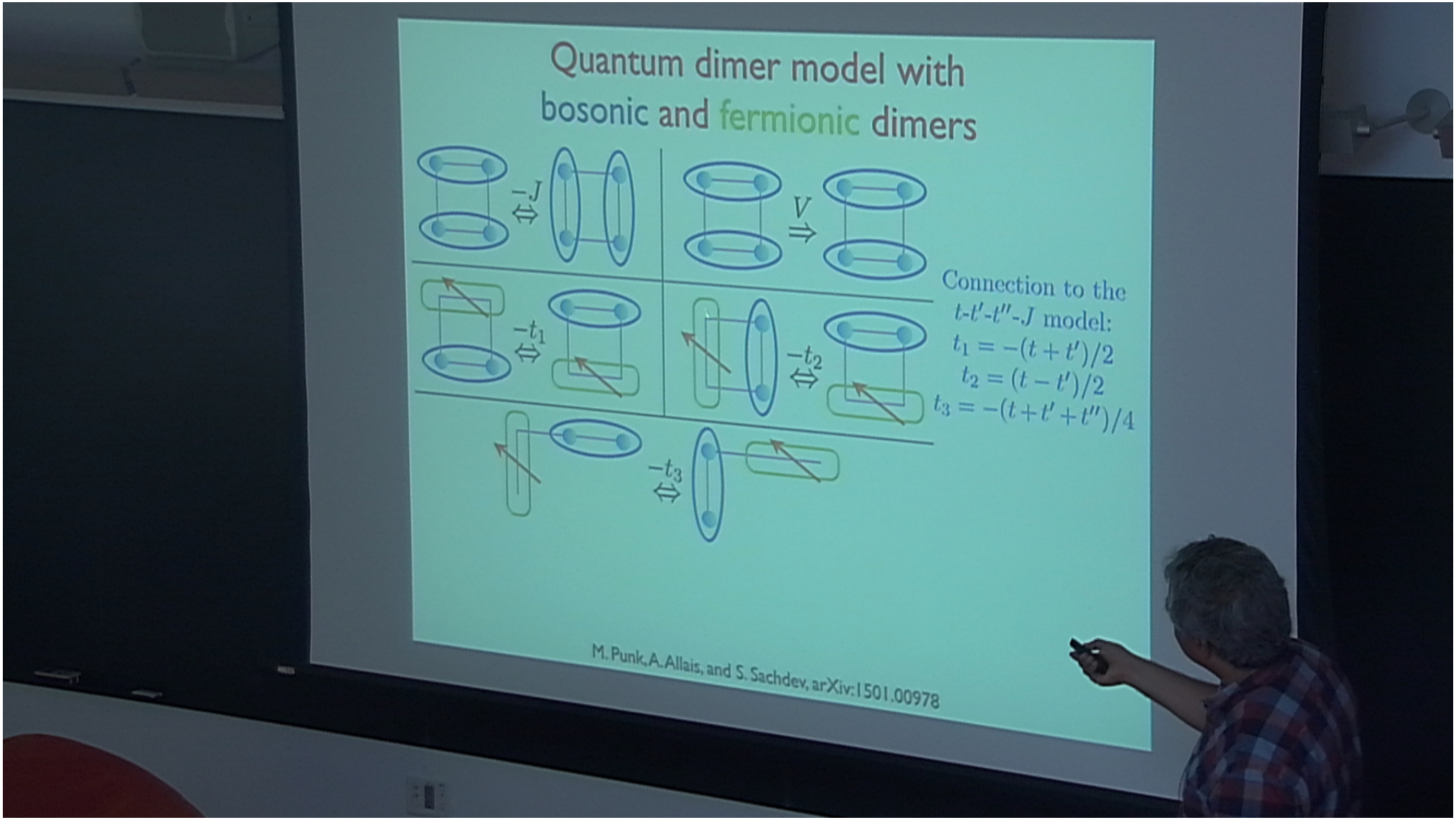
Quantum dimer model with
bosonic and fermionic dimers
$-J$
V
$-t_1$
$-t_2$
$-t_3$
Connection to the
t-t'-t''-J model:
$t_1 = -(t+t')/2$
$t_2 = (t-t')/2$
$t_3 = -(t+t'+t'')/4$
M. Punk, A. Allais, and S. Sachdev, arXiv:1501.00978

Electrical and optical evidence for Fermi surface of long-lived quasiparticles of density p

In-Plane Magnetoresistance Obeys Kohler's Rule in the Pseudogap Phase of Cuprate Superconductors

M. K. Chan,[1,*] M. J. Veit,[1] C. J. Dorow,[1,†] Y. Ge,[1] Y. Li,[1] W. Tabis,[1,2] Y. Tang,[1] X. Zhao,[1,3] N. Barišić,[1,4,5,‡] and M. Greven[1,§]

PRL 113, 177005 (2014)

We report in-plane resistivity (ρ) and transverse magnetoresistance (MR) measurements for underdoped $HgBa_2CuO_{4+\delta}$ (Hg1201). Contrary to the long-standing view that Kohler's rule is strongly violated in underdoped cuprates, we find that it is in fact satisfied in the pseudogap phase of Hg1201. The transverse MR shows a quadratic field dependence, $\delta\rho/\rho_0 = aH^2$, with $a(T) \propto T^{-4}$. In combination with the observed $\rho \propto T^2$ dependence, this is consistent with a single Fermi-liquid quasiparticle scattering rate. We show that this behavior is typically masked in cuprates with lower structural symmetry or strong disorder effects.

$$\rho_{xx} \sim \frac{1}{\tau}(1 + aH^2\tau^2 + \ldots)$$

$$\text{with } \frac{1}{\tau} \sim T^2$$

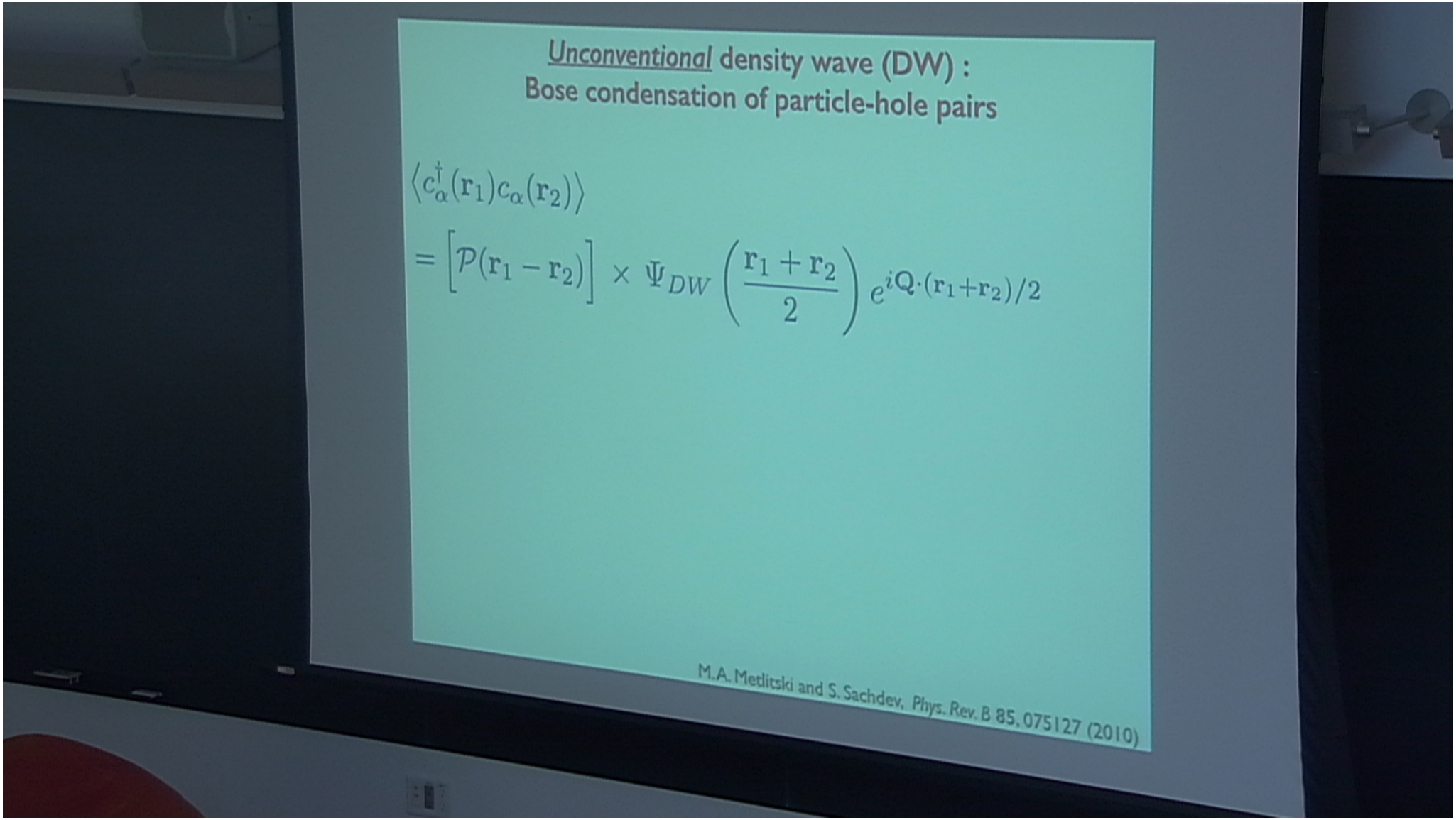
Unconventional density wave (DW) :
Bose condensation of particle-hole pairs
$\langle c^\dagger_\alpha(\mathbf{r}_1) c_\alpha(\mathbf{r}_2)\rangle$
$= \left[\mathcal{P}(\mathbf{r}_1 - \mathbf{r}_2)\right] \times \Psi_{DW}\left(\frac{\mathbf{r}_1+\mathbf{r}_2}{2}\right) e^{i\mathbf{Q}\cdot(\mathbf{r}_1+\mathbf{r}_2)/2}$
M.A. Metlitski and S. Sachdev, Phys. Rev. B 85, 075127 (2010)

See also
C. Howald, H. Eisaki, N. Kaneko, M. Greven, and A. Kapitulnik, Phys. Rev. B **67**, 014533 (2003);

M. Vershinin, S. Misra, S. Ono, Y. Abe, Yoichi Ando, and A. Yazdani, Science **303**, 1995 (2004).

W. D. Wise, M. C. Boyer, K. Chatterjee, T. Kondo, T. Takeuchi, H. Ikuta, Y. Wang, and E. W. Hudson, Nature Phys. **4**, 696 (2008).

Disordered uni-directional charge density waves ("stripes") with wavelength ≈ 4 lattice sites ?

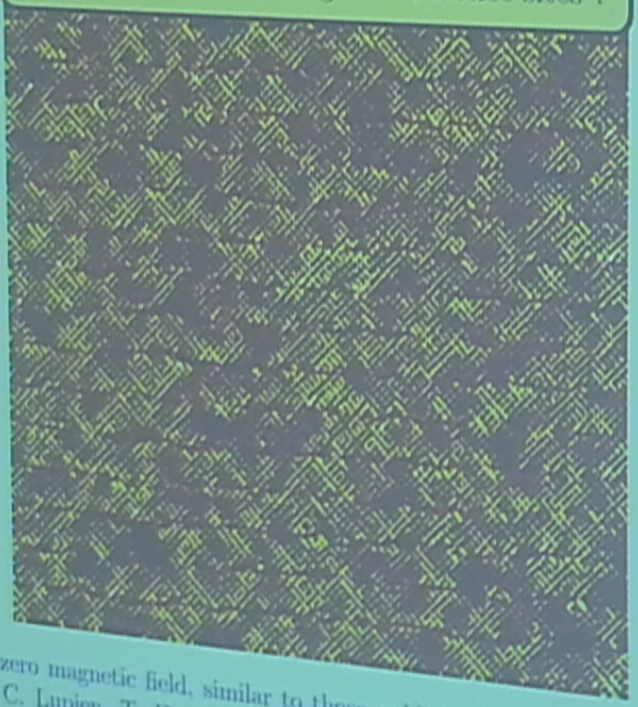

"R-map" of BSCCO in zero magnetic field, similar to those published in Y. Kohsaka, C. Taylor, K. Fujita, A. Schmidt, C. Lupien, T. Hanaguri, M. Azuma, M. Takano, H. Eisaki, H. Takagi, S. Uchida, and J. C. Davis, *Science* **315**, 1380 (2007). Davis group has sub-angstrom resolution capabilities, with lattice drift corrections, which make sublattice phase-resolved STM possible.

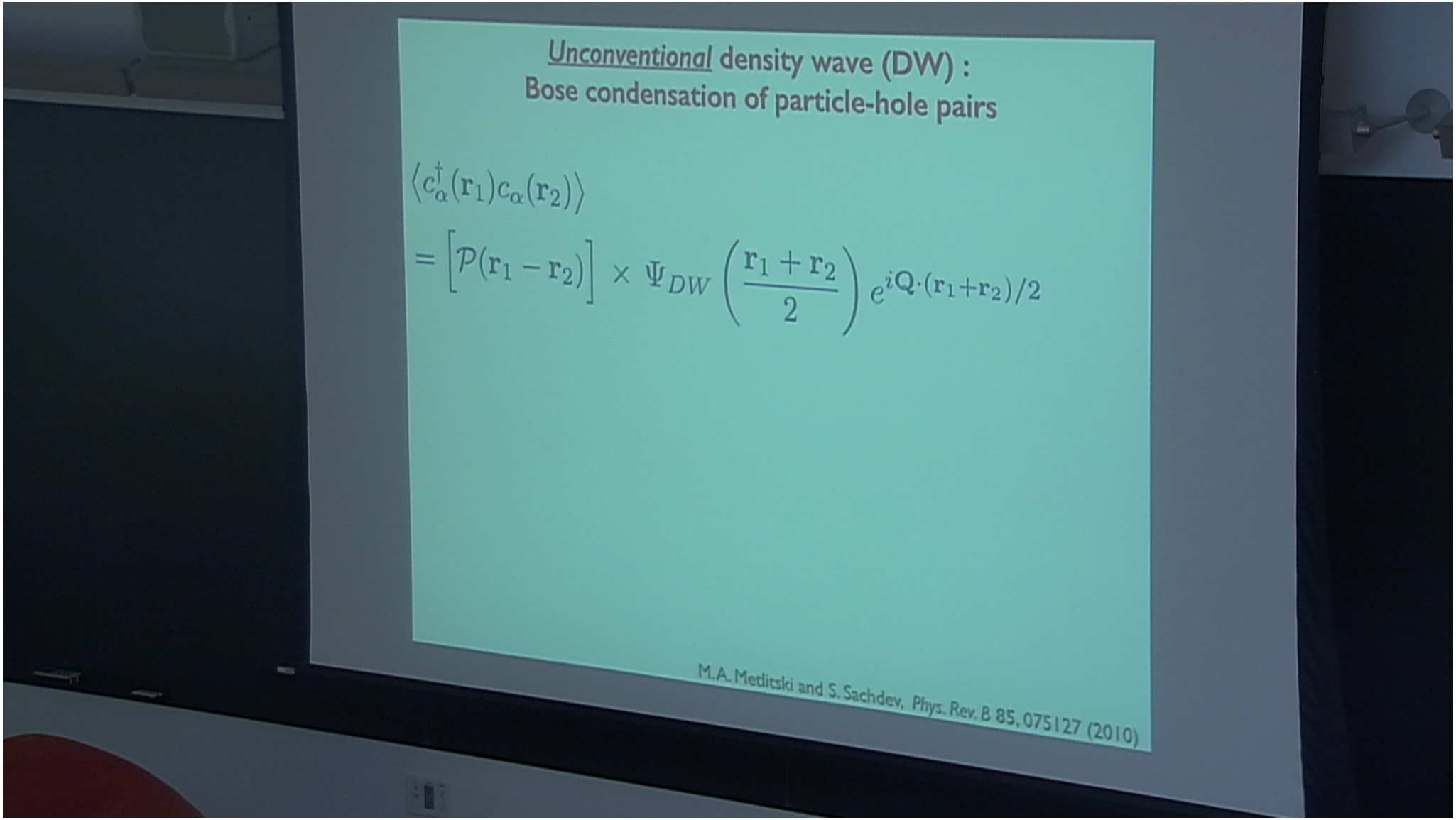
Unconventional density wave (DW) :
Bose condensation of particle-hole pairs
$\langle c^\dagger_\alpha(\mathbf{r}_1) c_\alpha(\mathbf{r}_2)\rangle$
$= \left[\mathcal{P}(\mathbf{r}_1 - \mathbf{r}_2)\right] \times \Psi_{DW}\left(\frac{\mathbf{r}_1+\mathbf{r}_2}{2}\right) e^{i\mathbf{Q}\cdot(\mathbf{r}_1+\mathbf{r}_2)/2}$
M.A. Metlitski and S. Sachdev, Phys. Rev. B 85, 075127 (2010)

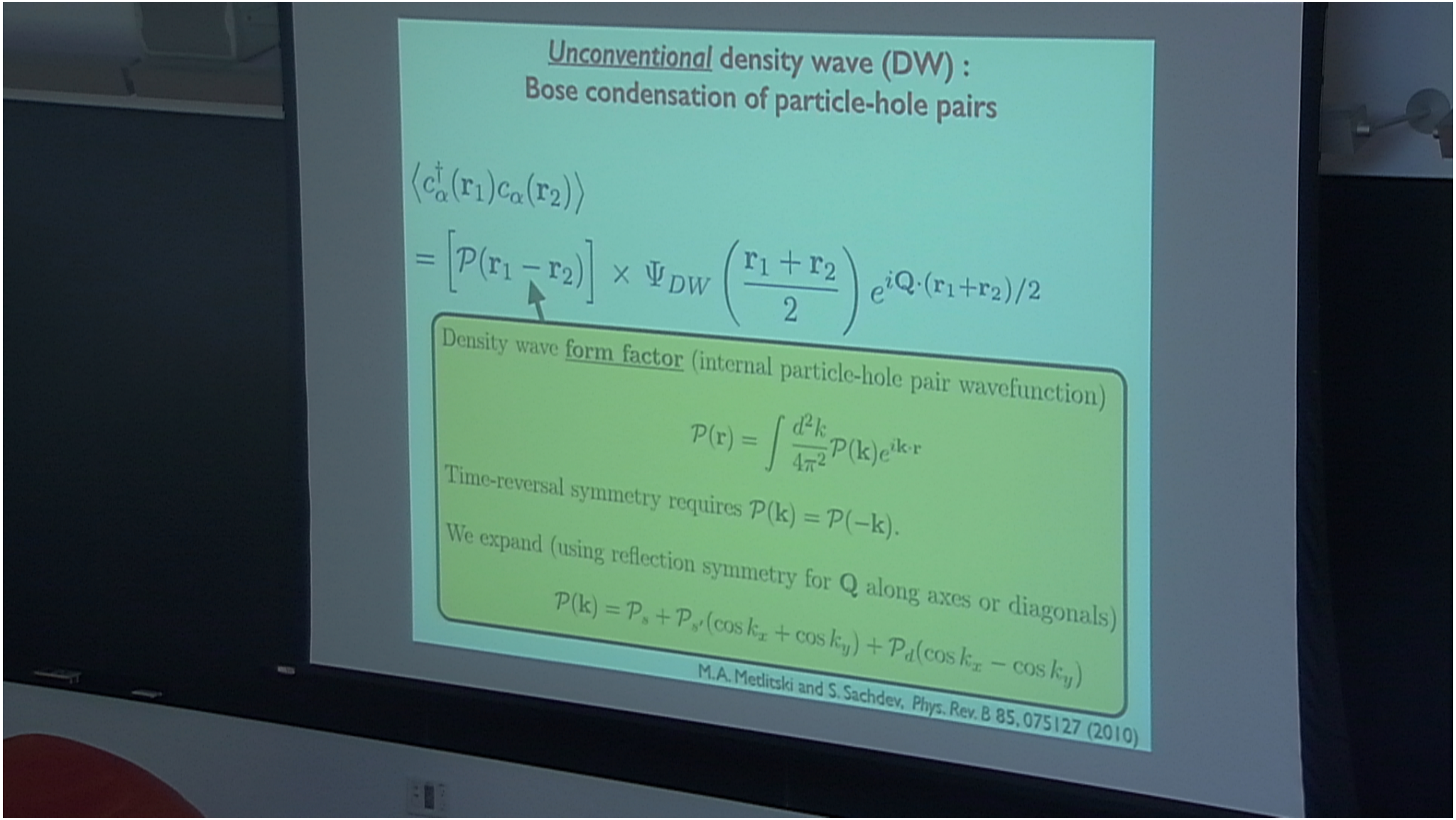
Unconventional density wave (DW) :
Bose condensation of particle-hole pairs
$\langle c^\dagger_\alpha(\mathbf{r}_1) c_\alpha(\mathbf{r}_2)\rangle$
$= \left[\mathcal{P}(\mathbf{r}_1 - \mathbf{r}_2)\right] \times \Psi_{DW}\left(\frac{\mathbf{r}_1+\mathbf{r}_2}{2}\right) e^{i\mathbf{Q}\cdot(\mathbf{r}_1+\mathbf{r}_2)/2}$
Density wave form factor (internal particle-hole pair wavefunction)
$\mathcal{P}(\mathbf{r}) = \int \frac{d^2k}{4\pi^2}\mathcal{P}(\mathbf{k})e^{i\mathbf{k}\cdot\mathbf{r}}$
Time-reversal symmetry requires $\mathcal{P}(\mathbf{k}) = \mathcal{P}(-\mathbf{k})$.
We expand (using reflection symmetry for $\mathbf{Q}$ along axes or diagonals)
$\mathcal{P}(\mathbf{k}) = \mathcal{P}_s + \mathcal{P}_{s'}(\cos k_x + \cos k_y) + \mathcal{P}_d(\cos k_x - \cos k_y)$
M.A. Metlitski and S. Sachdev, Phys. Rev. B 85, 075127 (2010)

Conventional CDW order: s-form factor

Plot of $P_{ij} = \left\langle c^{\dagger}_{i\alpha} c_{j\alpha} \right\rangle$ for $i = j$, and i, j nearest neighbors.

$$P_{ij} = \left[\int_{\mathbf{k}} \mathcal{P}(\mathbf{k}) e^{i\mathbf{k}\cdot(\mathbf{r}_i - \mathbf{r}_j)} \right] e^{i\mathbf{Q}\cdot(\mathbf{r}_i + \mathbf{r}_j)/2} + \text{c.c.}$$

$$\mathcal{P}(\mathbf{k}) = 1 \quad \text{and} \quad \mathbf{Q} = 2\pi(1/4, 0)$$

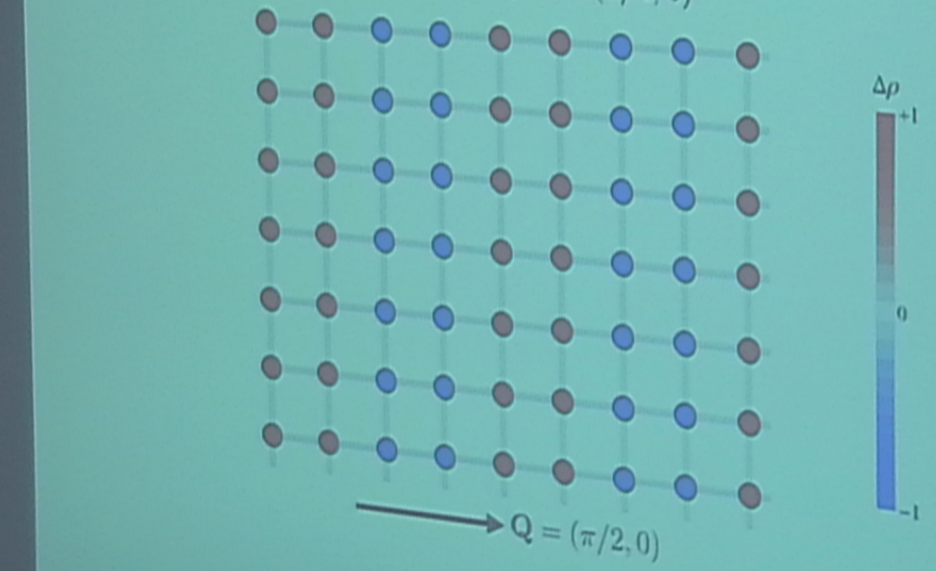

Unconventional DW order: s'-form factor

Plot of $P_{ij} = \left\langle c^\dagger_{i\alpha} c_{j\alpha} \right\rangle$ for $i = j$, and i, j nearest neighbors.

$$P_{ij} = \left[\int_{\mathbf{k}} \mathcal{P}(\mathbf{k}) e^{i\mathbf{k}\cdot(\mathbf{r}_i - \mathbf{r}_j)} \right] e^{i\mathbf{Q}\cdot(\mathbf{r}_i + \mathbf{r}_j)/2} + \text{c.c.}$$

$$\mathcal{P}(\mathbf{k}) = e^{i\phi} [\cos(k_x) + \cos(k_y)] \quad \text{and} \quad \mathbf{Q} = 2\pi(1/4, 0)$$

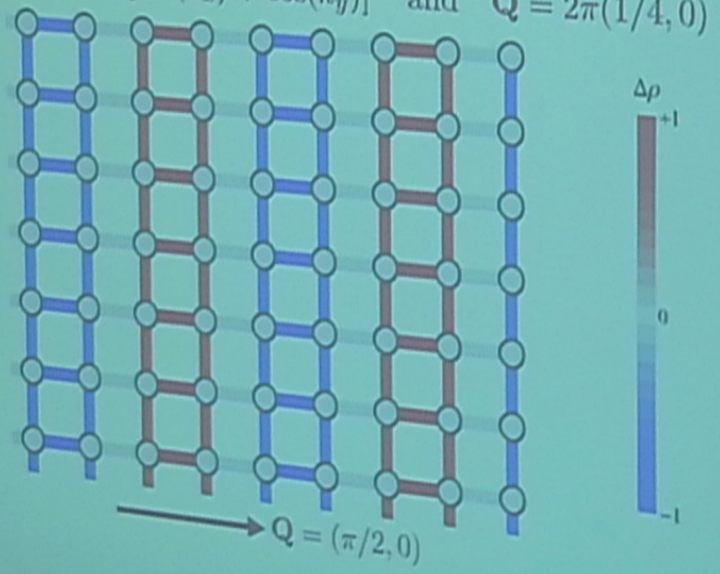

Unconventional DW order: $s + s'$-form factor

Plot of $P_{ij} = \left\langle c^{\dagger}_{i\alpha} c_{j\alpha} \right\rangle$ for $i = j$, and i, j nearest neighbors.

$$P_{ij} = \left[\int_{\mathbf{k}} \mathcal{P}(\mathbf{k}) e^{i\mathbf{k}\cdot(\mathbf{r}_i - \mathbf{r}_j)} \right] e^{i\mathbf{Q}\cdot(\mathbf{r}_i + \mathbf{r}_j)/2} + \text{c.c.}$$

$$\mathcal{P}(\mathbf{k}) = e^{i\phi}\left[1/2 + \cos(k_x) + \cos(k_y)\right] \quad \text{and} \quad \mathbf{Q} = 2\pi(1/4, 0)$$

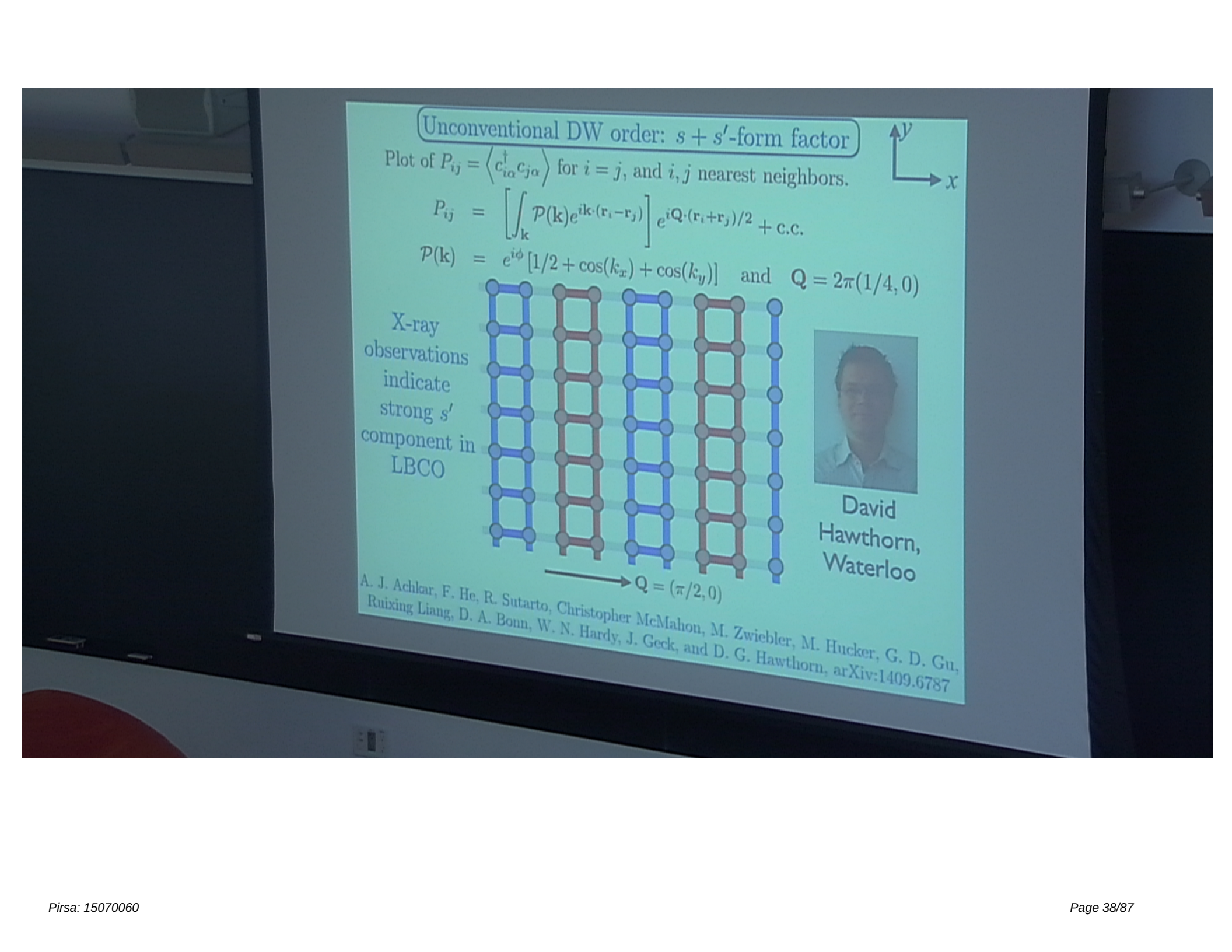

X-ray observations indicate strong s' component in LBCO

David Hawthorn, Waterloo

A. J. Achkar, F. He, R. Sutarto, Christopher McMahon, M. Zwiebler, M. Hucker, G. D. Gu, Ruixing Liang, D. A. Bonn, W. N. Hardy, J. Geck, and D. G. Hawthorn, arXiv:1409.6787

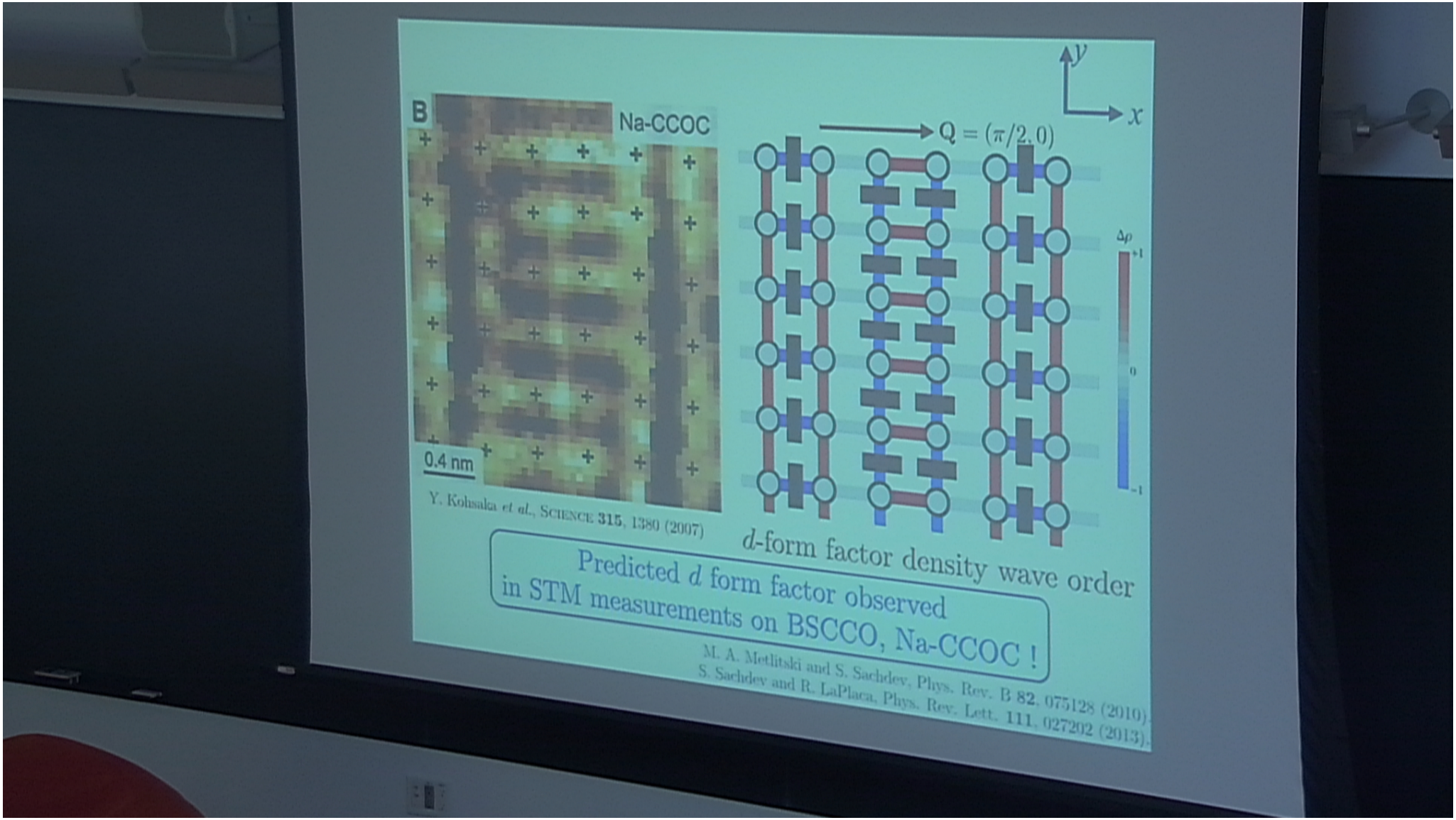
B
Na-CCOC
0.4 nm
Y. Kohsaka et al., SCIENCE 315, 1380 (2007)
y
x
Q = (π/2, 0)
Δρ
+1
0
−1
d-form factor density wave order
Predicted d form factor observed
in STM measurements on BSCCO, Na-CCOC !
M. A. Metlitski and S. Sachdev, Phys. Rev. B 82, 075128 (2010).
S. Sachdev and R. LaPlaca, Phys. Rev. Lett. 111, 027202 (2013).

d-form factor is peaked at the pseudogap energy, and does not disperse as a function of wavevector

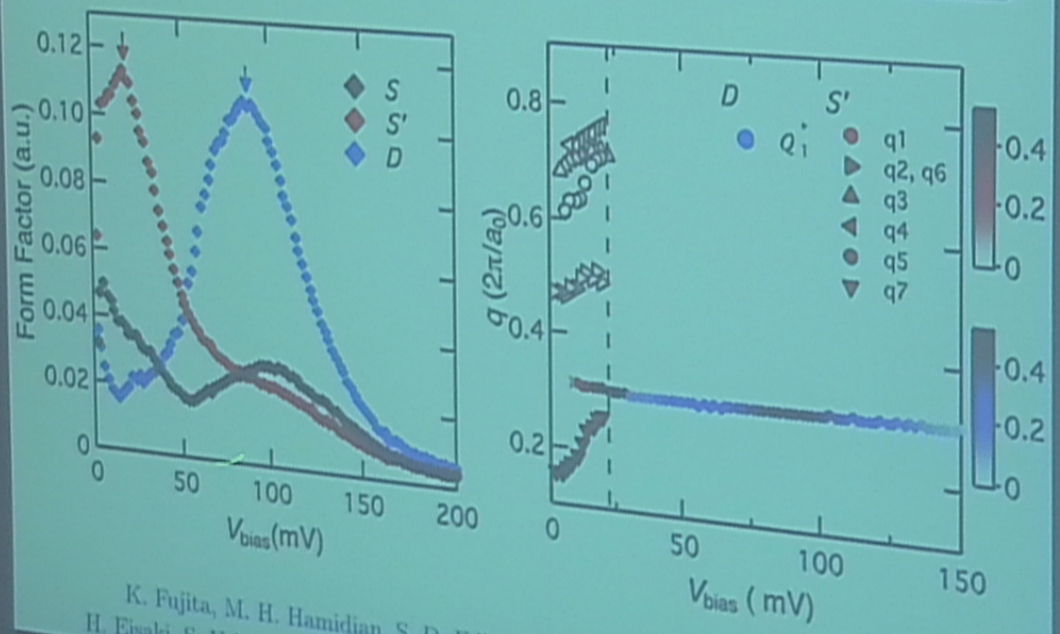

K. Fujita, M. H. Hamidian, S. D. Edkins, Chung Koo Kim, A. P. MacKenzie, H. Eisaki, S. Uchida, M. J. Lawler, E.-A. Kim, S. Sachdev, and J. C. Davis, to appear

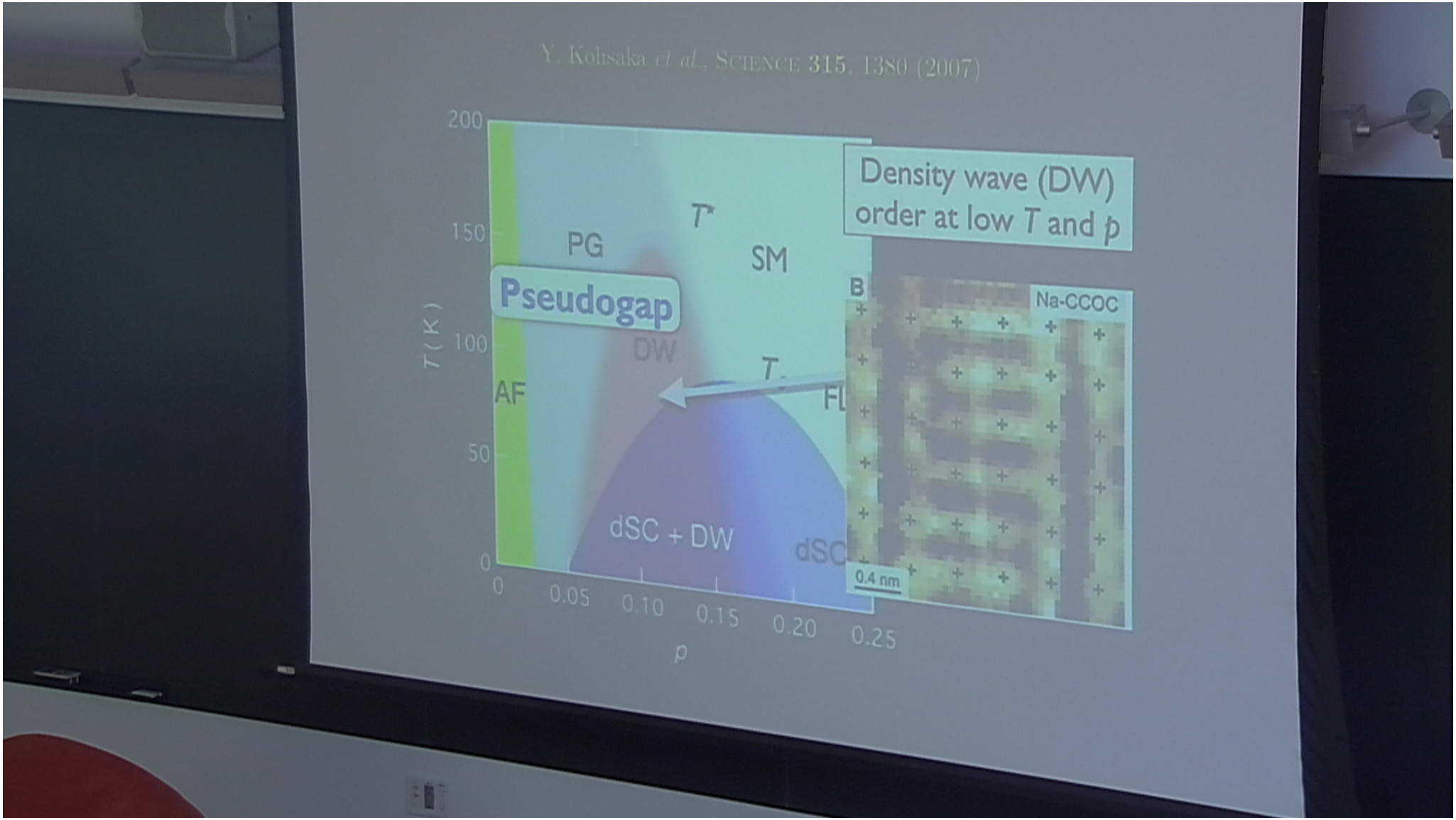
Y. Kohsaka et al., Science 315, 1380 (2007)
Density wave (DW) order at low T and p
Pseudogap
PG
SM
T*
DW
T
AF
dSC + DW
dSC
B
Na-CCOC
0.4 nm
T (K)
p
200
150
100
50
0
0
0.05
0.10
0.15
0.20
0.25

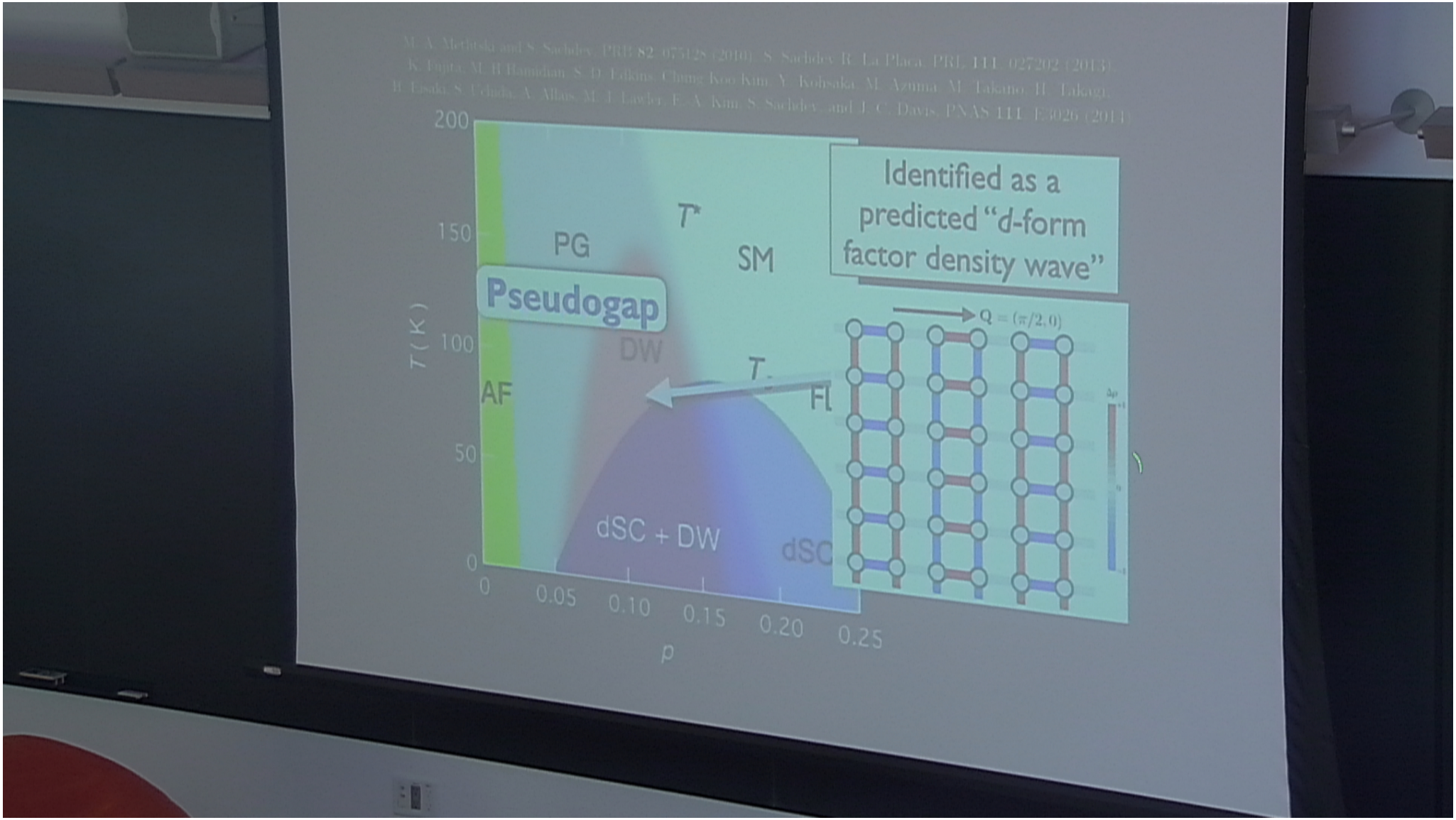
M. A. Metlitski and S. Sachdev, PRB 82, 075128 (2010). S. Sachdev, R. La Placa, PRL 111, 027202 (2013).
K. Fujita, M. H. Hamidian, S. D. Edkins, Chung Koo Kim, Y. Kohsaka, M. Azuma, M. Takano, H. Takagi,
H. Eisaki, S. Uchida, A. Allais, M. J. Lawler, E.-A. Kim, S. Sachdev, and J. C. Davis, PNAS 111, E3026 (2014)
Identified as a predicted "d-form factor density wave"
Pseudogap
PG
SM
T*
DW
T_c
AF
FL
dSC + DW
dSC
Q = (π/2, 0)
T (K)
200
150
100
50
0
0
0.05
0.10
0.15
0.20
0.25
p

Pairing "glue" for d-wave superconductivity from antiferromagnetic fluctuations

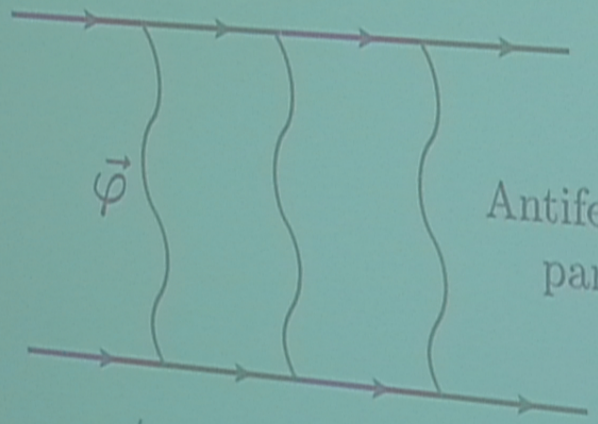

Antiferromagnetic paramagnon

Leads to $\left\langle c^{\dagger}_{\mathbf{k}\alpha} c^{\dagger}_{-\mathbf{k}\beta} \right\rangle = \varepsilon_{\alpha\beta}\Delta(\cos k_x - \cos k_y)$

V.J. Emery, J. Phys. (Paris) Colloq. 44, C3-977 (1983)
D.J. Scalapino, E. Loh, and J.E. Hirsch, Phys. Rev. B 34, 8190 (1986)
K. Miyake, S. Schmitt-Rink, and C. M. Varma, Phys. Rev. B 34, 6554 (1986)
P. Monthoux, A.V. Balatsky, and D. Pines, Phys. Rev. Lett. 67, 3448 (1991)

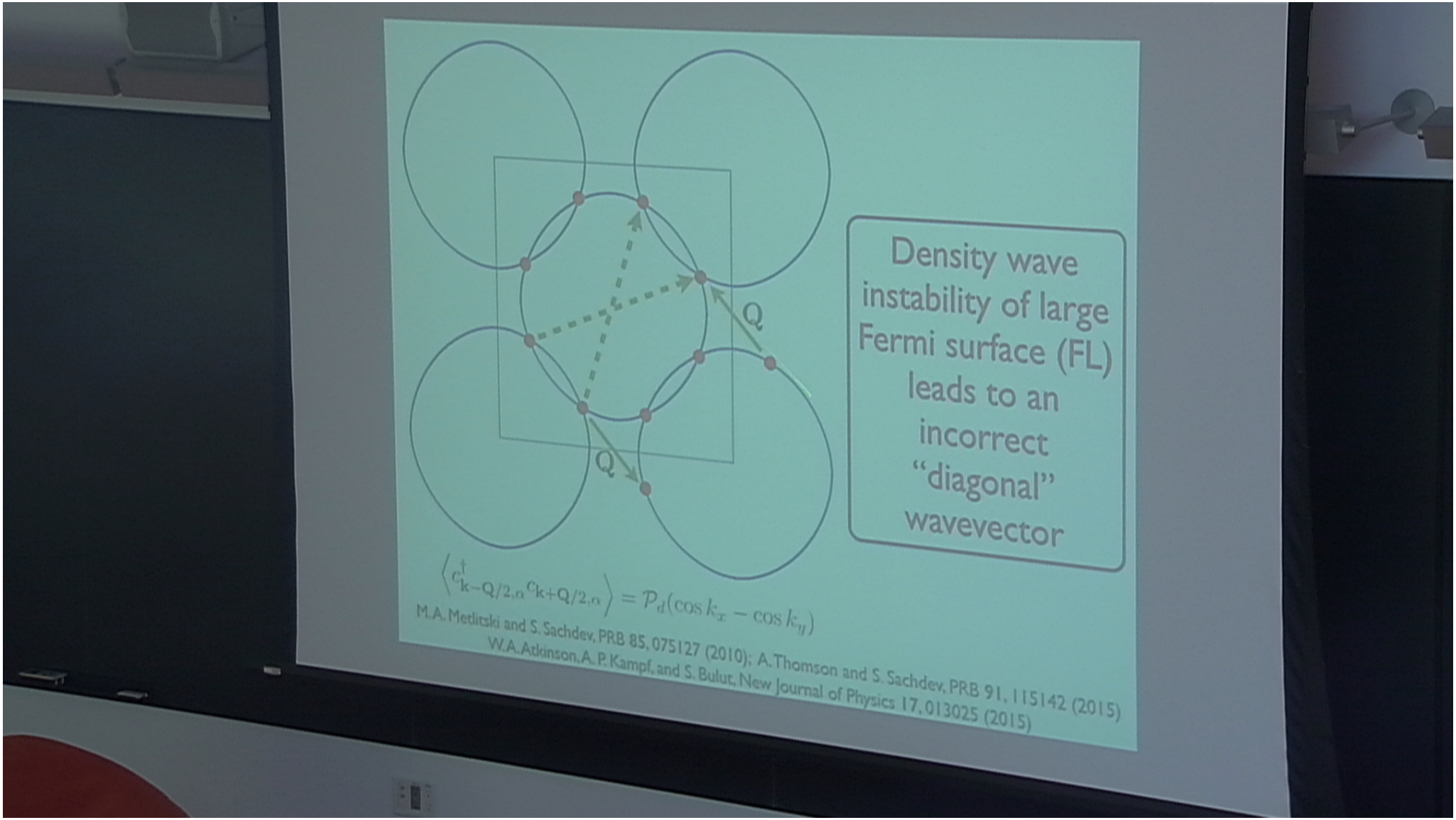
Q
Q
Density wave instability of large Fermi surface (FL) leads to an incorrect "diagonal" wavevector
$\left\langle c^{\dagger}_{\mathbf{k}-\mathbf{Q}/2,\alpha} c_{\mathbf{k}+\mathbf{Q}/2,\alpha} \right\rangle = \mathcal{P}_d(\cos k_x - \cos k_y)$
M.A. Metlitski and S. Sachdev, PRB 85, 075127 (2010); A. Thomson and S. Sachdev, PRB 91, 115142 (2015)
W.A. Atkinson, A. P. Kampf, and S. Bulut, New Journal of Physics 17, 013025 (2015)

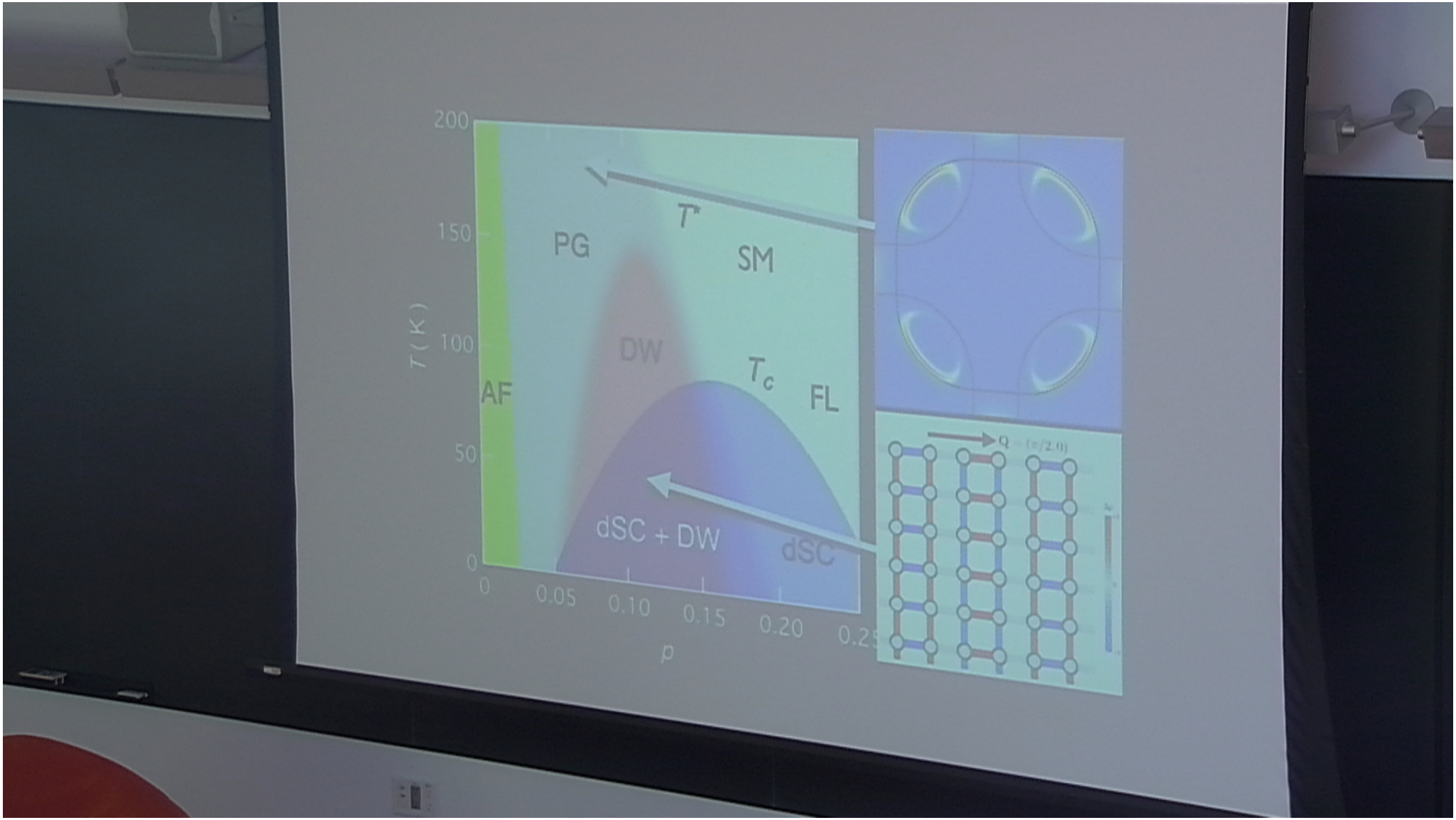
200
150
100
50
0
T (K)
PG
T*
SM
DW
Tc
AF
FL
dSC + DW
dSC
0
0.05
0.10
0.15
0.20
p

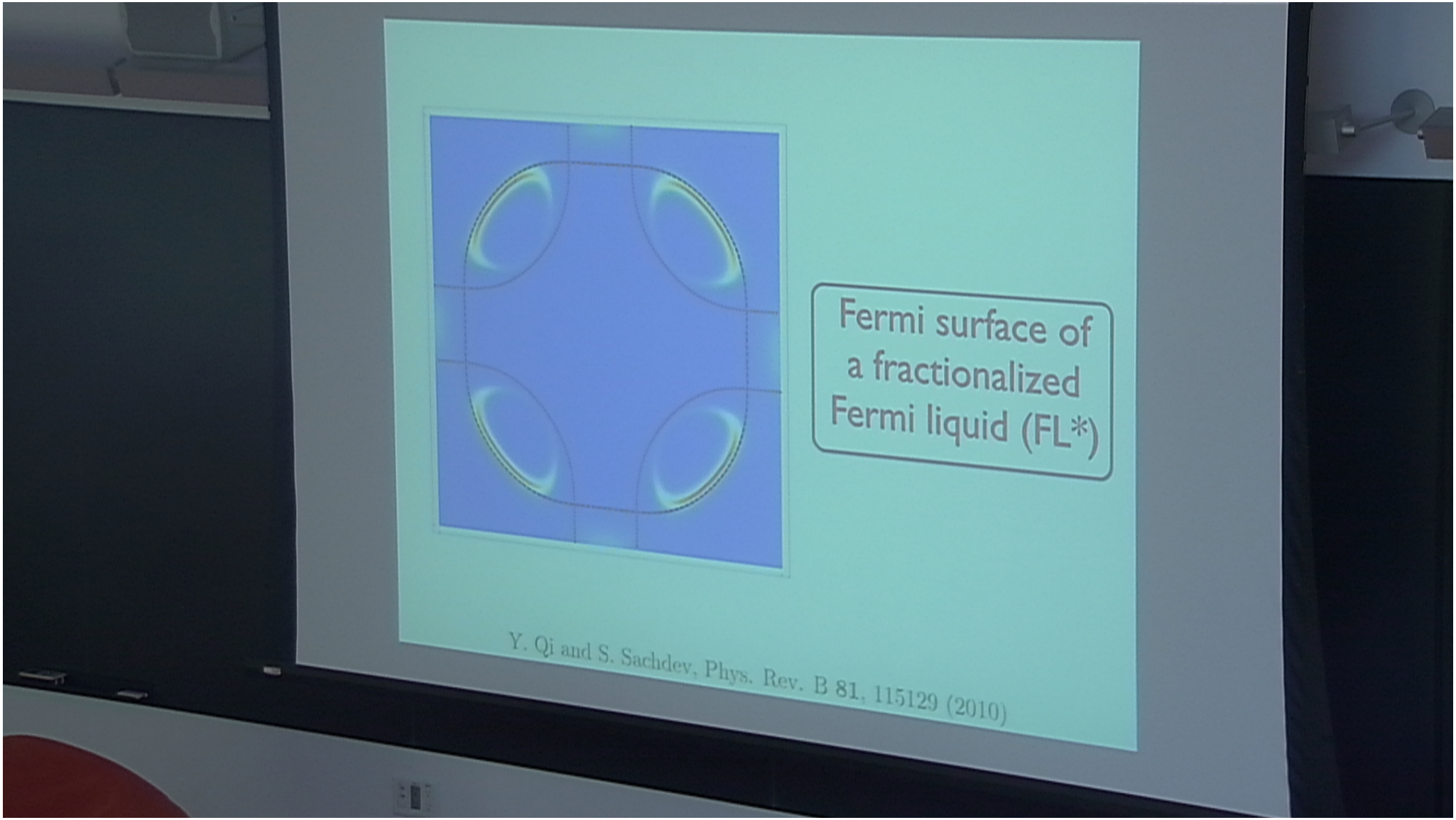
Fermi surface of
a fractionalized
Fermi liquid (FL*)
Y. Qi and S. Sachdev, Phys. Rev. B 81, 115129 (2010)

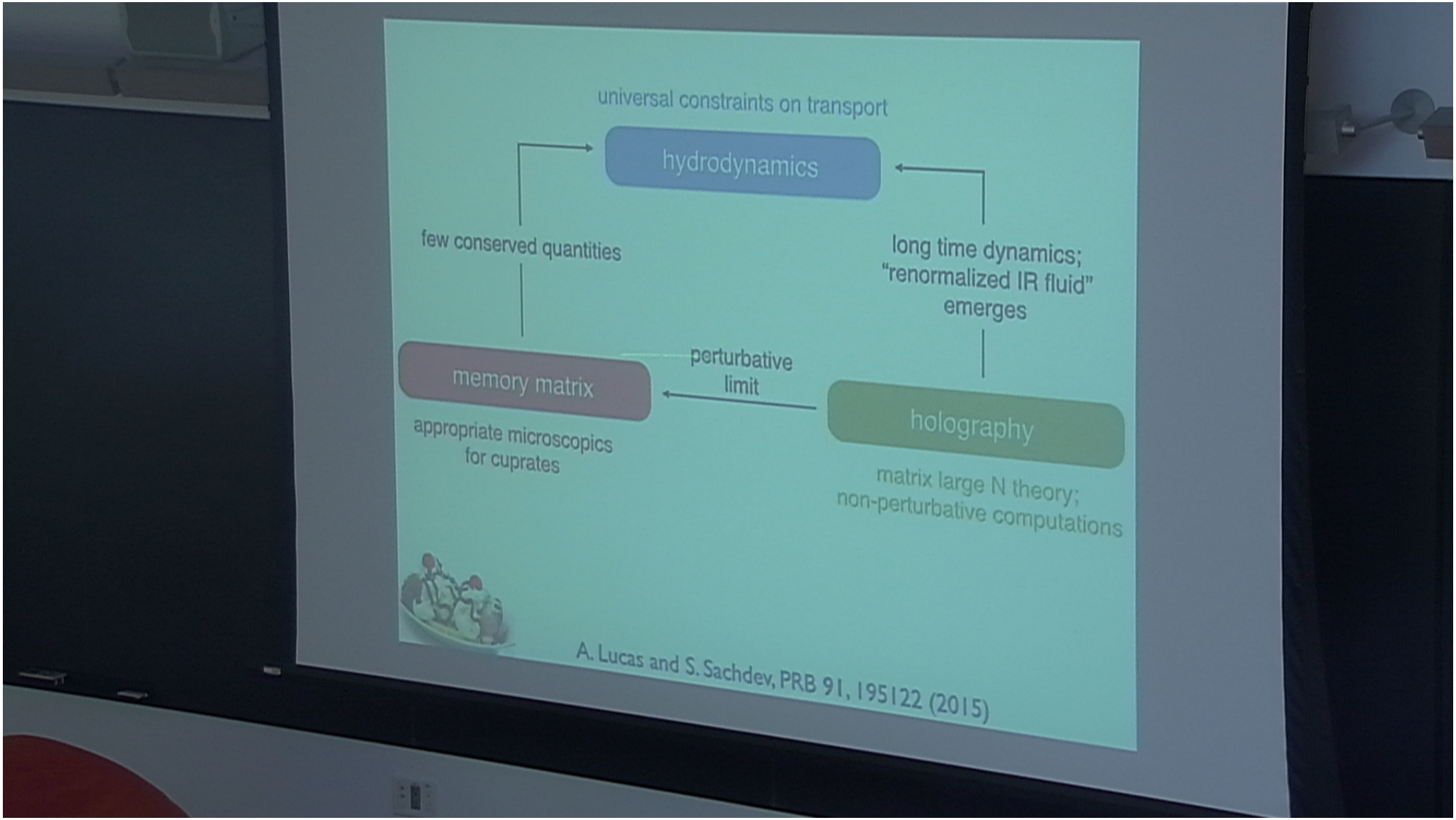
universal constraints on transport
hydrodynamics
few conserved quantities
long time dynamics;
"renormalized IR fluid"
emerges
perturbative
limit
memory matrix
holography
appropriate microscopics
for cuprates
matrix large N theory;
non-perturbative computations
A. Lucas and S. Sachdev, PRB 91, 195122 (2015)

Electrical transport at a strongly-coupled critical theory
without particle-hole symmetry,
with a conserved momentum P

$$\sigma = \sigma_Q + \frac{\mathcal{Q}^2}{\mathcal{M}} \pi \delta(\omega)$$

with $\mathcal{Q} \equiv \chi_{J_x,P_x}$ and $\mathcal{M} \equiv \chi_{P_x,P_x}$ thermodynamic response functions

Obtained in hydrodynamics, holography, and
by memory functions

S.A. Hartnoll, P.K. Kovtun, M. Müller, and S. Sachdev, PRB 76, 144502 (2007)
A. Lucas and S. Sachdev, PRB 91, 195122 (2015)

Electrical transport at a strongly-coupled critical theory *without* particle-hole symmetry, with an *almost* conserved momentum P, and an applied magnetic field B

$$\sigma_{xx} = \frac{(\tau_L^{-1} - i\omega)\mathcal{M}\sigma_Q + \mathcal{Q}^2 + B^2\sigma_Q^2}{\mathcal{Q}^2 B^2 + ((\tau_L^{-1} - i\omega)\mathcal{M} + B^2\sigma_Q)^2}\mathcal{M}\left(\frac{1}{\tau_L} - i\omega\right);$$

$$\sigma_{xy} = \frac{2(\tau_L^{-1} - i\omega)\mathcal{M}\sigma_Q + \mathcal{Q}^2 + B^2\sigma_Q^2}{\mathcal{Q}^2 B^2 + ((\tau_L^{-1} - i\omega)\mathcal{M} + B^2\sigma_Q)^2}B\mathcal{Q}.$$

Obtained in hydrodynamics, holography, and by memory functions

A. Hartnoll, P. K. Kovtun, M. Müller, and S. Sachdev, PRB 76, 144502 (2007)
M. Blake and A. Donos, PRL 114, 021601 (2015)
A. Lucas and S. Sachdev, arXiv:1502.04704

Electrical transport at a strongly-coupled critical theory *without* particle-hole symmetry, with an *almost* conserved momentum P, and an applied magnetic field B

$$\sigma_{xx} = \frac{(\tau_L^{-1} - i\omega)\mathcal{M}\sigma_Q + \mathcal{Q}^2 + B^2\sigma_Q^2}{\mathcal{Q}^2 B^2 + ((\tau_L^{-1} - i\omega)\mathcal{M} + B^2\sigma_Q)^2}\mathcal{M}\left(\frac{1}{\tau_L} - i\omega\right),$$

$$\sigma_{xy} = \frac{2(\tau_L^{-1} - i\omega)\mathcal{M}\sigma_Q + \mathcal{Q}^2 + B^2\sigma_Q^2}{\mathcal{Q}^2 B^2 + ((\tau_L^{-1} - i\omega)\mathcal{M} + B^2\sigma_Q)^2}B\mathcal{Q}.$$

Obtained in hydrodynamics, holography, and by memory functions

A. Hartnoll, P. K. Kovtun, M. Müller, and S. Sachdev, PRB 76, 144502 (2007)
M. Blake and A. Donos, PRL 114, 021601 (2015)
A. Lucas and S. Sachdev, arXiv:1502.04704

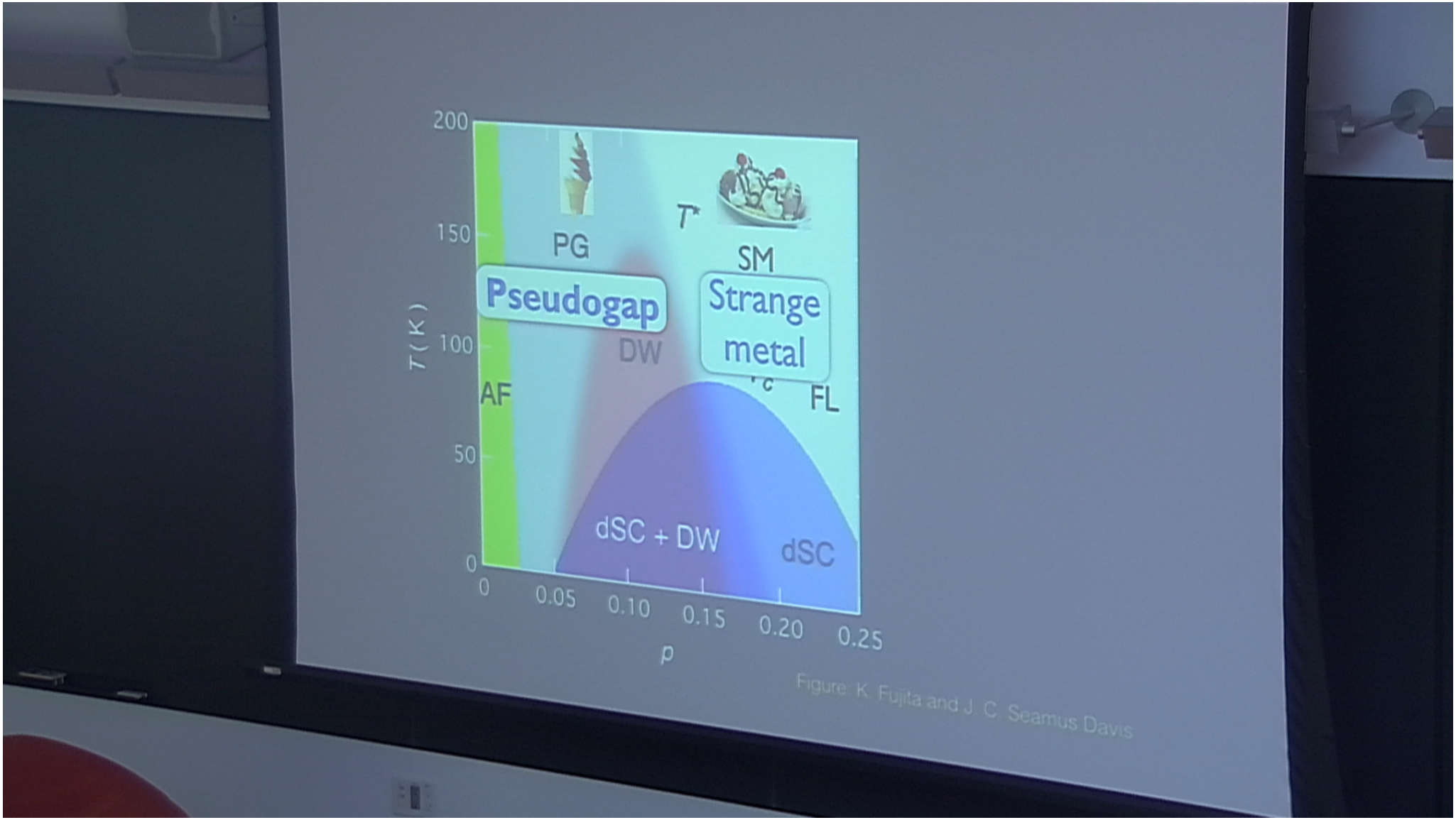
200
150
100
50
0
T (K)
PG
T*
SM
Pseudogap
Strange
metal
DW
AF
FL
dSC + DW
dSC
0
0.05
0.10
0.15
0.20
0.25
p
Figure: K. Fujita and J. C. Seamus Davis


Conclusions
1. Predicted d-form factor density wave order observed in the non-La hole-doped cuprate superconductors.
2. Proposed the pseudogap metal is a fractionalized Fermi liquid (FL*): a Fermi liquid co-existing with topological order
3. Can we experimentally detect possible "topological order" in the pseudogap metal ? (topological order is directly linked to Fermi surface size)
4. Hydrodynamic, memory-function, holographic, and field-theoretic approaches to transport without quasiparticles

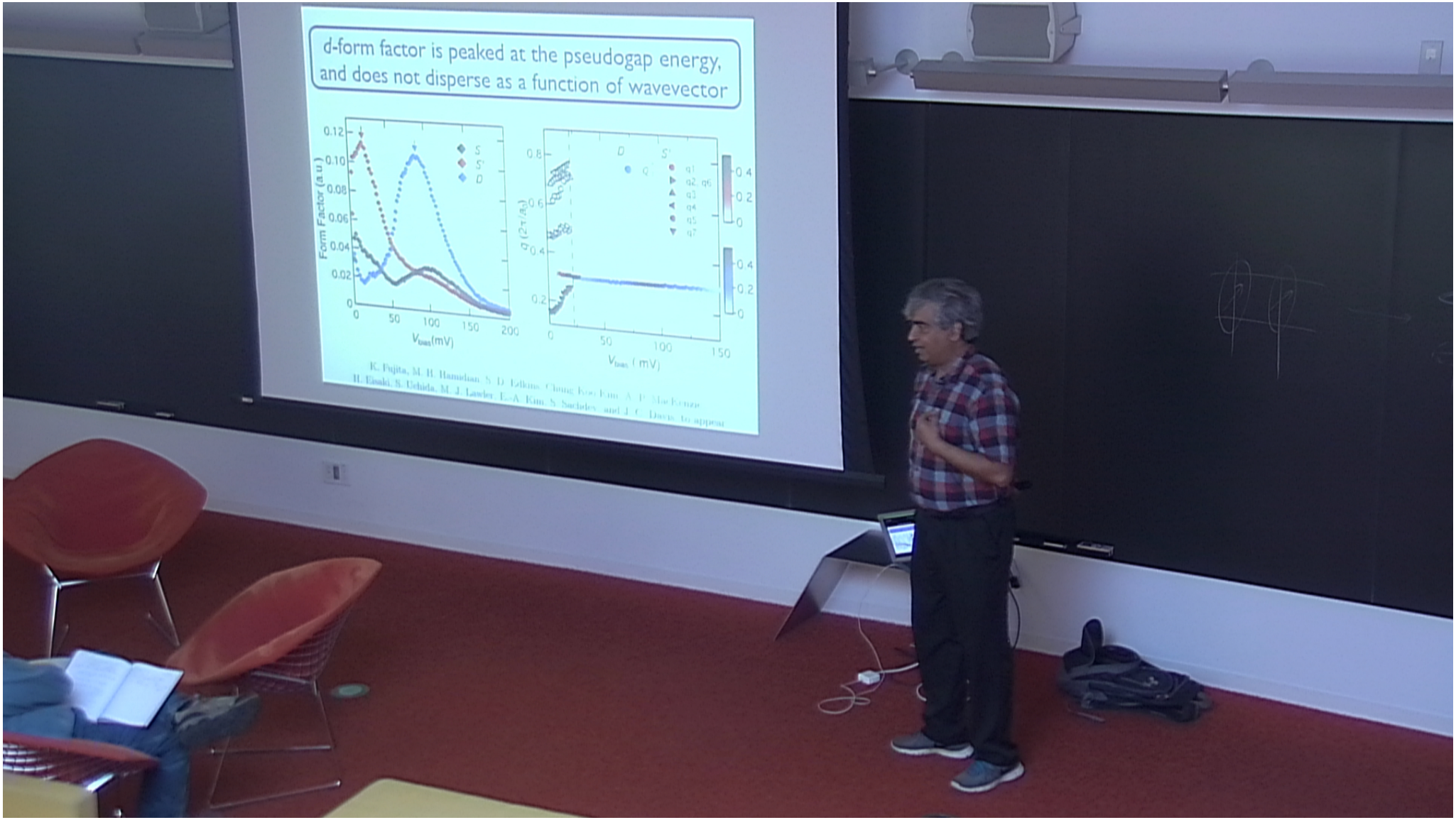
d-form factor is peaked at the pseudogap energy, and does not disperse as a function of wavevector
Form Factor (a.u.)
0.12
0.10
0.08
0.06
0.04
0.02
0
0
50
100
150
200
V_{bias}(mV)
S
S'
D
0.8
0.6
0.4
0.2
0
q ($2\pi/a_0$)
D
S'
q1
q2, q6
q3
q4
q5
q7
0.4
0.2
0
0.4
0.2
0
0
50
100
150
V_{bias} (mV)
K. Fujita, M. H. Hamidian, S. D. Edkins, Chung Koo Kim, A. P. MacKenzie
H. Eisaki, S. Uchida, M. J. Lawler, E.-A. Kim, S. Sachdev, and J. C. Davis, to appear

A tensor product state approach to spin-1/2 square J1-J2 Heisenberg model:

evidence for deconfined quantum criticality

Zheng-Cheng Gu

Perimeter Institute

Collaborator:

Dr. Ling Wang (Caltech)
Prof. Xiao-Gang Wen (MIT)
Prof. F. Verstraete (U. of Vienna)

Deconfined Quantum critical point (QCP) in cuprates?

Subir Sachdev, Science 288, 475, (2000)

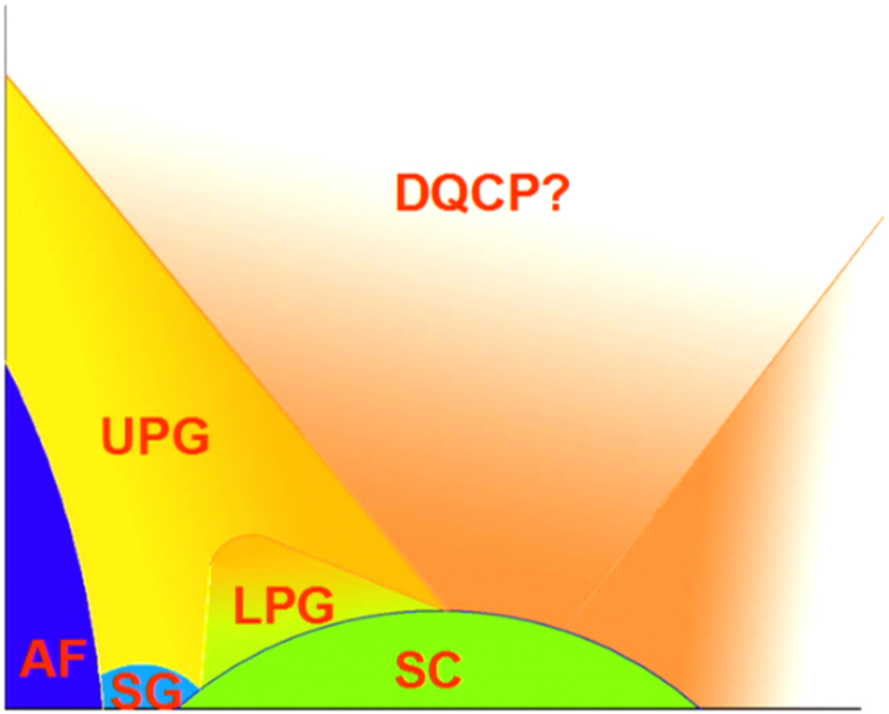

DQCP in spin models

Theory: beyond Landau's paradim

$$\mathcal{L}_z = \sum_{a=1}^{N} |\left(\partial_\mu - i a_\mu\right) z_a|^2 + s|z|^2 + u\left(|z|^2\right)^2 + \kappa\left(\epsilon_{\mu\nu\kappa}\partial_\nu a_\kappa\right)^2$$

$$Q = \frac{1}{4\pi}\int d^2 r\, \hat{n}\cdot\partial_x\hat{n}\times\partial_y\hat{n},$$

On square lattice, Q always changes by four, thus the instanton effect becomes dangerous irrelevant!

T. Senthil, Ashvin Vishwanath, Leon Balents, Subir Sachdev, M. P. A. Fisher, Science 303, 1490 (2004).

Numerical: J-Q model(simulated by using QMC)

$$H = J\sum_{\langle ij\rangle}\mathbf{S}_i\cdot\mathbf{S}_j - Q\sum_{\langle ijkl\rangle}(\mathbf{S}_i\cdot\mathbf{S}_j - \tfrac{1}{4})(\mathbf{S}_k\cdot\mathbf{S}_l - \tfrac{1}{4})$$

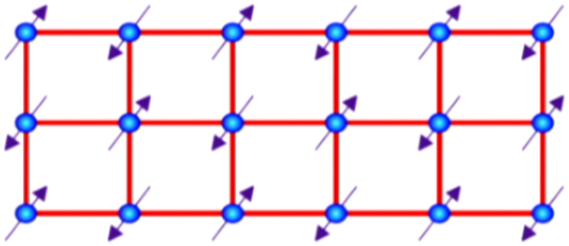

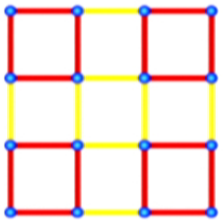

Anders W. Sandvik, Phys. Rev. Lett. 98, 227202 (2007)

DQCP in spin models

Theory: beyond Landau's paradim

$$\mathcal{L}_z = \sum_{a=1}^{N} |\left(\partial_\mu - i a_\mu\right) z_a|^2 + s|z|^2 + u\left(|z|^2\right)^2 + \kappa\left(\epsilon_{\mu\nu\kappa}\partial_\nu a_\kappa\right)^2$$

$$Q = \frac{1}{4\pi}\int d^2 r\, \hat{n}\cdot\partial_x\hat{n}\times\partial_y\hat{n},$$

On square lattice, Q always changes by four, thus the instanton effect becomes dangerous irrelevant!

T. Senthil, Ashvin Vishwanath, Leon Balents, Subir Sachdev, M. P. A. Fisher, Science 303, 1490 (2004).

Numerical: J-Q model(simulated by using QMC)

$$H = J\sum_{\langle ij\rangle}\mathbf{S}_i\cdot\mathbf{S}_j - Q\sum_{\langle ijkl\rangle}(\mathbf{S}_i\cdot\mathbf{S}_j - \tfrac{1}{4})(\mathbf{S}_k\cdot\mathbf{S}_l - \tfrac{1}{4})$$

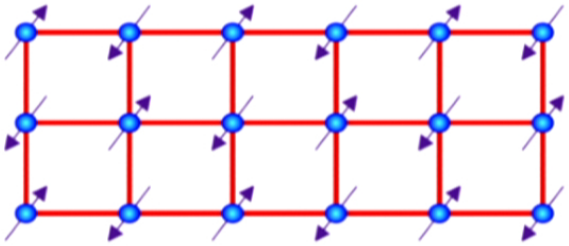

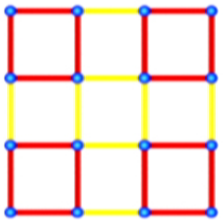

Anders W. Sandvik, Phys. Rev. Lett. 98, 227202 (2007)

Relevant spin model for cuprates

J1-J2 model: $$H = J_1 \sum_{\langle ij \rangle} \mathbf{S}_i \cdot \mathbf{S}_j + J_2 \sum_{\langle\langle ij \rangle\rangle} \mathbf{S}_i \cdot \mathbf{S}_j$$

Landau Paradigm: a meanfield phase diagram

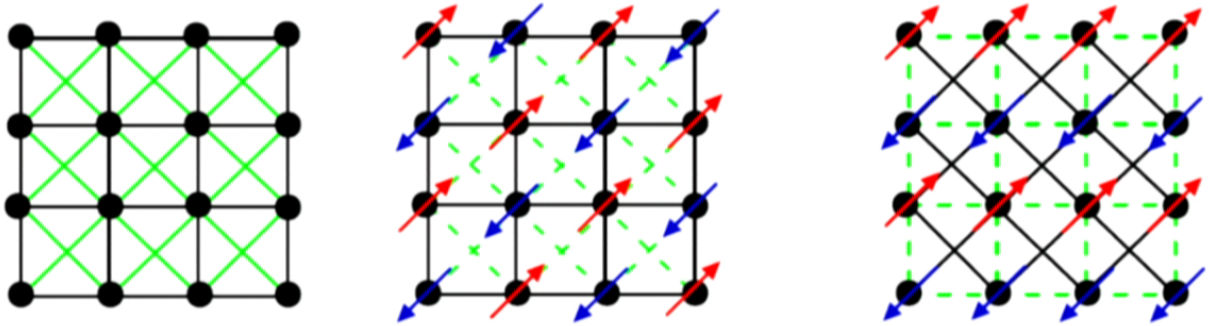

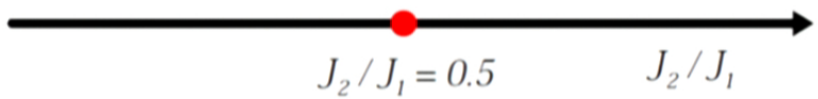

Recent progress

A recent work by using density matrix renormalization group(DMRG) algorithm claims a Z2 spin liquid

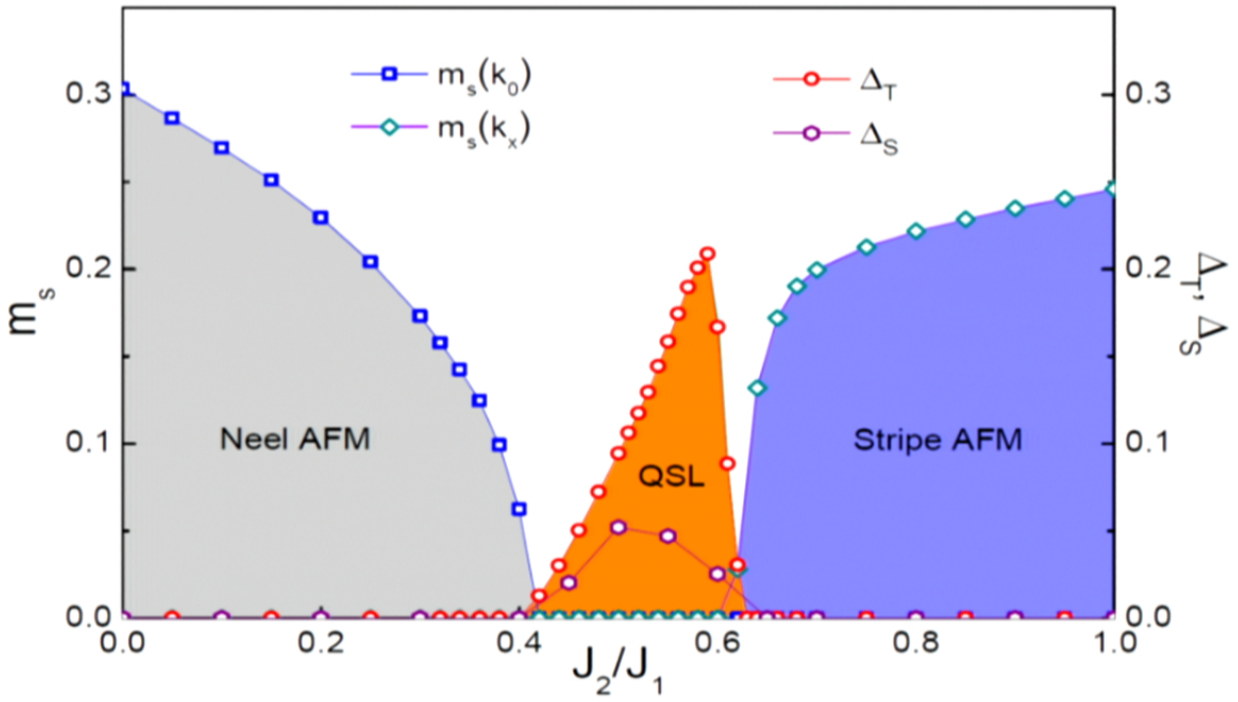

Hong-Chen Jiang, Hong Yao, Leon Balents, Phys. Rev. B 86, 024424 (2012)

Another work by using SU(2) symmetry DMRG algorithm suggests a different result

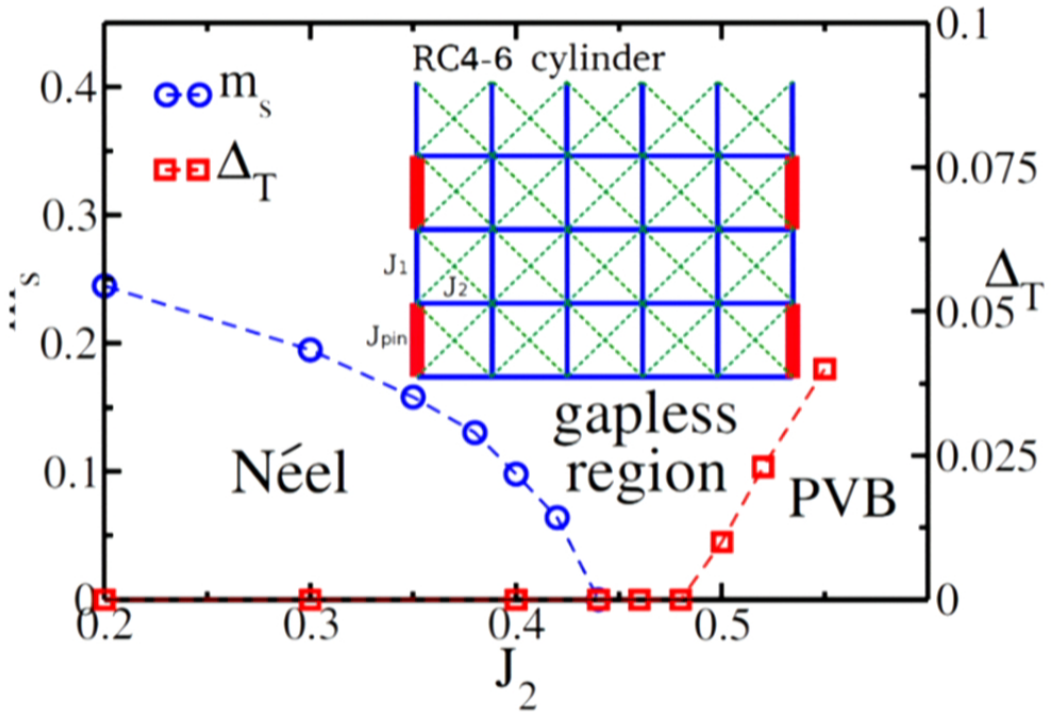

Shou-Shu Gong, Wei Zhu, D. N. Sheng, Olexei I. Motrunich, Matthew P. A. Fisher
Phys. Rev. Lett. 113. 027201 (2014)

Landau paradigm: meanfield approach

- The key concept is to find an ideal trial wave function, e.g., for a spin ½ system:

$$|\Psi_{trial}\rangle = \otimes \left(u^{\uparrow}|\uparrow\rangle_i + u^{\downarrow}|\downarrow\rangle_i\right)$$

- After minimizing the energy, we can find various symmetry ordered phases.

$$H = -\sum_{\langle ij\rangle} \sigma_i^z \sigma_j^z - h \sum_i \sigma_i^x$$

$$\begin{aligned} h_{MF}^c &= 4 \\ \beta_{MF}^c &= 0.5 \\ \langle \sigma_z \rangle &\propto |h - h_c|^{\beta} \end{aligned}$$

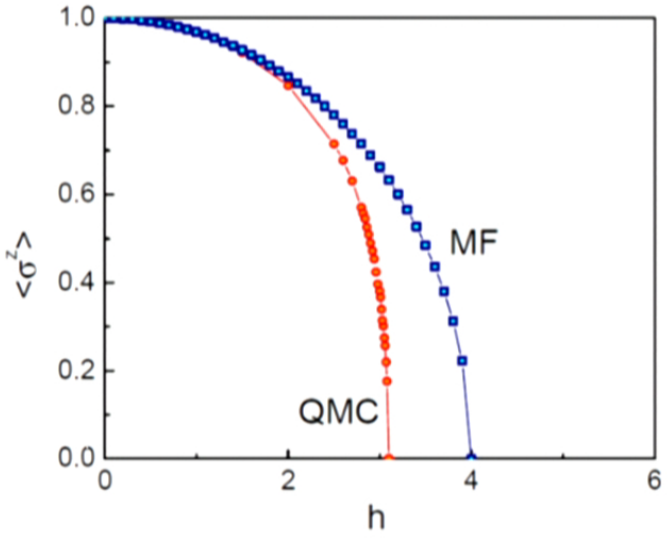

Tensor Product State approach

Mean-field states: $\uparrow \longrightarrow u^{\uparrow}; \quad \downarrow \longrightarrow u^{\downarrow}$

$$\Psi(\{m_i\}) = u^{m_1} u^{m_2} u^{m_3} u^{m_4} \cdots; \quad m_i = \uparrow, \downarrow$$

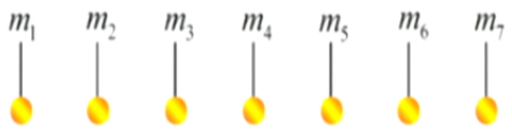

Tensor Product State approach

Mean-field states: $\uparrow \longrightarrow u^{\uparrow}; \quad \downarrow \longrightarrow u^{\downarrow}$

$$\Psi(\{m_i\}) = u^{m_1} u^{m_2} u^{m_3} u^{m_4} \cdots; \quad m_i = \uparrow, \downarrow$$

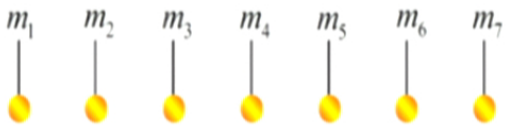

MPS/DMRG(the most powerful method in 1D):

$$\Psi(\{m_i\}) = \mathrm{Tr}\left[A^{m_1} A^{m_2} A^{m_3} A^{m_4} \cdots\right]; \quad m_i = \uparrow, \downarrow \quad \uparrow \longrightarrow A^{\uparrow}; \quad \downarrow \longrightarrow A^{\downarrow}$$

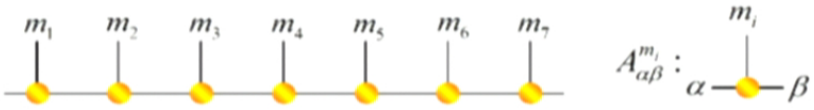

Tensor Product State approach

Mean-field states: $\uparrow \longrightarrow u^{\uparrow}; \quad \downarrow \longrightarrow u^{\downarrow}$

$$\Psi(\{m_i\}) = u^{m_1} u^{m_2} u^{m_3} u^{m_4} \cdots; \quad m_i = \uparrow, \downarrow$$

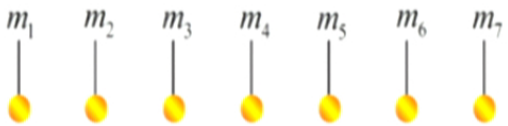

MPS/DMRG(the most powerful method in 1D):

$$\Psi(\{m_i\}) = \mathrm{Tr}\left[A^{m_1} A^{m_2} A^{m_3} A^{m_4} \cdots\right]; \quad m_i = \uparrow, \downarrow \quad \uparrow \longrightarrow A^{\uparrow}; \quad \downarrow \longrightarrow A^{\downarrow}$$

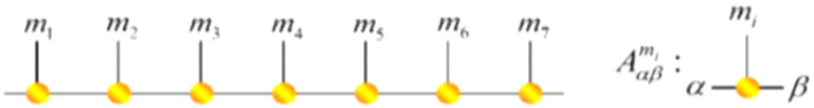

TPS: $\uparrow \longrightarrow T^{\uparrow}_{lrud}; \quad \downarrow \longrightarrow T^{\downarrow}_{lrud}$ (F. Verstraete and J. I. First 2004)

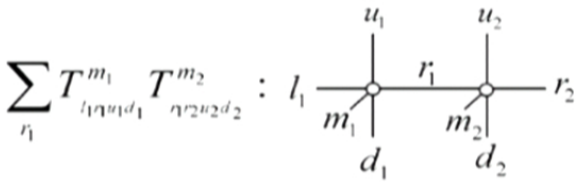

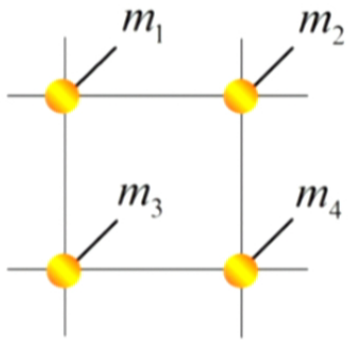

Properties of TPS:

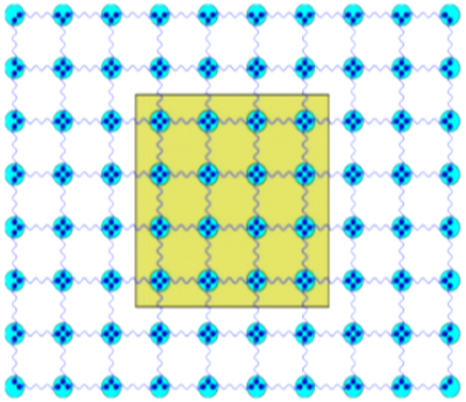

- Entanglement entropy satisfies area law

$$S(\rho_L) = \alpha L$$ (F. Verstraete *etal.*)

$$|\Psi_0\rangle = \prod_{link} |I\rangle \quad |I\rangle = \sum_{l=1}^{D} |ll\rangle$$

$$|\Psi_{TPS}\rangle = \prod_i P_i |\Psi_0\rangle \quad P_i = T^{m_i}_{lrud} |m_i\rangle\langle lrud|$$

Properties of TPS:

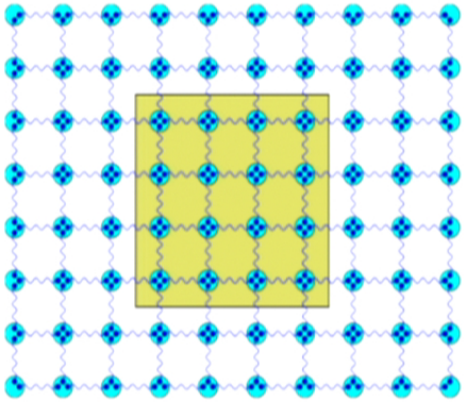

- Entanglement entropy satisfies area law

$$S(\rho_L) = \alpha L \quad \text{(F. Verstraete } \textit{etal.}\text{)}$$

$$|\Psi_0\rangle = \prod_{link} |I\rangle \quad |I\rangle = \sum_{l=1}^{D} |ll\rangle$$

$$|\Psi_{TPS}\rangle = \prod_i P_i |\Psi_0\rangle \quad P_i = T^{m_i}_{lrud} |m_i\rangle\langle lrud|$$

- TPS faithfully represent non-chiral topologically ordered states

(Z.C. Gu, *etal.*, PRB, 2008, O. Buerschaper, *etal.*, PRB, 2008)

Ground state energy

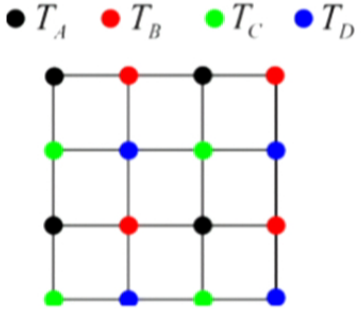

- We use an imaginary time evolution algorithm to find the variational ground state.

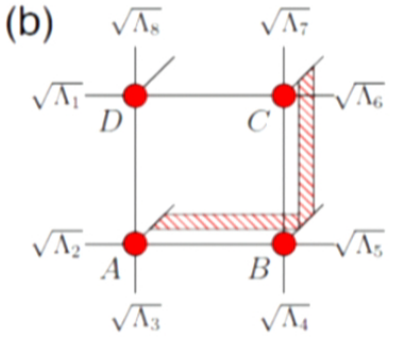

$$|\Psi_{GS}\rangle = \lim_{\tau\to\infty} e^{-\tau H}|\Psi_0\rangle = \lim_{N\to\infty} e^{-N\delta\tau H}|\Psi_0\rangle$$

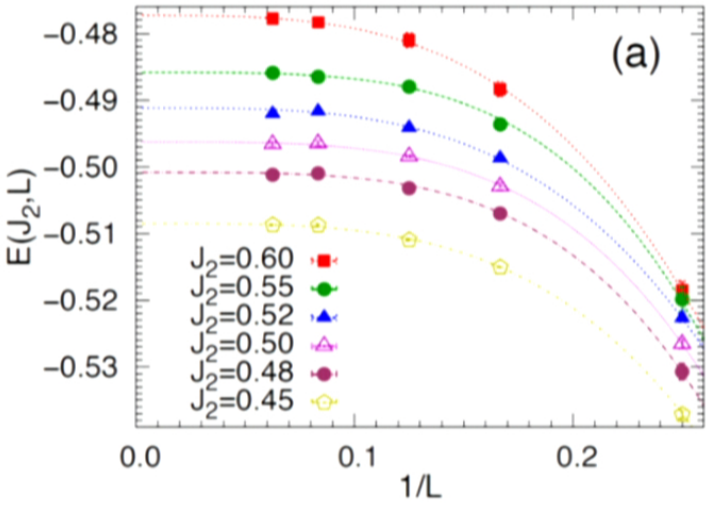

- D=9

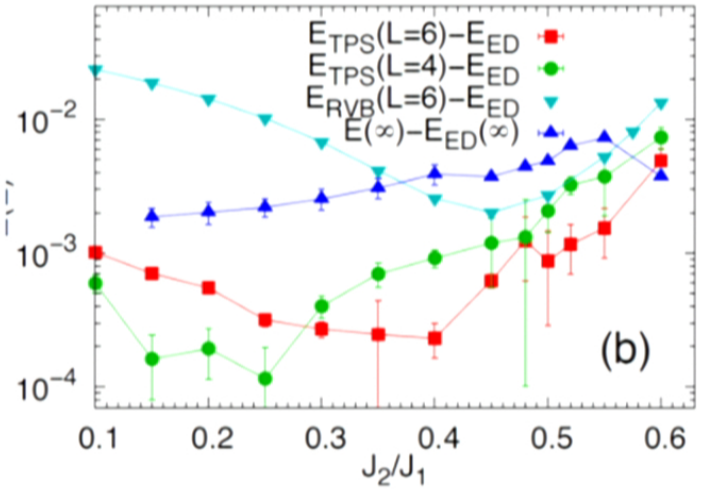

The TPS energy is lower than the best VMC energy!

Ground state energy

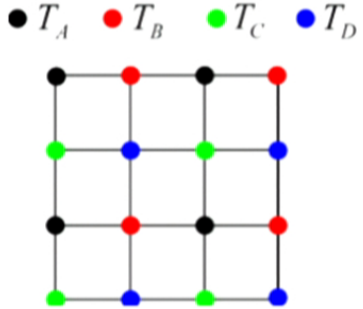

- We use an imaginary time evolution algorithm to find the variational ground state.

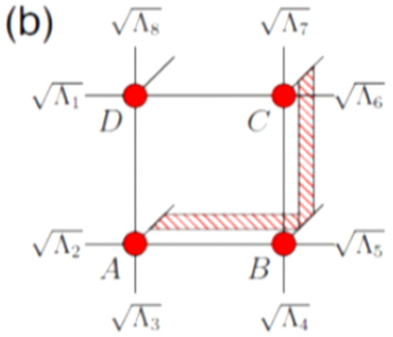

$$|\Psi_{GS}\rangle = \lim_{\tau\to\infty} e^{-\tau H}|\Psi_0\rangle = \lim_{N\to\infty} e^{-N\delta\tau H}|\Psi_0\rangle$$

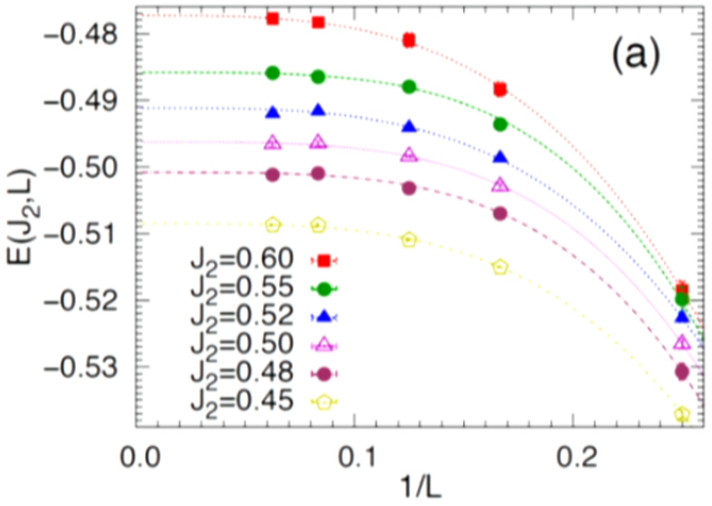

- D=9

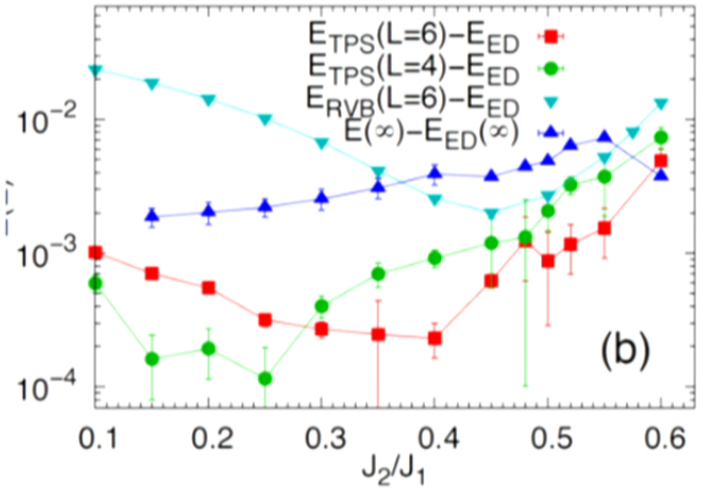

The TPS energy is lower than the best VMC energy!

Ground state energy

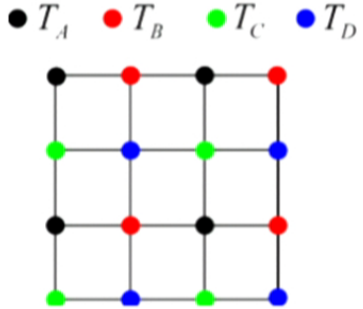

- We use an imaginary time evolution algorithm to find the variational ground state.

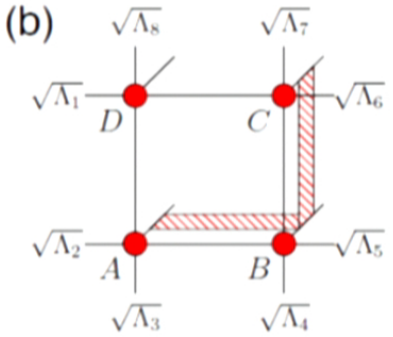

$$|\Psi_{GS}\rangle = \lim_{\tau\to\infty} e^{-\tau H}|\Psi_0\rangle = \lim_{N\to\infty} e^{-N\delta\tau H}|\Psi_0\rangle$$

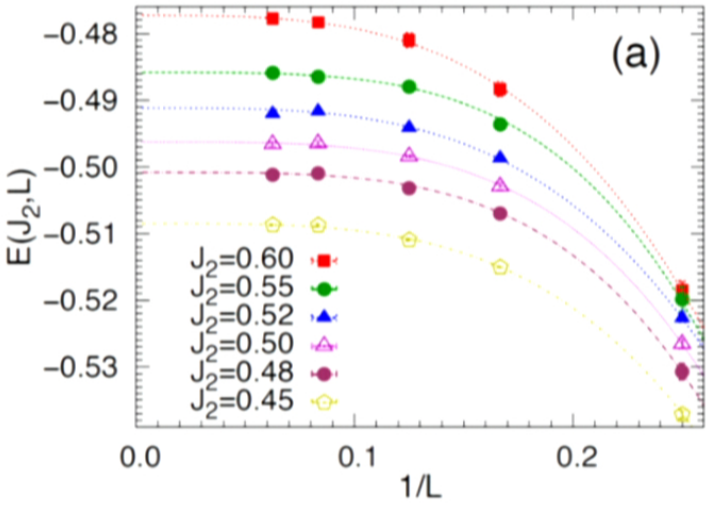

- D=9

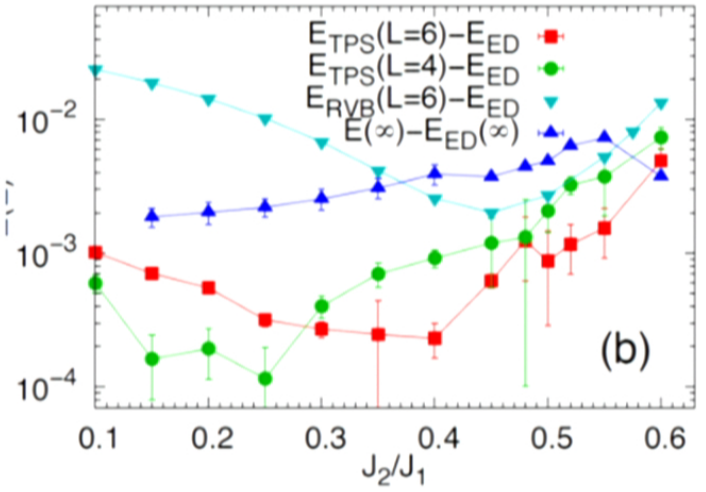

The TPS energy is lower than the best VMC energy!

Ground state energy

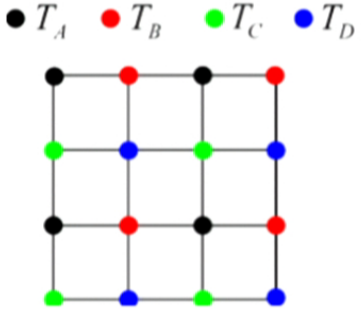

- We use an imaginary time evolution algorithm to find the variational ground state.

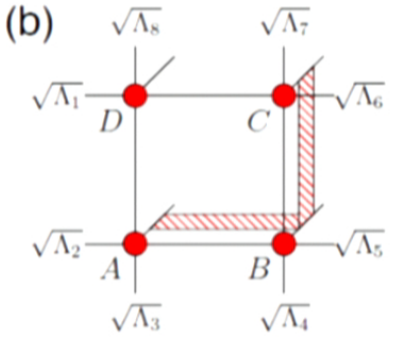

$$|\Psi_{GS}\rangle = \lim_{\tau\to\infty} e^{-\tau H}|\Psi_0\rangle = \lim_{N\to\infty} e^{-N\delta\tau H}|\Psi_0\rangle$$

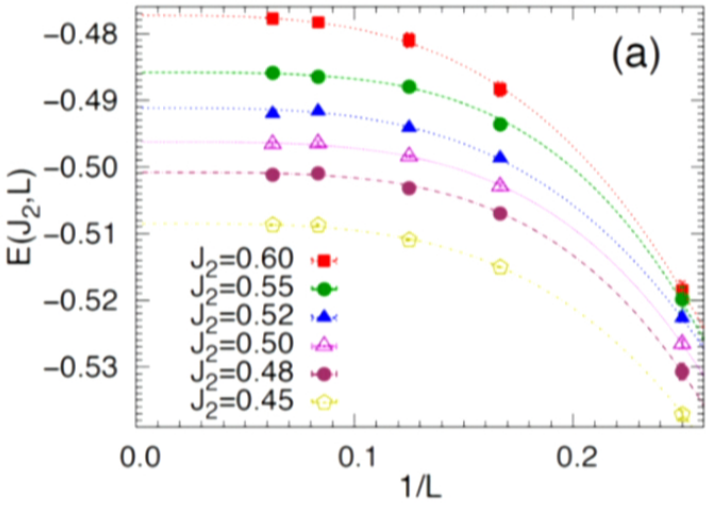

- D=9

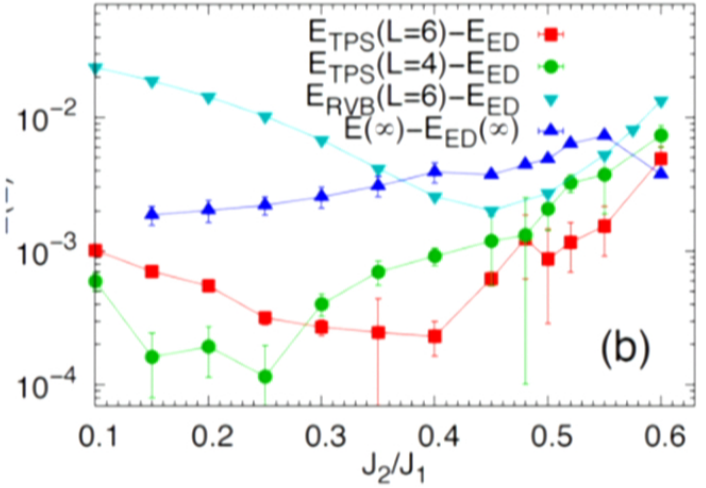

The TPS energy is lower than the best VMC energy!

AF order parameter:

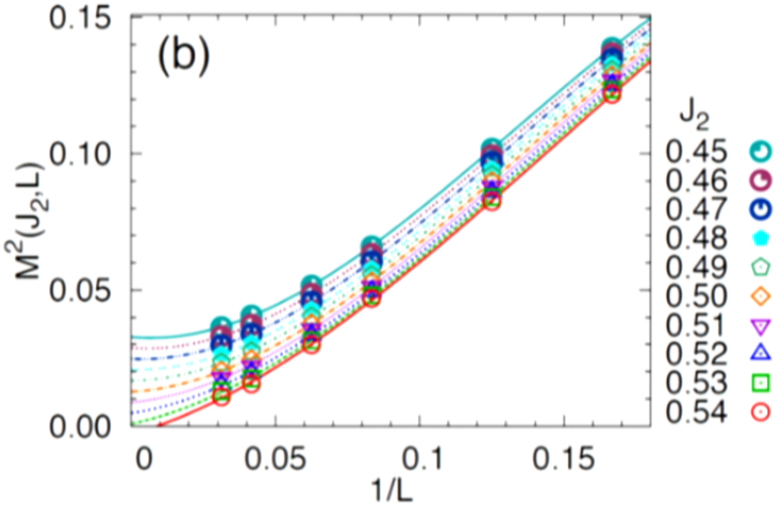

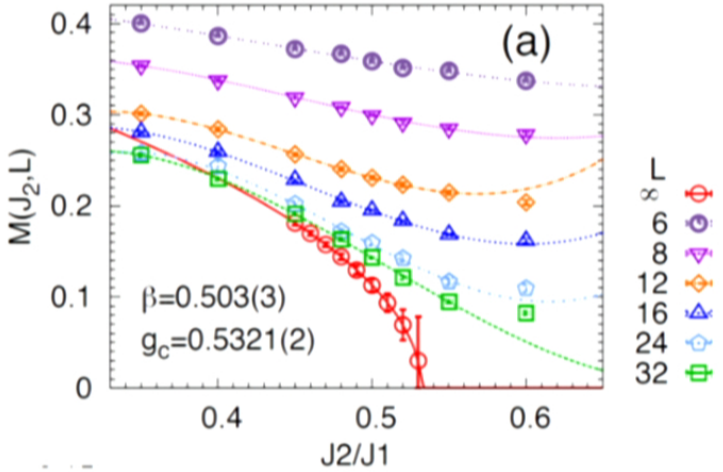

Spin-Spin Correlation:

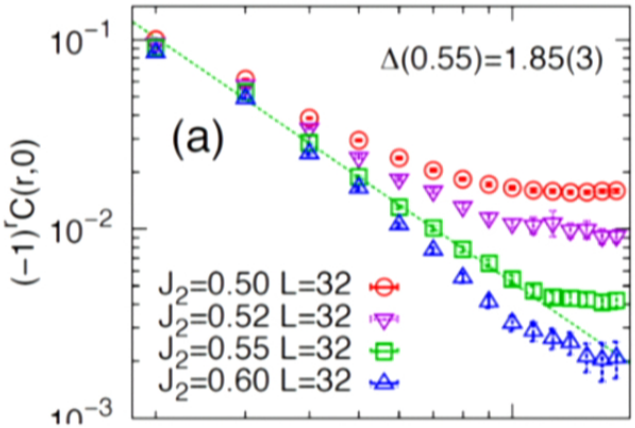

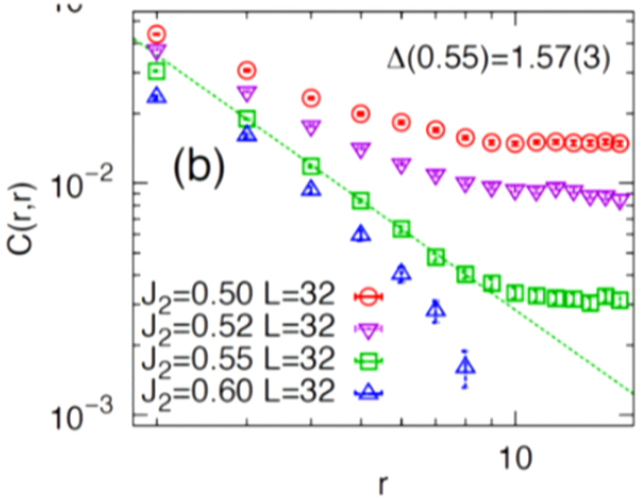

AF order parameter:

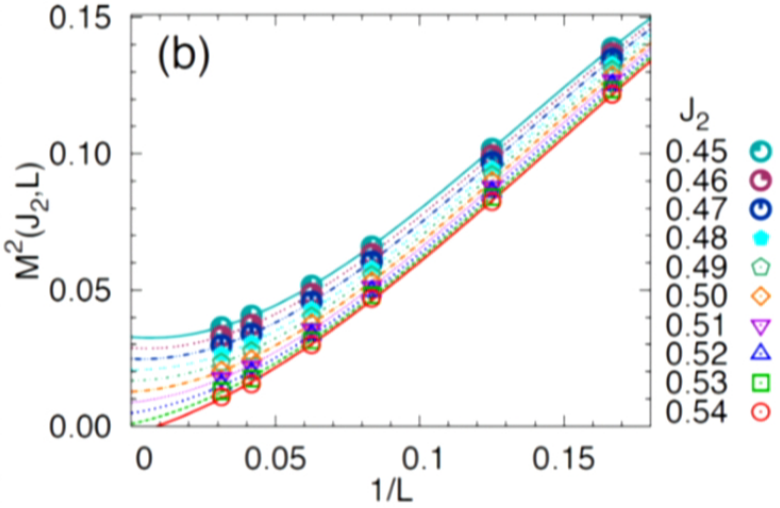

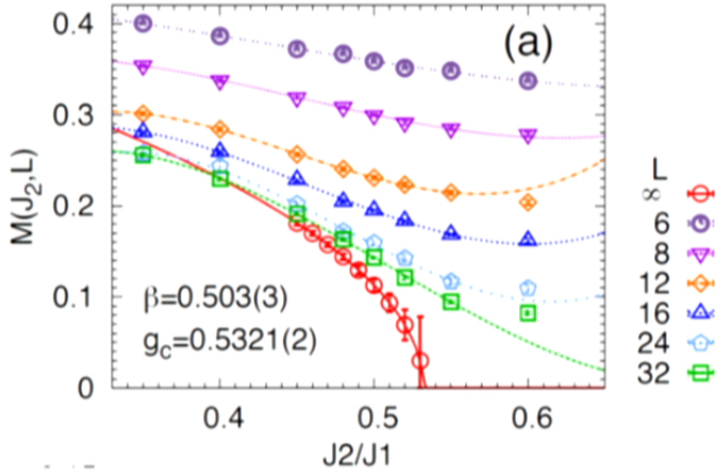

Spin-Spin Correlation:

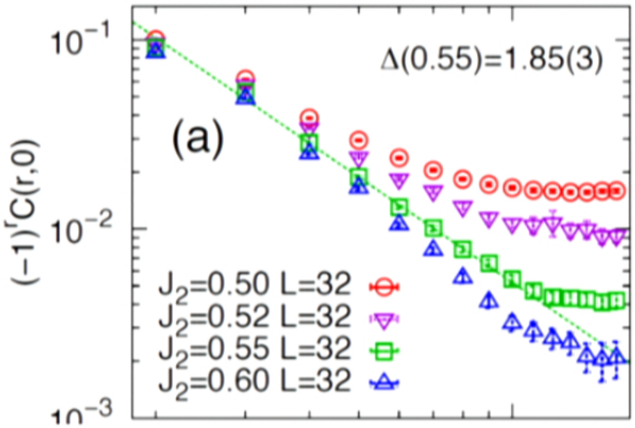

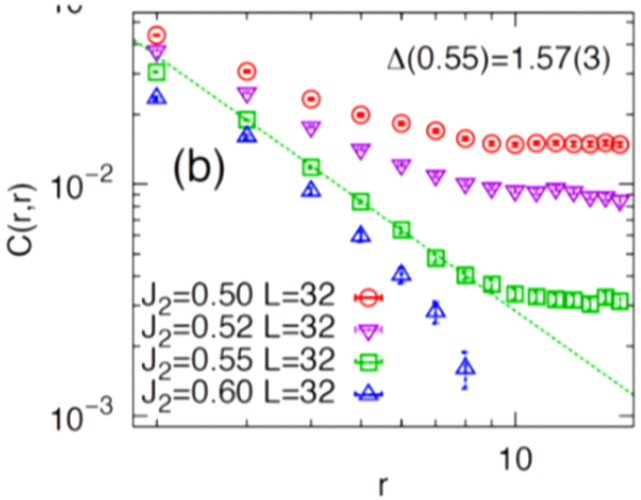

Dimer-Dimer Correlation:

$$C^*_{dx}(r,0) = C_{dx}(r,0) - C_{dx}(r-1,0), \qquad D_x(x,y) = \mathbf{S}_{(x,y)} \cdot \mathbf{S}_{(x+1,y)},$$
$$C^*_{dx}(r,r) = C_{dx}(r,r) - C_{dx}(r-1,r). \qquad D_y(x,y) = \mathbf{S}_{(x,y)} \cdot \mathbf{S}_{(x,y+1)}.$$

$$C_{dx}(r_x,r_y) = \frac{1}{N}\sum_{x,y} D_x(x,y)D_x(x+r_x,y+r_y),$$

$$C_{dy}(r_x,r_y) = \frac{1}{N}\sum_{x,y} D_y(x,y)D_y(x+r_x,y+r_y),$$

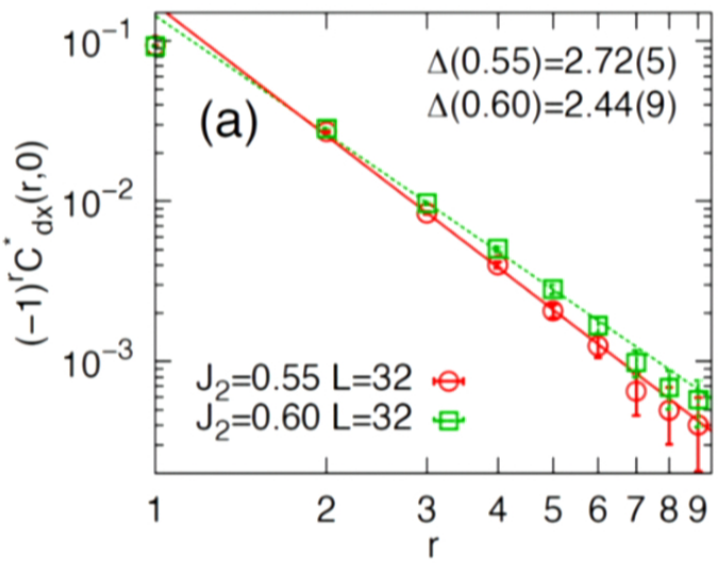

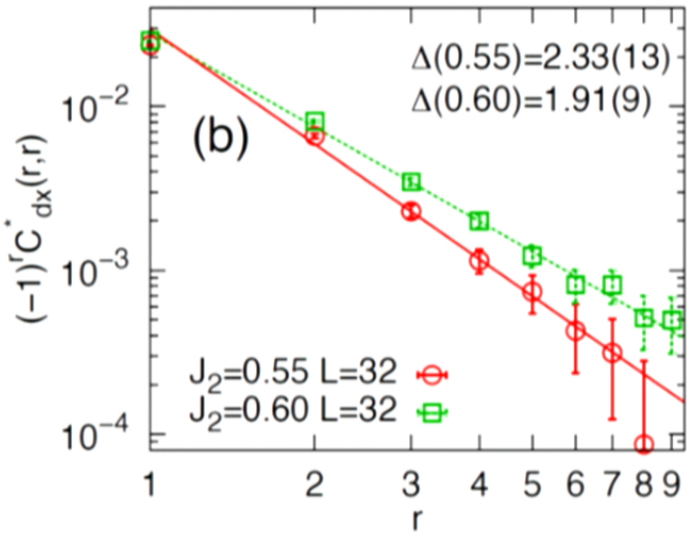

The universal scaling function

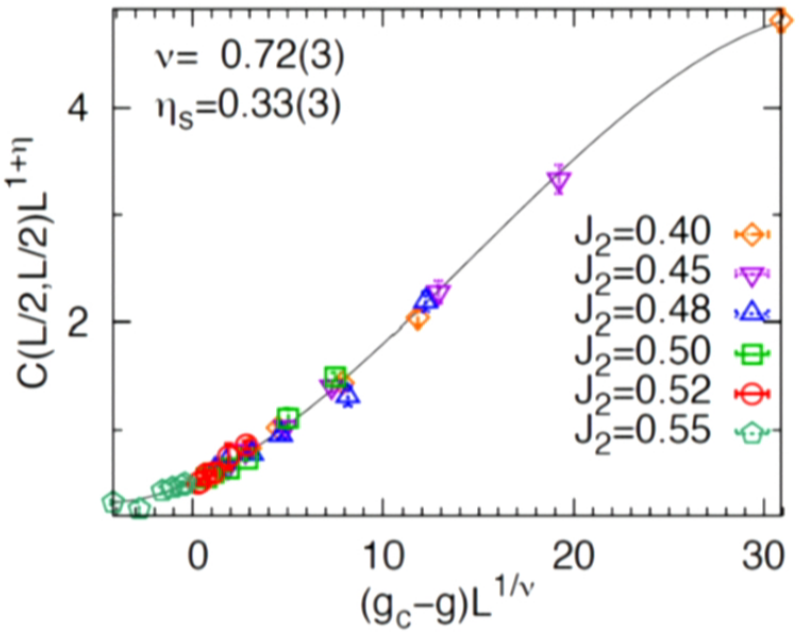

$$C(L/2, L/2) = L^{-1-\eta} f(L^{1/\nu}(g_c - g)/g_c),$$

The critical exponents are intrinsically close to the DQCP behavior observed in other systems, e.g., J-Q model

The universal scaling function

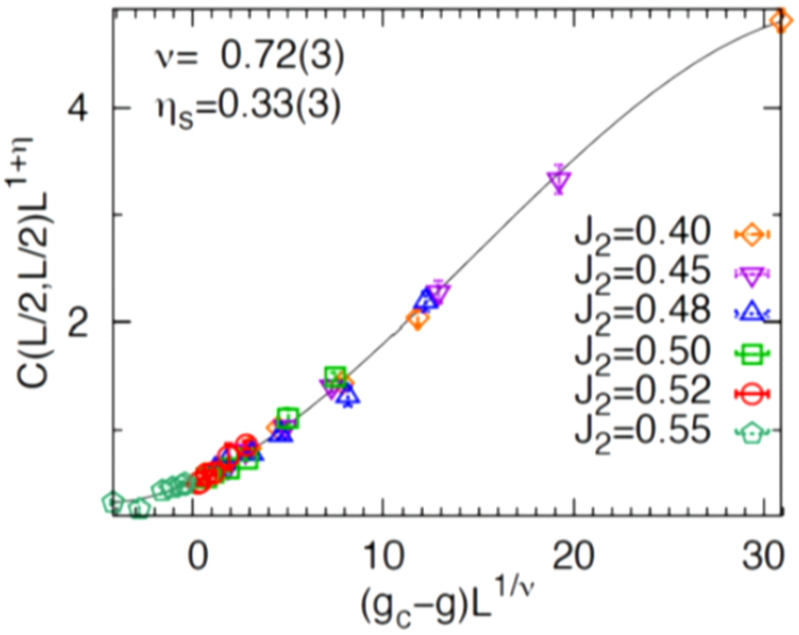

$$C(L/2, L/2) = L^{-1-\eta} f(L^{1/\nu}(g_c - g)/g_c),$$

The critical exponents are intrinsically close to the DQCP behavior observed in other systems, e.g., J-Q model

U(1) spin liquid is unstable, a VBS order with exponentially small amplitude might develop at long wave length

Dimer-Dimer Correlation:

$$C^*_{dx}(r,0) = C_{dx}(r,0) - C_{dx}(r-1,0), \qquad D_x(x,y) = \mathbf{S}_{(x,y)} \cdot \mathbf{S}_{(x+1,y)},$$
$$C^*_{dx}(r,r) = C_{dx}(r,r) - C_{dx}(r-1,r). \qquad D_y(x,y) = \mathbf{S}_{(x,y)} \cdot \mathbf{S}_{(x,y+1)}.$$

$$C_{dx}(r_x,r_y) = \frac{1}{N}\sum_{x,y} D_x(x,y)D_x(x+r_x,y+r_y),$$

$$C_{dy}(r_x,r_y) = \frac{1}{N}\sum_{x,y} D_y(x,y)D_y(x+r_x,y+r_y),$$

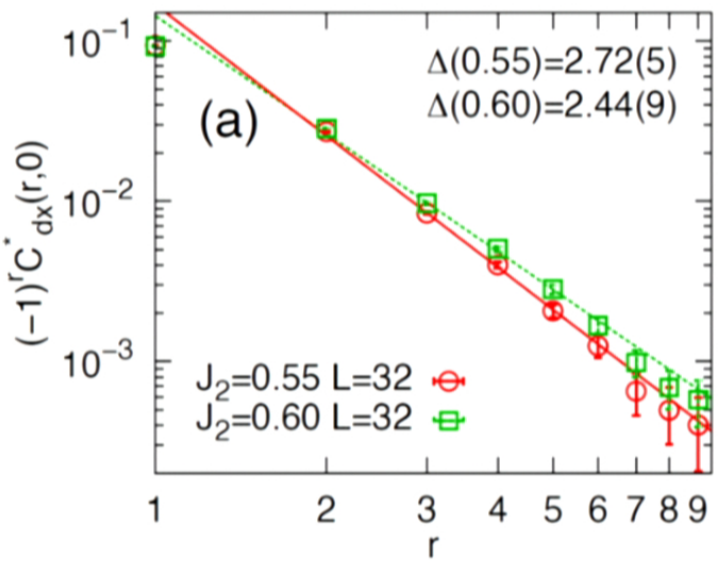

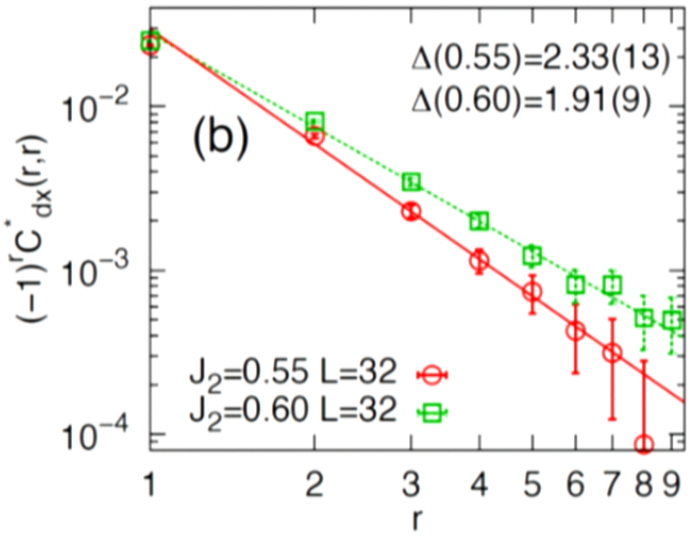

Single parameter variational approach

A D=3 TPS description of short range RVB state

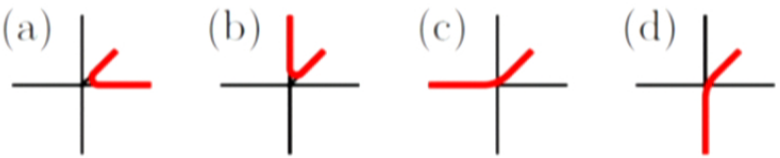

$$\mathcal{P}_1 = \sum_{k=1}^{4} (|\uparrow\rangle\langle 0|_k + |\downarrow\rangle\langle 1|_k) \otimes \langle 222|_{/k}$$

$$|\mathcal{S}\rangle = |01\rangle - |10\rangle + |22\rangle$$

$$|\Psi\rangle_{\mathrm{s-RVB}} = \prod_V \mathcal{P}_1 \prod_B |\mathcal{S}\rangle$$

Single parameter variational approach

A D=3 TPS description of short range RVB state

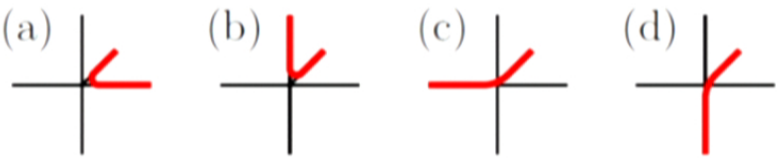

$$\mathcal{P}_1 = \sum_{k=1}^{4} (|\uparrow\rangle\langle 0|_k + |\downarrow\rangle\langle 1|_k) \otimes \langle 222|_{/k}$$

$$|\mathcal{S}\rangle = |01\rangle - |10\rangle + |22\rangle$$

Including longer range RVB

$$|\Psi\rangle_{\mathrm{s-RVB}} = \prod_V \mathcal{P}_1 \prod_B |\mathcal{S}\rangle$$

$$\mathcal{P}_2 = \sum_{i\neq j\neq k\neq l} (|\uparrow\rangle\langle 0|_i + |\downarrow\rangle\langle 1|_i) \otimes \langle 2|_j \otimes \langle \epsilon|_{kl}$$

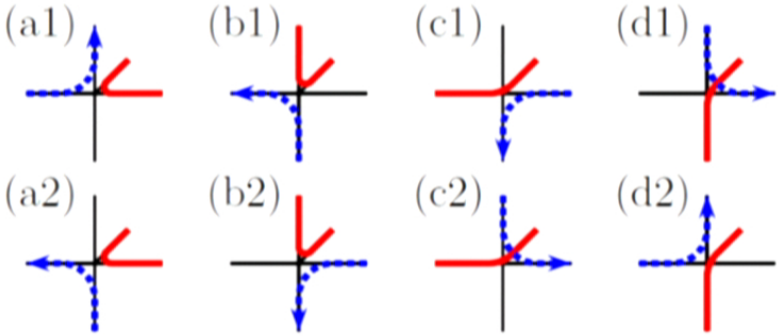

Topological sectors and variational energy

Similar to the short range RVB state, we can define four different topological sectors.

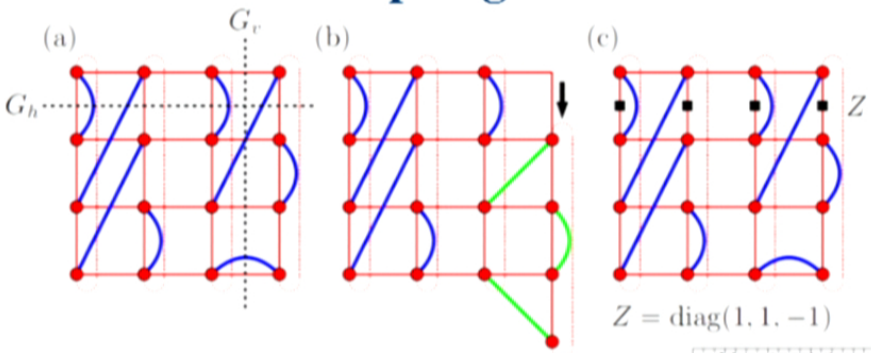

Vison sectors

$$|\Psi(\pm)\rangle \equiv |\Psi\rangle_{G_h=1} \pm |\Psi\rangle_{G_h=-1}$$

Best variational energy at c=0.35

- E=-0.4862/site on cylinder/stripe geometry
- Comparing to E=-0.494/site with D=9

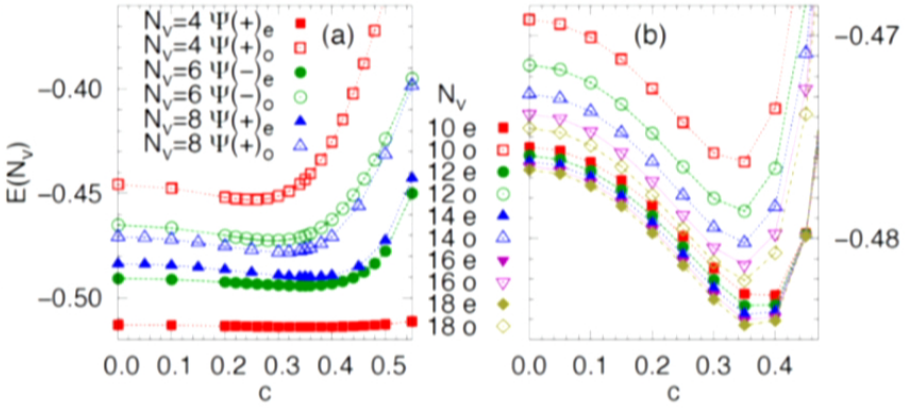

- Cylinder
- Stripe

Correlation functions

Dimer-dimer correlation shows different behaviors on cylinder and torus!(Challenges to DMRG)

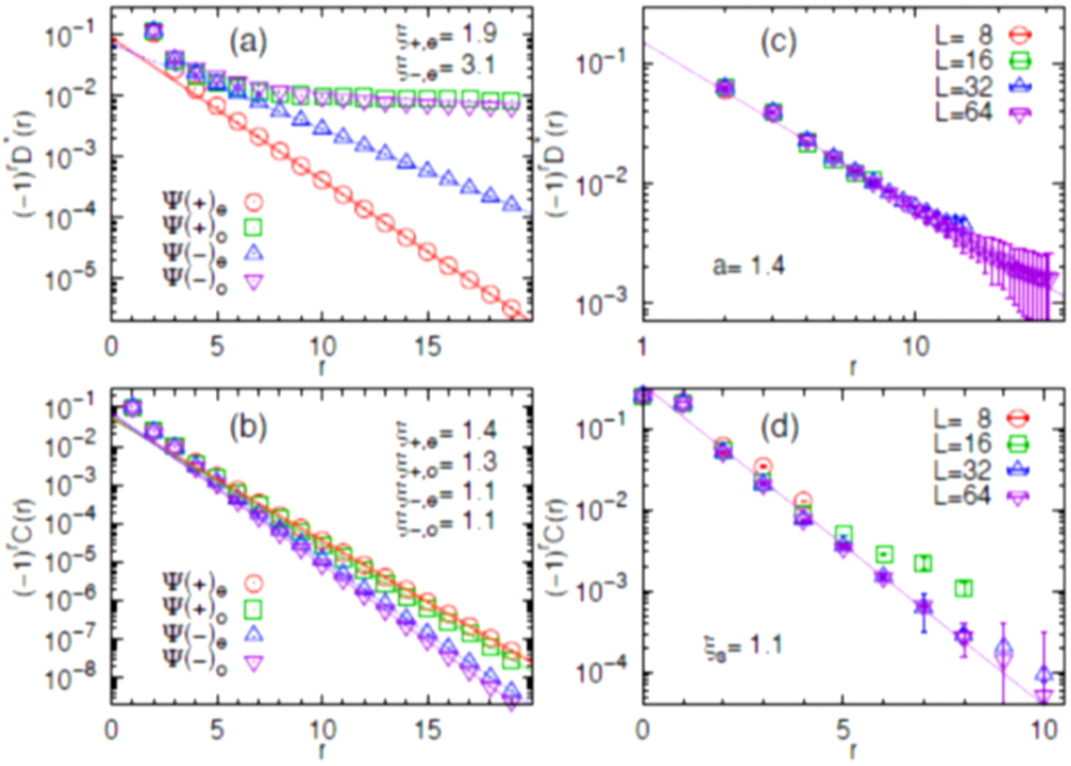

Entanglement entropy

Both dimer-dimer correlation and entanglement entropy indicate gapless spin liquid behaviors!

$$S_2(L) = a_1 L - \tfrac{1}{2} \ln L + b_1$$

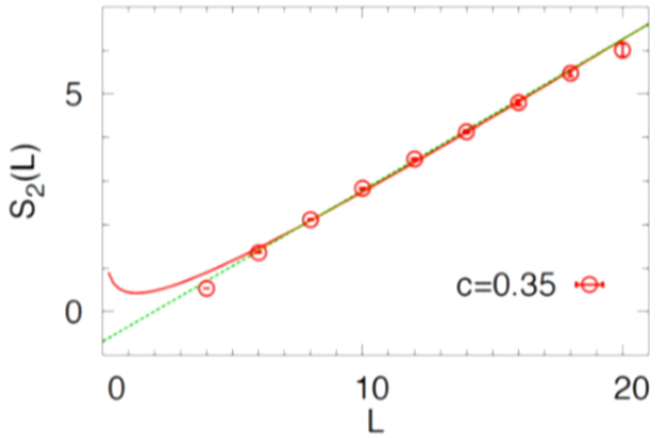

$$S_2(L) = a_2 L + b_2$$

$$b_2 = -0.68(1)$$

A linear fitting leads to a negative constant close to ln2

All these results can be understood as vanishing of same sublattice pairing in our variational ansatz, which describes a U(1) spin liquid

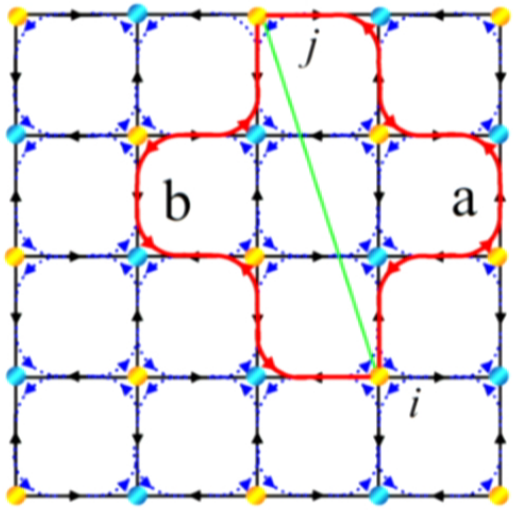

Entanglement entropy

Both dimer-dimer correlation and entanglement entropy indicate gapless spin liquid behaviors!

$$S_2(L) = a_1 L - \tfrac{1}{2} \ln L + b_1$$

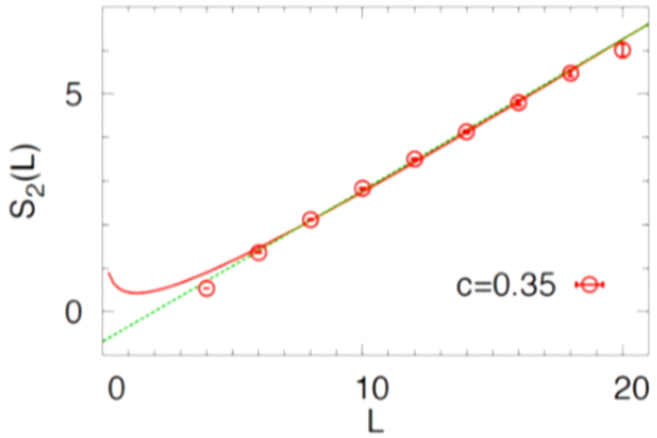

$$S_2(L) = a_2 L + b_2$$

$$b_2 = -0.68(1)$$

A linear fitting leads to a negative constant close to ln2

All these results can be understood as vanishing of same sublattice pairing in our variational ansatz, which describes a U(1) spin liquid

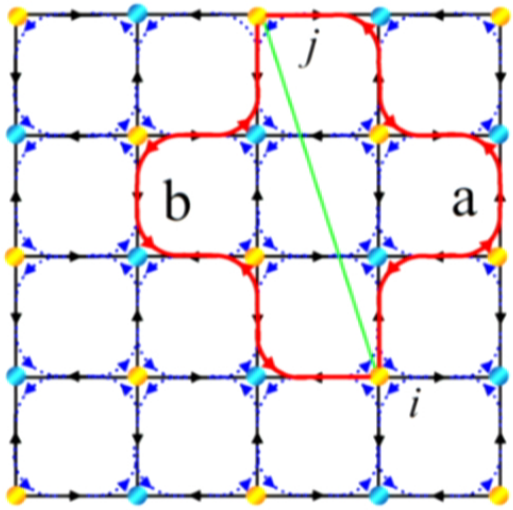

Entanglement entropy

Both dimer-dimer correlation and entanglement entropy indicate gapless spin liquid behaviors!

$$S_2(L) = a_1 L - \tfrac{1}{2} \ln L + b_1$$

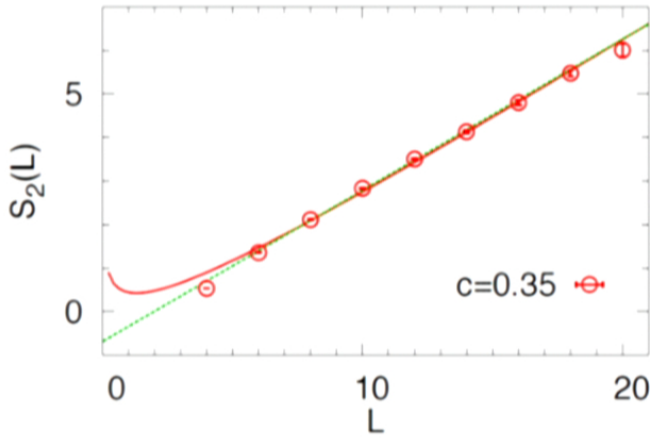

$$S_2(L) = a_2 L + b_2$$

$$b_2 = -0.68(1)$$

A linear fitting leads to a negative constant close to ln2

All these results can be understood as vanishing of same sublattice pairing in our variational ansatz, which describes a U(1) spin liquid

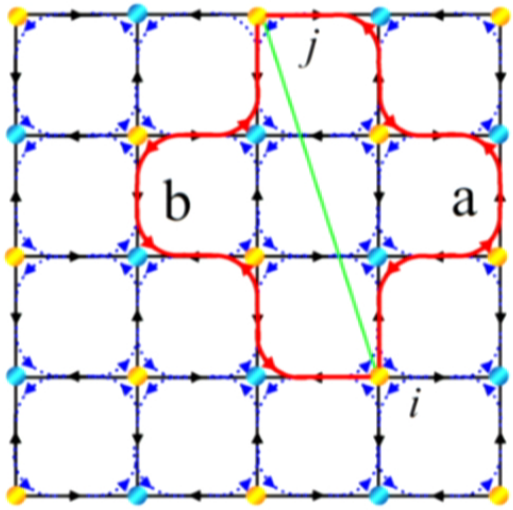

Topological sectors and variational energy

Similar to the short range RVB state, we can define four different topological sectors.

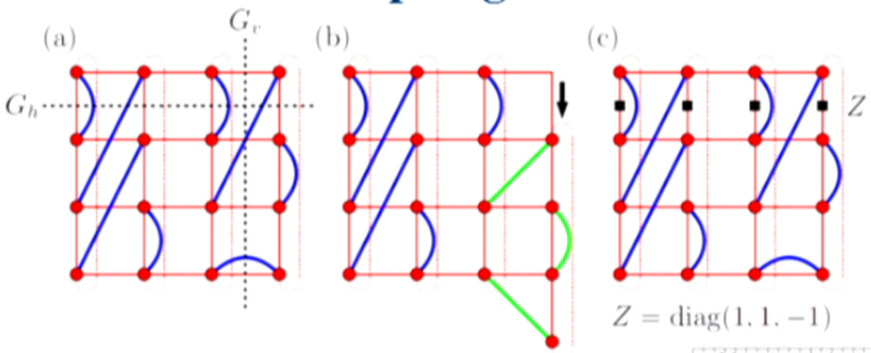

Vison sectors

$$|\Psi(\pm)\rangle \equiv |\Psi\rangle_{G_h=1} \pm |\Psi\rangle_{G_h=-1}$$

Best variational energy at c=0.35

- E=-0.4862/site on cylinder/stripe geometry
- Comparing to E=-0.494/site with D=9

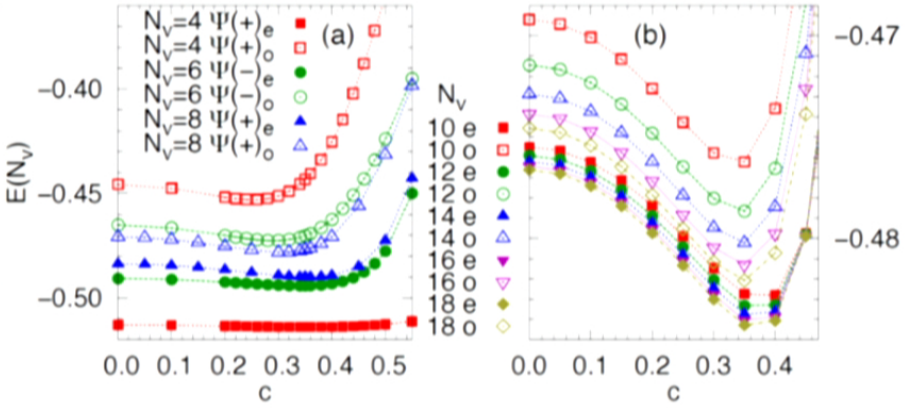

- Cylinder
- Stripe

Single parameter variational approach

A D=3 TPS description of short range RVB state

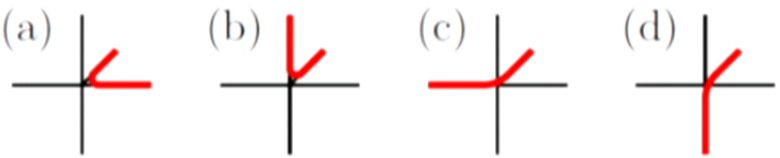

$$\mathcal{P}_1 = \sum_{k=1}^{4} (|\uparrow\rangle\langle 0|_k + |\downarrow\rangle\langle 1|_k) \otimes \langle 222|_{/k}$$

$$|\mathcal{S}\rangle = |01\rangle - |10\rangle + |22\rangle$$

Including longer range RVB

$$|\Psi\rangle_{\mathrm{s-RVB}} = \prod_V \mathcal{P}_1 \prod_B |\mathcal{S}\rangle$$

$$\mathcal{P}_2 = \sum_{i\neq j\neq k\neq l} (|\uparrow\rangle\langle 0|_i + |\downarrow\rangle\langle 1|_i) \otimes \langle 2|_j \otimes \langle \epsilon|_{kl}$$

A single-parameter ansatz

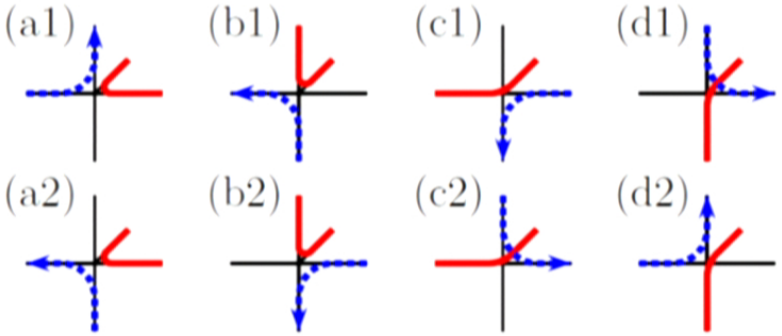

Discussions and future directions:

Other variational approach

- The best Schwinger VMC approach also predicts gapless U(1) spin liquid.
- The best Slave boson VMC approach predicts gapless Z2 spin liquid with a very small vison gap.
- In general, symmetric spin liquid must be gapless if it is close to AF state.

Properties of the variational state

Longer range RVB configurations can be generated through quantum teleportation

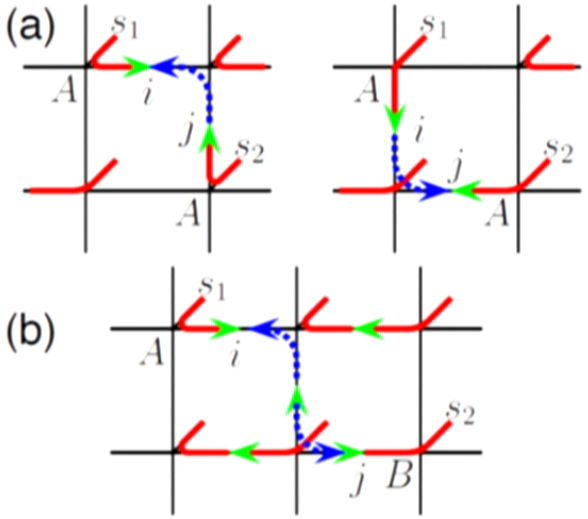

Longer range RVB decays exponentially

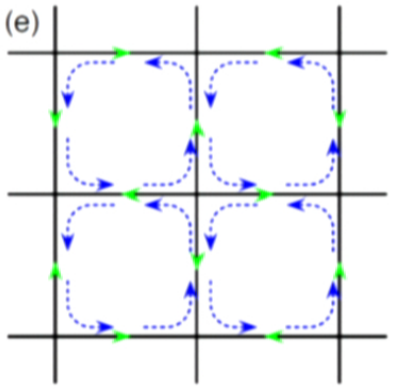

- Sign convention for bond singlets